Temperature Effects on Capillary Pressure in Unsaturated Soil

Debraj Biswas

Temperature Effects on Capillary Pressure in Unsaturated Soil

A Thesis Submitted in
Partial Fulfilment of the
Requirements for the Degree of

Doctor of Philosophy (Ph.D.)
in Civil Engineering

by

Debraj Biswas

to the

Department of Civil Engineering
Indian Institute of Technology Guwahati
Assam, India
December 2018

Declaration

I declare that the thesis entitled "**Temperature Effects on Capillary Pressure in Unsaturated Soil**" submitted by me is a presentation of my original research work done under the guidance of Dr. Suresh A. Kartha, Associate Professor, Department of Civil Engineering, Indian Institute of Technology Guwahati. This work has not been submitted elsewhere for the award of any degree, diploma, associateship, fellowship, titles in this institute or any other university or institution of higher learning.

December 2018

Debraj Biswas,
Department of Civil Engineering,
Indian Institute of Technology Guwahati,
Assam - 781039, India.

Statement

Department of Civil Engineering
Indian Institute of Technology Guwahati
Assam - 781039, India

Dr. Suresh A. Kartha
Associate Professor
Email: kartha@iitg.ac.in
Phone: +91-361-258-2422

Certificate

This is to certify that this thesis entitled "**Temperature Effects on Capillary Pressure in Unsaturated Soil**", submitted by **Debraj Biswas**, in partial fulfillment of the requirements for the award of the degree of Doctor of Philosophy, to the Indian Institute of Technology Guwahati, Assam, India, is a record of the *bona fide* research work carried out by him under my guidance and supervision at the Department Of Civil Engineering, Indian Institute of Technology Guwahati, Assam, India. To the best of my knowledge, no part of the work reported in this thesis has been presented for the award of any degree, diploma, associateship, fellowship, titles in this institute or any other university or institution of higher learning.

Date:
Place: IIT Guwahati

(Dr. Suresh A. Kartha)

Abstract

Subsurface temperature is generally affected by the natural trend of steady upward flux of heat from the interior of Earth. Temporal fluctuations of surface air temperature and sustained effect of it over ground surface temperature produce temperature anomaly up to a *certain* depth of subsurface. Subsurface temperature can affect the soil-water flow through the temperature derivative of capillary pressure (or, *temperature coefficient*), thereby, signifying the effects of existent temperature gradient in the subsurface. Temperature gradient, subsurface temperature, and the soil-water flow are thus interlinked and needs more study.

Capillary pressure is calculated as the product of the surface tension of the liquid and mean curvature of the air-liquid interface or meniscus in unsaturated soil (otherwise known as Young-Laplace (Y-L) equation). Researchers, who are working on the subject to model and to calculate the temperature coefficient at the constant moisture content, have used the Y-L equation to find the coefficient. Though they have managed to calculate coefficient from their model, however their model fails to give a coherent theory encompassing the effects of contact angle, moisture content and air phase along with the temperature coefficient. They have questioned the applicability of Y-L equation. These questions give us the objective of this thesis.

We have proposed a physical mechanistic model to calculate capillary pressure and the temperature coefficient. As we have started our research problem with entrapped air specifically in closed space like dead-end positions in soil (dead-end pore), the universally assumed spherical meniscus shape failed to provide proper answers on the capillary pressures. This veers us to trial with other shapes. *What is this shape?* First we introduce the catenary curve as the shape in 2-D form (upside down Igloo form in 3-D). Temperature coefficient of contact angle from this study validates with the published results. However, calculated capillary pressure from the proposed shape fails to validate the experimental results. We have presented a phenomenological meniscus equation (PME). This is incorporated in Y-L equation to calculate capillary pressure. Lastly we have given a more general algorithm (AoA) to simulate the soil or porous media using an unit-cell approach. We have compared the calculated and the experimental results.

As our results suggest that capillary pressure is a linear decreasing function of temperature regardless of the porous media or soil. Temperature affects capillary pressure in dead end pores in less pronounced way than that of open end pores. As the volume of entrapped air becomes

less, the capillary pressure becomes less sensitive with temperature and vice versa. Physical dimension of the pore size affects the pressure field values. Initial values of theoretical contact angle (SCA) i.e., wetting properties of the soil changes the temperature coefficient. Density values of air and liquid does influence the sensitivity of the temperature coefficient of SCA. Temperature is an intrinsic reason for contact angle hysteresis. The assumption of spherical meniscus imposed upon Y-L equation, i.e. the usual form of Y-L equation fails to incorporate real contact angle (ACA) and fails in more general term. Inclusion of gravity effects in the formation of meniscus as PME gives the effect of ACA with temperature and liquid content (or, 1 - air content) as found in experiments. Air phase has an impact on the variation of ACA with temperature. Presence or absence of air phase over meniscus changes the trend. Presence depicts the increasing trend and absence shows the decreasing trend of the temperature coefficient of ACA for hydrophilic soil and vice versa for hydrophobic soil. This shows that assumption of uniformity of air in porous domain is not the case and the effects of air or gaseous phase should be considered. The PME encompasses the whole effect of pore radius, contact angle and surface tension of liquid. We conclude that spherical shape may not be a good approximation universally, though it serves well for most cases. It is an assumption, *not* a fact. Emphasizing over last point, it is very important to note that curvature is an central factor in estimating the temperature coefficient of capillary pressure. We recommend a correction factor to the usual form of the Y-L equation to incorporate the effects of air or gaseous phase.

Acknowledgements

My principal debt is to my guide and thesis supervisor Dr. Suresh A. Kartha, who gave me the chance to work with him at the Department of Civil Engineering, IIT Guwahati, and who always supported me, encouraged me and helped me to shape my work in this thesis.

I owe much to the members of my doctoral committee - Prof. Gautam Barua (chairman), Dr. Sreeja P. and Dr. Ganesh Natarajan, for their pointed questions and suggestions every year, and my trying to find out answers to those questions over the years have eventually veered me onto the right direction.

My heartfelt thanks go to all my friends at IIT specifically Someswaran Da, Ratan, Arnab, Srikanth, Ashok, Subhadeep, Jagadish, Bhrigumani, Subhrangshu, Tanmoy, Rajeev, Dilip Da, Sudheer, Mamata, Sophia, Satish, Pranab, Bhaskar, Kamal, and my childhood friend Sudipta for all their time and being good friends.

I also convey my thanks to the WRE faculties who taught me about the subjects and life in general. My special thank goes to Prof. Rajib Kumar Bhattacharjya for setting up the Subsurface Hydrology Laboratory, where I have worked and written this thesis. I also thank to all the staffs of IIT for making all these years in this campus to be a pleasant experience.

I am really grateful to my Barda, Boudi, Didi, Rana Da, and my nephews Roop, Shaan, Shreyan for their presence in my life. Last but not the least, I am and always will be grateful and indebted to my Ma and Baba for giving me this life and supporting all the way whatever I chose till now. I dedicate this thesis to my parents.

To my *Ma* and *Baba*

Contents

List of Figures

List of Tables

List of Symbols

a	Molecular length	$[M^0\ L\ Q^0\ T^0]$
A_v	Area of void space in the representative cell	$[M^0\ L^2\ Q^0\ T^0]$
α_{vG}	van Genuchten's (1978) air-entry parameter	$[M^{-1}\ L\ Q^0\ T^2]$
Bo	Bond number ($=\rho g r^2/\sigma$)	$[M^0\ L^0\ Q^0\ T^0]$
$C_{\mathscr{H}}$	Contact angle hysteresis	$[^\circ]$
$\mathbf{C_f}$	Correction factor	$[M^0\ L^0\ Q^0\ T^0]$
D_T	Non-isothermal diffusivity	$[M^0\ L^2\ Q^{-1}\ T^{-1}]$
D_η	Isothermal diffusivity	$[M^0\ L^2\ Q^0\ T^{-1}]$
δ	Distance of maximum dominance of van der Waals force from the tube wall	$[M^0\ L\ Q^0\ T^0]$
d	Spacing parameter	$[M^0\ L\ Q^0\ T^0]$
η	Degree of fluid satuartion	$[M^0\ L^0\ Q^0\ T^0]$
ε	Thickness of a thin film	$[M^0\ L\ Q^0\ T^0]$
$\eth$	Number of carbon atoms in i-component of multicomponent fluid system	$[M^0\ L^0\ Q^0\ T^0]$
f_θ	Contact-angle sensitive temperature function	$[M^0\ L^0\ Q^0\ T^0]$
g	Acceleration due to Earth's gravity	$[M^0\ L\ Q^0\ T^{-2}]$
γ	Interfacial tension	$[M\ L^0\ Q^0\ T^{-2}]$
h	Height	$[M^0\ L\ Q^0\ T^0]$
$\mathbf{k}$	Permeability tensor	$[M^0\ L^2\ Q^0\ T^0]$
$\mathbf{K}$	Capillary conductivity tensor	$[M^0\ L\ Q^0\ T^{-1}]$
K_m	Mean curvature of the meniscus	$[M^0\ L\ Q^0\ T^0]$
λ	Fluid content	$[M^0\ L^0\ Q^0\ T^0]$
L	Total height of the capillary tube	$[M^0\ L\ Q^0\ T^0]$
μ	Dynamic viscosity	$[M\ L^{-1}\ Q^0\ T^{-1}]$
$\mathscr{M}$	Molar mass	$[M\ L^0\ Q^0\ T^0]$
n_g	No. of the moles of gas	$[M^0\ L\ Q^0\ T^0]$
n_{vG}	van Genuchten's (1978) parameter	$[M^0\ L^0\ Q^0\ T^0]$
ϕ	Volumetric porosity	$[M^0\ L^0\ Q^0\ T^0]$
P	Pressure	$[M\ L^{-1}\ Q^0\ T^{-2}]$
P'	Hydrostatic pressure ($=-\rho g h$)	$[M\ L^{-1}\ Q^0\ T^{-2}]$
P_c	Capillary pressure	$[M\ L^{-1}\ Q^0\ T^{-2}]$

q	Specific discharge	$[M^0\ L\ Q^0\ T^{-1}]$
ρ	Density	$[M\ L^{-3}\ Q^0\ T^0]$
R_g	Universal gas constant	$[M\ L^2\ Q^{-1}\ T^{-1}]$
R	Radius	$[M^0\ L\ Q^0\ T^0]$
R_1, R_2	Principal radii of the meniscus	$[M^0\ L\ Q^0\ T^0]$
$r, z(r)$	Cartesian co-ordinate axis of the meniscus taking water table as reference	$[M^0\ L\ Q^0\ T^0]$
r_s	Radius of soil separate (say, 's')	$[M^0\ L\ Q^0\ T^0]$
ψ	Capillary or matric head	$[M^0\ L\ Q^0\ T^0]$
σ	Surface tension	$[M\ L^0\ Q^0\ T^{-2}]$
θ	Contact angle	$[^\circ]$
T	Temperature	$[M^0\ L^0\ Q\ T^0]$
T_n	Combinations of specific pore space inside a particular cell while taking three out of 'n' soil separates	$[M^0\ L^0\ Q^0\ T^0]$
$\triangle$	Triangular face area of the representative cell	$[M^0\ L^2\ Q^0\ T^0]$
υ	Mass-flow factor	$[M^0\ L^0\ Q^0\ T^0]$
u	Meniscus velocity	$[M^0\ L\ Q^0\ T^{-1}]$
φ	Energy potential	$[M^0\ L^2\ Q^0\ T^{-2}]$
v	Velocity	$[M^0\ L\ Q^0\ T^{-1}]$
V	Volume	$[M^0\ L^3\ Q^0\ T^0]$
ϖ	Tortuosity factor	$[M^0\ L^0\ Q^0\ T^0]$
ς	A factor accounting for interaction of vapor and liquid phase	$[M^0\ L^0\ Q^0\ T^0]$
$\mathscr{V}$	Molar volume	$[M^0\ L^3\ Q^0\ T^0]$
ϑ_i	Superficial volume fraction of i-component of multicomponent fluid system	$[M^0\ L^0\ Q^0\ T^0]$
w	Weight function	$[M\ L^{-1}\ Q^0\ T^{-2}]$
w	Statistical weight	$[M^0\ L^0\ Q^0\ T^0]$

N.B. We have included only important symbols in this list. All the symbols are defined wherever they are first appeared in this work. [M] = [Mass], [L] = [Length], [Q] = [Temperature], and [T] = [Time].

CHAPTER 1

Introduction

1.1 General

Human population is ever rising*. To cater the need of the human demands, infrastructural development on the surface as well as beneath the surface of earth are constructed in the cities and human settlement zones. The stresses on the natural environment and resources are, therefore, immense and require caution for sustainable development. The ambient temperature of the surface and subsurface environment plays a crucial role in the ecological balances. In general, subsurface temperature linearly decreases from the center of Earth to the ground surface over the radius of the Earth due to steady upward flux of heat from the interior of Earth (Beltrami et al., 2005). This natural trend can be affected by daily, seasonal, and annual changes in surface air temperature (Smerdon et al., 2006). Accumulated effect of ground water temperature over a long period can reach up to a *certain* depth of subsurface (e.g. 140 m, 80 m, 50 m, and 50 m as estimated by Taniguchi et al., 2007 in Tokyo, Osaka, Seoul and Bangkok respectively). Depth of the ground water table typically ranges from 0.25 m to 200 m (Fan et al., 2013). Thermal fluctuations thus directly influence physics of soil-water and eventually impact all the terrestrial water storage (sum of groundwater, soil moisture, surface water, snow and ice) (Rodell et al., 2018).

Soil is a particular case of *porous media*. At this point, we digress to the definitions and the terminologies involving porous media (specifically, soil) appeared throughout the thesis before we go any further.

1.1.1 Preliminaries

Fluid movement in porous media is ubiquitous in nature (e.g. movement of water or oil or gas in geological aquifers, concrete, ceramic materials, bricks etc.). Following the different porous materials, one can see some basic characteristics.

*see an interesting display on http://www.worldometers.info/world-population/ about ever-rising human population.

Definition 1. Porous Media (Muskat and Wyckoff, 1937) *Porous media consist of 'solid matrix' and interstices in between them or 'void space' or 'pore space', which are interconnected and through which fluid may flow.*

In simple term, 'interconnectedness' can be understood if one can connect the void space of porous media from one end to other one through a single line. Some pores may not be part of the flow path or imaginary line as described without contributing to flow and some may be just disconnected from the whole main flow path. Whenever we mention void space or pore in this thesis, we mean interconnected pores only. Pores are usually filled up with either one fluid (i.e. saturated) or, two to more fluids (i.e. unsaturated). In unsaturated case, one of these fluids can be gas and a single liquid or both can be liquids. These fluids meet at an interface or a surface. All fluids are assumed to be *homogeneous* (A1[†]).

We focus on soil and fluids in its void spaces. What is soil? Soil is 'the weathered and fragmented outer layer of the earth's terrestrial surface' (Hillel, 1980). Void spaces in soil are occupied typically by two fluids – water and air. Sometime, whole voids are fully filled up or *saturated* by water or air. Rain or precipitation is the source of water on earth. Some portion of rain water *infiltrates* and stores in the soil and other portion gets lost due to *evaporation*, *surface*, and *subsurface water flow*. Water starts accumulating over bedrock (bottom limit of the soil domain) due to Earth's gravitational pull. Above the bedrock, soil becomes saturated up to a limit, known as *water table*. Above water table, water is still there, however coexisting with air and this soil zone above water table is known as *unsaturated zone*.

In 1738 Daniel Bernoulli and later on in 1755 Leonhard Euler showed that an inviscid, incompressible fluid holds constant total *potential* i.e., total mechanical energy per unit elemental mass (total potential = sum of gravitational, pressure and kinetic potentials), along its flow path or *streamline* in steady flow field (Batchelor, 2000). In soil, the total potential as water possesses can be defined as follows

Definition 2. Soil water potential (Soil Science Society of America, 2008) *The amount of 'work' that must be done per unit of a specified quantity of pure water in order to transport reversibly and isothermally an infinitesimal quantity of water from a specified source to a specified destination.*

In soil, water is not inviscid i.e. not frictionless, thus the mechanical energy is not constant over the flow path and it diminishes over its path. Velocity of soil water is very slow (generally in the order of few centimeters per day) and thus the kinetic energy ($\sim$velocity^2) can be neglected without the loss of generality (Hubbert, 1940). We, therefore, consider in this

[†]A1 represents assumption 1 or first assumption. Throughout this work, we shall refer all assumptions as 'A#'.

thesis two potentials that are predominant in the unsaturated soil zone – *gravitational energy potential* and *pressure potential*.

Gravitational energy potential (φ_g, [J kg^{-1}]) can be defined as gravitational potential energy *stored* (due to Earth's gravitational force field) per unit mass of soil water at a specific destination (say, z, [m]) above specified source (taking free flat surface of water or water table as source).

$$\varphi_g = gz, \tag{1.1}$$

where g is acceleration due to Earth's gravity (9.81 m s^{-2}).

Pressure potential[‡] (φ_P, [J kg^{-1}]) can defined as work done by *pressure gradient force* to move a unit mass of fluid from source to destination point (Richards, 1931).

$$\varphi_P = \int_{P \text{ at source point}}^{P \text{ at destination point}} \frac{dP}{\rho} = \int_{P_0}^{P} \frac{dP}{\rho}. \tag{1.2}$$

Here P implies *mechanical pressure* (from here onwards, we call P as simply *pressure* [N m^{-2} or Pa]) and ρ is the density of fluid involved [kg m^{-3}]. Mechanical pressure can be defined as average compression stress on fluid (see p. 67 of White, 1991). The pressures P_0 and P are pressures at reference level and the point in soil water zone respectively.

Momentum-balance of fluid in the soil zone generates an equation of flow (Hall, 1956; Hubbert, 1956; Bear and Bachmat, 1990). This flow equation is known as Darcy's law after Henry Darcy (1856), who found the form empirically. In general terms, Darcy's law describes *specific discharge* relative to moving soil (Bear and Corapcioglu, 1981) as

$$\vec{q}_r \equiv \phi\eta\left(\vec{v} - \vec{v}_s\right) = -\frac{\rho}{\mu}\mathbf{k}\cdot\nabla\varphi^*, \tag{1.3}$$

where $\vec{v}$ is velocity [m s^{-1}] of water (or any fluid) and $\vec{v}_s$ is velocity [m s^{-1}] of soil grains (or solid matrix), μ is dynamic viscosity of water (or any fluid) [N s m^{-2}], ϕ is volumetric porosity [m^3 m^{-3}], and η is water content [m^3 m^{-3}] in porous medium. The coefficient $\mathbf{k}$ [m^2] characterizes the geometrical configuration of void space (Bear and Bachmat, 1990). The term φ^* is known as Hubbert's potential and is sum of $\varphi_g + \varphi_P$. Edgar Buckingham (1907) independently came to same law as Darcy in terms of energy potential in soil water (Sposito, 1986). L. A. Richards (1928) discussed the importance of energy potential and later in 1931, he introduced a new pressure potential to accommodate soil water in unsaturated zone. This improvement gives a full picture of soil water from fully saturated to unsaturated

[‡]The necessary condition to be this term as potential is $\nabla \times \nabla\left(P/\rho\right) = 0$ (De Wiest, 1966; Hubbert, 1940, p. 841).

zone.

In unsaturated soil zone, two *phases*[§] of fluid exist – water (subscripted as w) and air (subscripted as a). Fundamentally, phases can be described as their *wetting* characteristic in porous media other than obvious density difference. One of the two phases adheres to solid much more than the other phase. Thus, one phase *wets* the solid matrix and the other does not. The two fluids are known as - *wetting* and *non-wetting* fluid. In soil, water functions as wetting fluid and air as non-wetting fluid. The fluids move relative only to the solid but *not* relative to each other fluid phases at their interfaces. In this thesis, we assume that there is no interfacial *drag* due to movement of water or air over each other (A2). This is due to high viscosity ratio of air and water (Hoffmann, 2003). Water movement in unsaturated zone is very slow and thus *consolidation* due to water drainage and imbibition can be neglected. Porosity is fixed with respect to time and thus, solid matrix is fixed at space or *non-deformable*, i.e. $\vec{v}_s = 0$ (Bear and Corapcioglu, 1981) (A3).

In *Einstein summation* symbols (Schutz, 1980, p. 56), the fluid pore velocity from Darcy's equation in terms of 3-D Cartesian coordinate system (taking $x_1 = x,\ x_2 = y,\ x_3 = z$) is:

$$v_{\alpha i} = -\frac{k_{\alpha ij}}{\phi \eta_\alpha \mu_\alpha}\left(\rho_\alpha g \frac{\partial z}{\partial x_j} + \frac{\partial P_\alpha}{\partial x_j}\right);\ \alpha = w \text{ or } a;\ i,j = 1,2,3. \tag{1.4}$$

In saturated soil, the permeability coefficient k_{ij} is only dependent upon geometry of the void space. However in unsaturated soil, each phase has different permeability coefficient depending upon its partial fill of void space or η_α. The permeability in unsaturated zone is known as *effective permeability* $k_{\alpha ij}(\eta_\alpha)$.

Another important concept in unsaturated hydrology is *capillary pressure*. The pressure difference across the interface of two *immiscible* fluids is *defined* as capillary pressure (P_c).

$$P_c \equiv P_a - P_w. \tag{1.5}$$

On assuming the pressure of air and density of water being *uniform* over space (A4), Darcy's equation for water phase is:

$$v_{wi} = -\frac{\rho_w g k_{wij}}{\phi \eta_w \mu_w}\left(\frac{\partial}{\partial x_j}\left(z - \frac{P_c}{\rho_w g}\right)\right). \tag{1.6}$$

[§]A *phase* is defined as a chemically homogeneous portion of a system under consideration that is separated from other such portions by a definite physical boundary (interface, or inter-phase boundary)' (Bear and Bachmat, 1990)

As one can see that the dimension of $P_c/\rho_w g$ is in length scale [m], it can be replaced with *head* term ψ, which is otherwise known as *capillary* or *suction* head. Therefore, the Darcy's equation for specific discharge of water is:

$$v_{wi} = -\frac{K_{wij}}{\phi\,\eta_w}\frac{\partial\,(z-\psi)}{\partial x_j}, \tag{1.7}$$

where $K_{wij} = \rho_w g k_{wij}/\mu_w$ is capillary conductivity of water [m s^{-1}] and varies with the saturation of water phase, i.e. $K_{wij} = K_{wij}(\eta_w)$. This describes with how *ease* the fluid flows through void space and thus, combines both fluid and porous medium properties in its description.

There are three unknown variables or dependent variables of importance – ψ, η_w and η_a. Three equations are, therefore, required to extract the values of unknowns – 1. The *continuity* equation for water (see p. 5 of Lamb, 1932), 2. Saturation constraint of void space and 3. Constitutive relationship of water saturation and capillary potential.

$$\frac{\partial \eta_w}{\partial t} + \frac{\partial \eta_w v_{wi}}{\partial x_i} = 0, \tag{1.8}$$

$$\eta_w + \eta_a = 1, \tag{1.9}$$

$$\eta_w = \eta_w(\psi). \tag{1.10}$$

At this juncture, it is important to note that all the terms mentioned above are averaged over a representative *elementary* volume of the porous media. Any property in this volume is averaged with respect to the centroid of the volume. This centroid possesses the averaged values of the properties and behaves as a *physical* or *material point*. All differential equation is based on the idea of *smoothness* and *continuity* of physical properties as functions of these spatial *material* points. Intuitively, it is assumed that single dimension of this volume is much bigger than *microscopic* characteristic length (or *local* scale) of solid or void space, but much less than the length scale over which averaged terms vary (A5) (Whitaker, 1969). The averaging terms can be said as *macroscopic* terms. Averaging process smooths out the microscopic heterogeneities to get macroscopic value. Now, the averaging process of any term (say, p) over the averaging volume (V) can be described (Whitaker, 1986) as

$$p \equiv \langle p \rangle^{\alpha} = \frac{1}{V_\alpha}\int_{V_\alpha} p\,dV = \frac{V}{V_\alpha}\frac{1}{V}\int_{V_\alpha} x\,dV = \frac{\langle p \rangle}{\lambda_\alpha}. \tag{1.11}$$

Here $\lambda_\alpha = V_\alpha/V = \phi\,\eta_\alpha$ is the α-fluid content, V_α is the volume of α-fluid in void space,

$\phi = V_v/V$ is the porosity, V_v is the volume of void space, and $\eta_\alpha = V_\alpha/V_v$ is the degree of saturation of α-fluid in the averaging volume V. The $\langle p \rangle$ is known as *phase average* and $\langle p \rangle^\alpha$ is known as *intrinsic phase average* of p. The integrand pdV in Eq. (1.11), must be an additive quantity to be physically meaningful (see the criterion 1 of Hassanizadeh and Gray, 1979). Phase average gives the value of the variable in term of whole volume, whereas intrinsic phase average expresses phase values inside pore or void space, like pressures are intrinsic to its phase. Whitaker (1986) mentioned that intrinsic phase average is 'more representative of the conditions' in a particular phase. As an example, relative specific discharge of α-phase is,

$$\langle \vec{q}_r \rangle \equiv \lambda_\alpha \langle \vec{v} \rangle^\alpha = -\mathbf{K} \cdot \nabla \left(z + \frac{P_c}{\langle \rho \rangle^\alpha g} \right). \tag{1.12}$$

The solution of unsaturated porous media flow equations is intricately linked to the relation of capillary potential with wetting phase saturation. Capillary potential is first introduced by Buckingham (1907) and is a scalar quantity under 'capillary field' (Richards, 1928). L. A. Richards (1928) himself said that the concept of this field force is 'obscure'. This force can be understood as pressure gradient experienced due to attractive forces of porous solid matrix towards wetting phase (Richards, 1928). This definition combines both *matric* and *osmotic* potential (Passioura, 1980). In this work, we ignore the effect of osmotic potential in capillary potential and by that, we mean that soil water is assumed as *homogeneous* (A4). As defined before, capillary potential can be evaluated from macroscopic capillary pressure per unit specific weight of water (or wetting phase). We can write the macroscopic capillary pressure as

$$P_c \equiv \langle P_a \rangle^a - \langle P_w \rangle^w. \tag{1.13}$$

The intrinsic phase pressure $\langle P_\alpha \rangle^\alpha$ is 'a good macroscopic representation for statistically uniform fluid distributions' (Nordbotten et al., 2008) (A6). Under above assumptions, macroscopic capillary pressure can be known from *local* values (pore level) of capillary pressure.

Capillary pressure is realized *locally* within *mathematically thin* interfacial line of non-wetting and wetting fluids, by *mean* curvature of the interface (K_m, [m]) and tension force parallel to interface per unit length (σ, [N m^{-1}]). This is known as *Laplace Theorem* (De Gennes et al., 2004). Thomas Young (1805) was the first one to give the idea of the theorem and Pierre Simon Laplace (1805) differently came to the theorem in formal form. The equation described in the theorem is thus also known as Young-Laplace (Y-L) equation.

$$P_c = \sigma \times K_m. \tag{1.14}$$

At the pore level, we are assuming that interface from the liquid phase to its vapor phase is *zero* width and this ideal interface is known as *Gibbs dividing plane* (Butt et al., 2003) (A7). Mean curvature of this interface is an arithmetic average of two curvatures measured at two principal directions orthogonal to each other at *desired* point. Curvature at the point can be defined as the inverse of radius of osculating circle at the point. Tension force per unit length of the interface parallel to it (required surface *free* energy[¶] to create unit new interfacial area of liquid) is termed as surface tension or interfacial tension of liquid ([N m^{-1}] or [J m^{-2}]).

Liquid interface meets at the solid surface of soil particle and creates a three-phase (liquid-air-solid) contact line. This contact line (in its vicinity) at its equilibrium state are resultant of balances of forces at every point on its periphery (Young, 1805; Dupré and Dupré, 1869). Interfacial tensions among solid-liquid (γ_{sl}), solid-air (γ_{sa}) and liquid-air (σ) are in balance at every point on the contact line. This force-balance along the tangential line at desired point of solid surface can be described as an equation, which otherwise is known as Young-Dupré equation (Bear, 1972).

$$\gamma_{sl} - \gamma_{sa} = \sigma \cos\theta. \tag{1.15}$$

The tangent line of liquid-air meniscus and solid surface makes the angle of contact or *contact angle* θ [°] in the side of liquid (more generally, in the side of wetting fluid). Perpendicular to the tangential line of solid, interfacial forces are counterbalanced by *perfectly rigid*[‖] solid. Henceforth, whenever we mention solid (e.g. soil particle), we assume a perfectly rigid solid (A8).

1.2 A historical perspective

Different anthropogenic and climatic factors are influencing soil temperature drastically especially in the last few decades (As described in Section-1.1). Heat is transferred generally through *conduction*, *convection* and *radiation* in a system (Çengel, 2003). Conductive heat transfer is due to the existence of temperature gradients and convective heat transfer is due to fluid flow (Lu and Dong, 2015). Depending on the hydro-geologic setting, either or both of them could be important for heat transfer in soil (e.g., De Vries, 1987; Noborio et al., 1996; Lipiec et al., 2007). Heat transfer in soil by radiation is neglected (De Vries, 1987) (A9).

[¶]Free energy or Helmholtz free energy is *available* energy to work and is defined as difference from *internal* energy to product of temperature and *entropy* of a system (Blundell and Blundell, 2006).

[‖]This means, elastic modulus of the solid substrate is *theoretically* infinity (see Marchand et al., 2012 for deeper understanding).

1.2.1 Literature review on moisture transfer under temperature gradient in soil

George Bouyoucos (1915) first showed through experiments that soil moisture or soil water moves towards the temperature gradient, meaning from warm to cold area in soil (as in Smith, 1943). Smith (1943) found that soil water moves from higher to lower temperature in his experiments. However, he argued against Bouyoucos's reasoning that moisture movement happened within air space. He attributed the moisture movement as liquid flow than that of vapor diffusion and vapor condensation may be a reason for moisture movement in capillary pores. This line of argument is then followed by Winterkorn (1948) and he theorized that liquid flow of the film from warm to cold region is due to change in liquid affinity with change in temperature. He put an emphasis on this change in liquid affinity mechanism over vapor diffusion. Gurr et al. (1952) showed in closed system through experiments that apparent vapor diffusion coefficient is much more than predicted by the vapor diffusion equation adaptations of Fick's law (the 'simple' theory as described by Philip and De Vries, 1957 later). Krischer and Rohnalter (1940), Taylor and Cavazza (1954), and Rollins (1954) have confirmed same conclusions independently but with different techniques. Philip and De Vries (1957) (hereafter PD57) proposed the theory of non-isothermal moisture movement in porous materials for the first time. They distinctively analyzed vapor flux and liquid flux and their interactions at 'liquid islands'. Their equations can be written in terms of above mentioned variables:

Liquid flux:

$$v_{li} = -D_{Tlij}\frac{\partial T}{\partial x_j} - D_{\eta lij}\frac{\partial \eta}{\partial x_j} - \frac{K_{lij}}{\phi \eta_l} e_j;\ e_j = j\text{-th component of } \frac{\vec{x}}{|\vec{x}|}. \tag{1.16}$$

Vapor flux:

$$v_{vi} = -D_{Tvij}\frac{\partial T}{\partial x_j} - D_{\eta vij}\frac{\partial \eta}{\partial x_j}. \tag{1.17}$$

Total moisture flux:

$$v_{Ti} = -D_{Tij}\frac{\partial T}{\partial x_j} - D_{\eta ij}\frac{\partial \eta}{\partial x_j} - \frac{K_{lij}}{\phi \eta_l} e_j. \tag{1.18}$$

Here $D_{Tlij} = -\frac{K_{lij}}{\phi \eta_l}\frac{\partial \psi}{\partial T}\Big|_\eta$, $D_{\eta lij} = -\frac{K_{lij}}{\phi \eta_l}\frac{\partial \psi}{\partial \eta}\Big|_T$, $D_{Tvij} = \varsigma \varpi \eta_a D_{\text{atm}} \upsilon \frac{d\rho_0}{dT}\delta_{ij}$, $D_{\eta vij} = \frac{\varpi \eta_a D_{\text{atm}} \upsilon g \rho_v}{R_g T \rho_l}\frac{\partial \psi}{\partial \eta}\Big|_T \delta_{ij}$ and $D_{Tij} = D_{Tlij} + D_{Tvij}$, $D_{\eta ij} = D_{\eta lij} + D_{\eta vij}$. The variables T is the temperature [K], D_T and D_η are the non-isothermal [$m^2\ s^{-1}\ K^{-1}$] and isothermal [$m^2\ s^{-1}$] diffusivities respectively, and $\eta = \eta_w$. The subscripts 'l' and 'v' represent bulk liquid and liquid vapor respectively. Here R_g is universal gas constant [$J\ K^{-1}\ mol^{-1}$], ρ_0 is

the saturated water vapor density at a given temperature [kg m^{-3}], ϖ is a tortuosity factor, D_{atm} is the diffusivity of liquid vapor in still air [m^2 s^{-1}], υ is a mass-flow factor and ς is a factor that accounts for additional pore space available for the liquid vapor to move through, due to the ability of liquid vapor to condense on one side of a saturated pore and evaporate on the other (Parlange et al., 1998), and δ_{ij} is the Kronecker delta, and repeated subscripts or dummy indices imply summation (Nobre and Thomson, 1993). The PD57 theory describes qualitatively the majority of experimental data (Grifoll et al., 2005) and though different researchers (Milly, 1982; Cass et al., 1984; De Vries, 1987; Nassar and Horton, 1992; Nassar et al., 1992; Nassar and Horton, 1997; Nassar et al., 1997; Grifoll et al., 2005, and others) worked on the theory and later on some of them have modified and improved upon the PD57 theory to match the broader class of experimental values. Recent work of Vanderborght et al. (2017) based on the 'coupling concept' developed by Mosthaf et al. (2011), gave a novel set of equations on heat and water transport in soils.

All these fundamental flow equations of soil-water hinge upon an important relationship of capillary pressure with respect to moisture content and temperature or, $\psi = \psi(\eta, T)$. Gradient of capillary head drives soil-water in unsaturated zone and the gradients of isothermal and non-isothermal capillary heads contribute to the whole gradient of the head as shown below:

$$\nabla\psi = \underbrace{\left.\frac{\partial\psi}{\partial\eta}\right|_T \nabla\eta}_{\text{isothermal}} + \underbrace{\left.\frac{\partial\psi}{\partial T}\right|_\eta \nabla T}_{\text{non-isothermal}} . \tag{1.19}$$

We discuss briefly about literatures regarding the isothermal relation of $\psi(\eta, T = \text{constant})$, and then we shall go on to give a brief account of literature on $\psi(\eta = \text{constant}, T)$, before putting out the objectives of the thesis.

1.2.2 Literature review on the relationship of ψ-*vs.*-η

There have been many efforts to find out the relationship between capillary potential (ψ) and moisture content (η) (capillary pressure saturation relation or abbreviated as 'CPSR') as well as relationship with capillary conductivity. Soil zone has been divided into two zones to simplify the complexity of soil pores; one is composed of networks of 'pores' and 'channels' and other one is composed of networks of fractures (Bear et al., 2011). We here generally will concentrate over works done considering soil as networks of pores and channels (A10).

Gardner (1956), Brooks and Corey (1964), van Genuchten (1978), Durner (1994), Kosugi (1994), Fredlund and Xing (1994), Seki (2007) and others suggested formulas obtained by curve fitting techniques to experimental soil data with parameters adjusted as per the type of porous media. Over the years, many researchers tried to include complicated network of

pore using statistical parameters in their formulas, however they always missed the point of intricate forces within pores especially in dry ranges. Nitao and Bear (1996) identified that the lack of considerations of adsorptive surface forces and liquid films in unsaturated flow phenomena, may contribute to the varying fitting responses of above empirical relations one over other in different soils. They pointed out that this variation is because of the vague definition of matric potential where capillary and adsorptive forces are taken together rather than explicitly. Following this explanation from Nitao and Bear (1996), Tuller et al. (1999) took into account both the capillary and adsorptive forces individually. In classical theoretical approaches (Collins, 1961), the previous researchers considered the porous media as bundles of cylindrical capillaries and also the portion of interconnected cylindrical pores is considered fully filled, whereas larger pores are considered as completely empty. Tuller et al. (1999) considered aforementioned hindrances and replaced the cylindrical pore networks with more realistic angular pore geometry and slit shaped spaces. In the next paper, Or and Tuller (1999) proposed the closed form expressions of interfacial areas as function of chemical potential considering the unitary approach of capillary and adsorptive forces. Peters and Durner (2008) claimed that Or and Tuller's (1999) approach is mathematically complex and is more specific rather than generalized. Lebeau and Konrad (2010) partitioned the water retention into capillary and adsorptive components and described that capillary component is dominant in the wet to moderately wet ranges whereas a thin film flow prevails in dry ranges. For the capillary component, they used a conventional statistical predictive model whereas a theoretical model of soil-water flow in thin films was derived to describe the adsorptive part. This model is simple and more flexible compared to Or and Tuller's (1999) which often fails to follow the trend of experimental data in the intermediate saturation ranges. Wang et al. (2018) mentioned that Lebeau and Konrad's (2010) model agrees poorly with the observations, and gives uncertain results of the film conductivity. Iden and Durner (2014) modified the Peters' (2013) model and included the capillary flow using the models developed by van Genuchten (1978) and Mualem (1976) and film flow based on the Tokunaga's (2009) model. It is difficult to accurately distinguish the contribution of capillary and adsorption forces, and as well soil hydraulic behavior due to the complexity of pores and the heterogeneity of soil as mentioned by Wang et al. (2018). Thus, they proposed a single equation to capture the conductivity behaviors resulting from both capillarity and adsorption forces based on the EMFX-K model proposed by Wang et al. (2016, 2017).

1.2.3 Literature review on the relationship of ψ-*vs.*-T

Richards and Neal (1937), Richards et al. (1938), Moore (1941) and Richards and Weaver (1944) reported the effect of temperature on the moisture percentage indirectly, but no data were given on the effect of temperature on moisture tension at constant moisture percentage

(Gardner, 1955). Gardner (1955), for the first time, presented a consistent tendency for soil moisture tension decrease with increase in temperature for three types of soils and said firmly that variations of tension due to temperature cannot be ignored in the studies of soil moisture movement. Wilkinson and Klute (1962) did experiment on three soils regarding drainage curve of P_c- or ψ-*vs.*-η at two different temperatures and showed that experimental value of the temperature derivative of pressure or tension at constant moisture contents $\left(\partial\psi/\partial T\big|_{\eta}\right)$ is much more than calculated temperature derivatives surface tension of water i.e. $\left(\psi/\sigma\right)d\sigma/dT$ (just as implicitly assumed in PD57 or PD57's approach). They speculated that the possible explanation for the higher experimental values is that surface-active contaminants at the air-water interface. Other researchers have reported that the effect of temperature on ψ-*vs.*-η was larger than the expected value from surface tension changes alone (Moore, 1941; Taylor et al., 1961; Haridasan and Jensen, 1972; Jury and Miller, 1974; Nimmo and Miller, 1986; Constantz, 1991). Peck (1960) theorized that the temperature derivative of the moisture tension may be composed of temperature derivatives of the entrapped air volume, water moisture and surface tension of water. Hopmans and Dane (1986) showed after experimentation on a glass beads medium and a Norfolk sandy loam at two temperatures that neither temperature derivative of entrapped air volume nor of surface tension of soil solution could account for observed discrepancy. Grant and Salehzadeh (1996) were first to take into account temperature effects on contact angle along with surface tension and using the chemical thermodynamics of interfaces arguments, modified van Genuchten's (1978) model to be a one-parameter temperature sensitive empirical CPSR. She and Sleep (1998) confirmed the effectiveness of Grant and Salehzadeh's (1996) one-parameter model from their recently experimental studies of the effect of temperature on CPSRs for water-air and water-tetrachloroethylene systems. Their data contradicted with the Grant and Salehzadeh's (1996) results on temperature derivative of contact angle. Grant and Bachmann (2002) reviewed the previous literatures extensively and they cited PD57 for their implicit assumption of relative changes of capillary pressure being equal to only surface tension changes relative to temperature and shortcomings of the assumption. Above literatures showed the disparity between PD57's approach and the experimental verifications. This disparity baffled many young researchers and inspired them to pursue this subject for their doctoral dissertations (Wilkinson, 1960; Meeuwig, 1964; Haridasan, 1970; Jury, 1973; Okandan, 1974; Miller, 1983; Salehzadeh, 1990; She, 1997, etc.) (Grant and Bachmann, 2002). Grant and Bachmann (2002) proposed four possible mechanisms that explain the above discrepancy and these are – expansion of water; expansion of entrapped air; solute effects on the surface tension of water; and thermal-sensitivity of contact angles. Going through each point they concluded that the most likely mechanisms are solute effects on the soil solution surface tension or temperature-induced changes in contact angles. Bachmann and van der Ploeg (2002) pointed out that

previous researchers did not differentiate capillary-bound and adsorbed-bound water at low saturation. Thus, the Grant and Salehzadeh's (1996) model fails to fit at low water saturation. Bachmann and van der Ploeg (2002) utilized the extended version of thermal derivation of Y-L equation as found in Grant and Salehzadeh (1996), in which there are two terms – (i) the term involving the conventional PD57's approach, and (ii) the extension due to contact angle, where the derivative of contact angle is prominent. Bachmann et al. (2002) performed experiments to determine the dependence of water retention curves on temperature for wettable and water-repellent soils and confirmed the applicability of Grant and Salehzadeh's (1996) one-parameter model over PD57's approach. Grant (2003) derived a series expression of interfacial energy in terms of temperature to incorporate the effect of temperature on van Genuchten's (1978) CPSR. He improved and generalized Grant and Salehzadeh's (1996) one-parameter model with introducing another parameter and thus included broader spectrum of temperatures for homogeneous and heterogeneous porous media as well. Gao and Shao (2015) suggested formulas of temperature dependence of surface tension, viscosity and soil porosity to quantify CPSR and hydraulic properties. The deviation in predicted and experimental results of relative changes in capillary pressure with respect to temperature still exists and as per Gao and Shao (2015), these deviations may be due to the effects of temperature on entrapped air and also the presence of contaminants (or solutes) that affects the surface tension at the air-water interface.

1.3 Objectives of the thesis

One fact always remains intact across all porous media and that capillary pressure of water in soil at a constant degree of saturation is a linearly decreasing function of temperature. Grant (2003) claims this behavior to be universal one. The current state-of-the-art literature (especially, Grant, 2003 and Gao and Shao, 2015) for the effects of temperature on capillary pressure put some questions forward:

- Can Y-L equation alone explain the existed disparity among model and experimental values?
- Is the temperature sensitivity of capillary pressure affected by the degree of liquid saturation?
- Is any model consistent with the measured apparent effect of temperature on contact angles?
- Is the effects of temperature enough on entrapped air to influence capillary pressure?

Our central objective is to understand capillary pressure behavior in soil (more generally, in porous media), and try to develop a physical and conceptual model to answer the questions. We organize our thesis as the evolution of our research, i.e. starting from the effects of

entrapped air veer us unexpectedly to the form of meniscus shape and then the eventual development of a conceptual framework to study capillary pressure and temperature effects on it in the scale of pore space to an averaging volume of unsaturated soil.

1.4 Organization of the thesis

Capillary pressure in soil can be understood through equivalent system of capillary tubes of different radii as same as pore radii at constant temperature with proper assumptions (see Fig. 2 of Richards, 1928). "If moisture of the soil is in equilibrium, the curvature of all water surfaces at uniform level is the same" (Briggs and McCall, 1904). That is to say that in equilibrium, curvature of the meniscus in soil and in capillary tube, where both share same water source and ambient condition, will have same values at uniform level. It allows to probe and prod into soil indirectly through capillary tube.

In chapter 2, we venture into our objective in effect of Gao and Shao's (2015) claim to understand the effect of entrapped-air on capillary pressure due to temperature with one-end close and both-end open capillary tube, and then we find out that assumption of meniscus shape being spherical may be a limiting factor while calculating capillary pressure. This work has been published in Biswas and Kartha (2019).

Consequently, in chapter 3 we assume the meniscus shape to be a catenary curve and do the analysis of temperature effects on contact angle. We do compare calculated results with experimental and analytical results. The proposed meniscus shows effectiveness of proposed meniscus shape and encourages us to investigate further in the next chapter. Part of this work has been presented as a poster in a conference (Biswas and Kartha, 2017).

In chapter 4 we generalize the assumption of this shape. Lastly, we give an algorithm of averaging to combine the effects of single capillary tubes to get a singular picture of the particular effect in a representative porous media or soil. We compare the calculated and experimental results for soil. This work is under preparation for publication.

Lastly in chapter 5 we conclude with remarks on the above questions and about our understanding of the phenomena. Then we discuss future directions of the research.

CHAPTER 2

Temperature Effects on Capillary Pressure in Dead-end Pores with Spherical Meniscus

2.1 Introduction

In this chapter, we are trying to understand the role of entrapped air in dead-end pores on the capillary pressure-*vs.*-temperature relation. In wet situation, residual air remains trapped in the crevices of pores or in dead-end pores due to presence of water. During air-sparging, which is a groundwater remediation technique to displace water with injection of air (Clayton, 1999; Jang and Aral, 2009) and as well volumetric air content (η_a) never gets to zero in soil as continuum percolation theory suggests (Hunt, 2005) and there are chances that air remains in dead-end pores. Dead-end pores are also known as stagnant pockets (Bear, 1972). Their geometry i.e. closed-end (one end is closed and other is connected to the *active* pores) makes the fluids in these zones stagnant as the name suggests. Thus any change in these zones affects capillary pressure or CPSR for a given degree of saturation and affects the flow characteristics in soil. Trapping of non-wetting fluid is one of the reasons for the hysteresis effect of CPSR and vice versa (Lenhard and Parker, 1987). Dead-end pores are generally studied in reference to diffusion within mobile and immobile or dead-end pores (Goodknight et al., 1960; Coats and Smith, 1964; Jackson and Klute, 1967; Philip, 1968; De Smedt and Wierenga, 1979) and in reference to oil-recovery through different techniques (Zhang and Yue, 2008; Jamaloei and Kharrat, 2009; Sedaghat et al., 2013; Kar et al., 2015; Mosavat and Torabi, 2016; Santiago et al., 2016). Here we consider the dead-end pore as a capillary tube with one end closed and other end in touch to an infinite source of wetting fluid. This assumption is justified as one end of dead-end pores is usually connected to a main flow channel or *active* pores. The Y-L equation is invoked and differentiated with respect to temperature with some assumptions for our problem domain. A differential equation of a *temperature function* is obtained and consequently capillary pressure is deduced from this function. Through example problems, we present the effects of properties of air, liquid and solid as well as physical dimension of dead-end pore on capillary pressure-*vs.*-temperature relation.

2.2 Mathematical modeling

Capillary pressure (P_c) [N m^{-2} or Pa] can be introduced as an explicit function of two distinct variables – temperature-dependent variables (say $G(T)$) and temperature-independent variables (say M) i.e. $P_c(T) = P_c(G(T), M)$. The capillary pressure *vs.* temperature is assumed to be a non-hysteretic one for a particular liquid saturation, as suggested and verified by researchers (Faybishenko, 1983; Grant and Bachmann, 2002; Grant, 2003). Therefore, a single relationship will be sufficient for both heating and cooling curve i.e. both curves are actually the same - no hysteresis - no two values of P_c at single T.

Then the total derivative of $P_c(G,M)$ with respect to temperature T will be:

$$\frac{\mathrm{d}P_c}{\mathrm{d}T} = \frac{\partial P_c}{\partial G}\frac{\mathrm{d}G}{\mathrm{d}T} + \frac{\partial P_c}{\partial M}\frac{\mathrm{d}M}{\mathrm{d}T} = \frac{\partial P_c}{\partial G}\frac{\mathrm{d}G}{\mathrm{d}T} + 0 = \frac{\partial P_c}{\partial G}\frac{\mathrm{d}G}{\mathrm{d}T}. \tag{2.1}$$

Similarly, from here onwards, it is assumed that every other physical property to be also either function of temperature only or not.

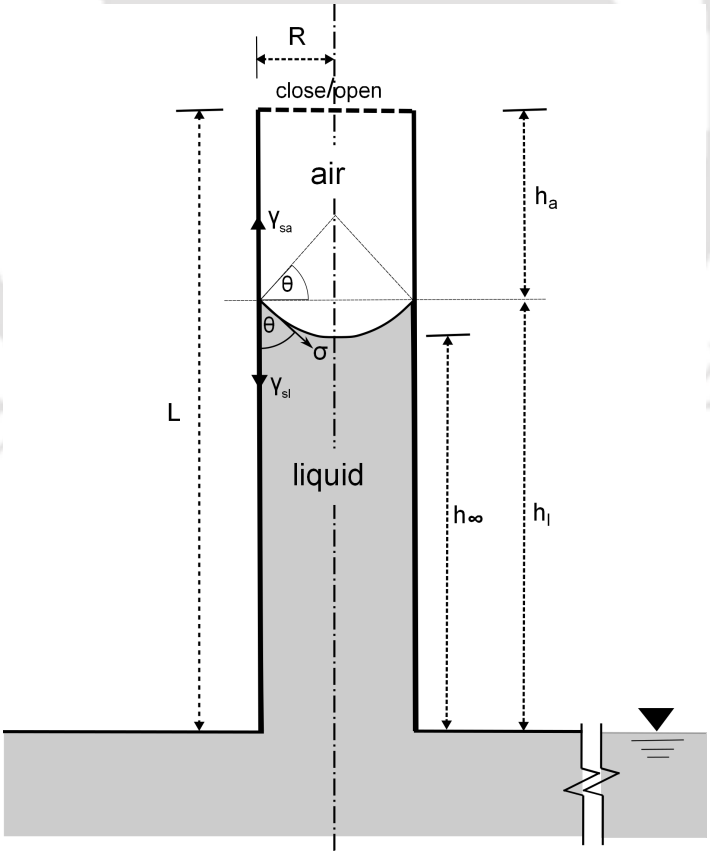

Figure 2.1: A schematic of liquid rise in a capillary tube

Under static equilibrium scenario in a cylindrical capillary tube with a spherical meniscus (Fig. 2.1), the Young-Laplace equation is (Lu and Likos, 2004),

$$P_c = \frac{2\sigma}{R_m}, \tag{2.2}$$

where σ is the surface tension of the liquid [N m^{-1}] and R_m the mean radius of the curvature of the meniscus [m]. For a spherical meniscus in a vertical tube with circular cross section of radius R [m] (Fig. 2.1), the mean radius of curvature of spherical meniscus is related with the radius of the tube by $R = R_m \cos\theta$. Applying Eq. (2.2) to the problem domain (Fig. 2.1), the capillary pressure is:

$$P_c = \frac{2\sigma}{R}\cos\theta, \tag{2.3}$$

where θ is the contact angle* between the air-liquid interface and the solid surface [°].

The Young's equation at static equilibrium is (Hassanizadeh and Gray, 1993):

$$\gamma_{sa} - \gamma_{sl} = \sigma\cos\theta, \tag{2.4}$$

where γ_{sl} is the interfacial tension between solid (subscripted as 's') and liquid (subscripted as 'l') [N m^{-1}], and γ_{sa} is the interfacial tension between solid and air (subscripted as 'a') [N m^{-1}].

Therefore, substituting Eq. (2.4) in Eq. (2.3), the capillary pressure is:

$$P_c = \frac{2\left(\gamma_{sa} - \gamma_{sl}\right)}{R} = G(T).M, \tag{2.5}$$

where $G(T) = (\gamma_{sa} - \gamma_{sl})$ is a function of temperature, and $M = 2/R$ is independent of temperature.

Assuming the whole system is in static equilibrium in capillary tube, the capillary pressure is: $P_c = P_a - P_l$, where P_a is the pressure of air in the closed section of the tube [Pa] (temperature dependent), and P_l is the pressure in liquid immediately under the meniscus [Pa] (Lu and Likos, 2004; De Gennes et al., 2004). Air in the closed section is assumed as an *ideal* gas (where there are no intermolecular forces and interactions among gas molecules) and thus follows the ideal gas law (Çengel and Boles, 2015):

$$P_l = \frac{n_g R_g T}{V_a} - P_c, \tag{2.6}$$

*This angle is otherwise known as microscopic contact angle (see Section-3.1).

where n_g is no. of moles of gas [mol] and V_a is volume of air [m^3]. The liquid pressure in the capillary tube is assumed to conform to the laws of hydrostatics (De Gennes et al., 2004). Since the pressure in the liquid is connected to an active or main channel, the pressure in the liquid in capillary gets reduced towards meniscus level above the channel and thus the liquid pressure at the bottom of the meniscus is:

$$P_l = P_{\text{ref}} - \rho_l g h_\infty, \tag{2.7}$$

where P_{ref} is the pressure at the bottom of the tube (taken as atmospheric pressure like water table, P_{atm} for simplicity and assumed to be temperature-independent) [Pa], ρ density of liquid [kg m^{-3}], g the acceleration due to gravity [m s^{-2}], and h_∞ equilibrium height of liquid rise in the tube [m] (or Jurin height[†] and Fig. 2.1).

Comparing Eq. (2.6) and Eq. (2.7):

$$P_{\text{atm}} + P'_l = \frac{n_g R_g T}{V_a} - P_c, \tag{2.8}$$

where the term $\rho_l g(-h_\infty)$ is assigned as P'_l.

As the air cannot escape in the case of closed-end tube, the mass of air will be a constant and, therefore, the number of moles of air (n_g) is treated as temperature-independent. Differentiating Eq. (2.8) with respect to temperature T and using the relationship of Eq. (2.5),

$$\frac{dP'_l}{dT} = \frac{n_g R_g}{V_a} - \frac{n_g R_g T}{{V_a}^2}\frac{dV_a}{dT} - \frac{2}{R}\left(\frac{d\gamma_{sa}}{dT} - \frac{d\gamma_{sl}}{dT}\right). \tag{2.9}$$

Volume of the air section above the air-liquid interface in the capillary tube (see Fig. 2.1) is:

$$V_a = \pi R^2 h_a + \frac{\pi R^3}{\cos^3\theta}\left(\frac{1}{3}\sin^3\theta - \sin\theta + \frac{2}{3}\right), \tag{2.10}$$

where h_a is the height of the air section in the capillary tube (see Fig. 2.1).

Differentiating Eq. (2.10) with respect to T:

$$\frac{dV_a}{dT} = \pi R^2 \frac{dh_a}{dT} - \frac{\pi R^3}{\left(\sin\left(\frac{\theta}{2}\right) + \cos\left(\frac{\theta}{2}\right)\right)^4}\frac{d\theta}{dT}. \tag{2.11}$$

According to the studies done by other researchers (Elliott and Riddiford, 1967; Slattery and

[†]This height is first confirmed by extensive experiments done by Francis Hauksbee in 1713 and then by a English physiologist James Jurin in 1718 (De Gennes et al., 2004).

Flumerfelt, 1982; Poynting and Thomson, 1902; Hassanizadeh and Gray, 1993), the liquid-air interface or meniscus can adjust itself for small pressure changes to nullify the imbalance without any vertical movement. Hence the meniscus gets stuck or pinned at the *hardly* smooth natural surface of the solid. This pinning phenomenon or formally *contact line pinning* (CLP) causes the contact angle hysteresis (a difference between maximum and minimum θ) (Kuchin and Starov, 2016). Contact angle hysteresis, therefore, suggests that there is no unique value for contact angle even at static equilibrium (Makkonen, 2017). The authors in this research opine that this phenomenon may or rather probable to happen for temperature variation within a certain range of temperatures (say ΔT). Within this range, meniscus behaves as elastic and liquid sticks to the solid surface before meniscus starts moving (after surpassing some *energy barrier* (see Johnson Jr and Dettre, 1964; Marmur, 1994, for more details)). As an example, it takes $T \sim 10^3$ K for water-air meniscus even to overcome one nanometer of defect on quartz glass substrate if pinned (Pompe and Herminghaus, 2000; Quéré, 2008; Whyman et al., 2008). Thus CLP infers that h_a is independent of temperature within this small interval of temperature, in which the translation motion of the meniscus along the solid surface is absent i.e. $\mathrm{d}h_a/\mathrm{d}T = 0$.

Applying $\mathrm{d}h_a/\mathrm{d}T = 0$ in Eq. (2.11) and substituting this equation in Eq. (2.9), we get:

$$-\frac{n_g R_g T}{\left(\sin\left(\frac{\theta}{2}\right)+\cos\left(\frac{\theta}{2}\right)\right)^4}\frac{\mathrm{d}\theta}{\mathrm{d}T} = \frac{n_g R_g V_a}{\pi R^3} - \frac{{V_a}^2}{\pi R^3}\frac{\mathrm{d}P'_l}{\mathrm{d}T} - \frac{{V_a}^2}{\pi R^3}\frac{2}{R}\left(\frac{\mathrm{d}\gamma_{sa}}{\mathrm{d}T} - \frac{\mathrm{d}\gamma_{sl}}{\mathrm{d}T}\right). \tag{2.12}$$

Rearrangement of Eq. (2.10) gives a contact angle sensitive *temperature function* $f_\theta(T)$ as shown,

$$\frac{V_a}{\pi R^3} - \frac{h_a}{R} = \frac{1}{\cos^3\theta}\left(\frac{1}{3}\sin^3\theta - \sin\theta + \frac{2}{3}\right) = f_\theta\left(\theta\left(T\right)\right) = f_\theta\left(T\right). \tag{2.13}$$

Substituting Eq. (2.13) in Eq. (2.12):

$$\begin{aligned} n_g R_g T\frac{\mathrm{d}f_\theta\left(T\right)}{\mathrm{d}T} = n_g R_g\left(f_\theta\left(T\right)+\frac{h_a}{R}\right) - \pi R^3\left(f_\theta\left(T\right)+\frac{h_a}{R}\right)^2\frac{\mathrm{d}P'_l}{\mathrm{d}T} \\ -2\pi R^2\left(f_\theta\left(T\right)+\frac{h_a}{R}\right)^2\left(\frac{\mathrm{d}\gamma_{sa}}{\mathrm{d}T} - \frac{\mathrm{d}\gamma_{sl}}{\mathrm{d}T}\right). \end{aligned} \tag{2.14}$$

Grant (2003) argued that interfacial tension is a linear function of temperature, and their difference of temperature derivatives $(d\gamma_{\mathrm{sa}}/dT - d\gamma_{\mathrm{sl}}/dT)$ in Eq. (2.14) becomes a constant (lets say this constant be C_γ).

Meniscus height (h_m) is defined as (see Fig. 2.1):

$$h_m = h_l - h_\infty = R\left(\sec\theta - \tan\theta\right), \tag{2.15}$$

where h_l is the height of the liquid section $= L - h_a$ and L is the total height of the capillary tube (henceforth, subscript T means *total*) (see Fig. 2.1).

Therefore, Eq. (2.13) can be rewritten as:

$$\frac{1}{3}(\sec\theta - \tan\theta)^2\left(\tan\theta + 2\sec\theta\right) = f_\theta\left(T\right). \tag{2.16}$$

Using Eq. (2.15) and performing some simplifications in Eq. (2.16), a cubic equation of h_m is obtained as:

$$h_m^3 + \left(3R^2\right)h_m + \left(-6R^3 f_\theta\right) = 0. \tag{2.17}$$

On solving Eq. (2.17), since it is a cubic equation of h_m, there are three roots or values possible for h_m. There is one *real* value and two other *conjugate complex* values for h_m from Eq. (2.17) and the real value is taken as the solution of Eq. (2.17) (because h_m is length and cannot have complex values). The real solution of Eq. (2.17) is:

$$h_m\left(f_\theta\right) = -\frac{R^2}{\left(3f_\theta R^3 + \sqrt{R^6 + 9f_\theta^2 R^6}\right)^{1/3}} + \left(3f_\theta R^3 + \sqrt{R^6 + 9f_\theta^2 R^6}\right)^{1/3}. \tag{2.18}$$

From Eq. (2.8) and Eq. (2.15), $P_l' = -\rho_l g h = -\rho_l g(h_l - h_m(f_\theta))$. The derivative of P_l' with respect to T is:

$$\frac{\mathrm{d}P'_l}{\mathrm{d}T} = \frac{\mathrm{d}P'_l}{\mathrm{d}f_\theta}\frac{\mathrm{d}f_\theta}{\mathrm{d}T} = \rho_l g\frac{\mathrm{d}h_m}{\mathrm{d}f_\theta}\frac{\mathrm{d}f_\theta}{\mathrm{d}T} \quad (\because h_l \text{ is constant}). \tag{2.19}$$

Substituting Eq. (2.19) in Eq. (2.14) and performing some arithmetic operations and simplifications, an ordinary differential equation of f_θ with respect to T is obtained:

$$T\frac{\mathrm{d}f_\theta}{\mathrm{d}T} + \left[\rho_l\left(A_1 f_\theta^2 + A_2 f_\theta + A_3\right)\frac{\mathrm{d}h_m}{\mathrm{d}f_\theta}\right]\frac{\mathrm{d}f_\theta}{\mathrm{d}T} + \left(B_1 f_\theta^2 + B_2 f_\theta + B_3\right) = 0, \tag{2.20}$$

where $A_1 = g\pi R^3/n_g R_g$, $A_2 = 2g\pi R^2 h_a/n_g R_g$, $A_3 = g\pi R h_a^2/n_g R_g$, $B_1 = 2\pi R^2 C_\gamma/n_g R_g$, $B_2 = 4\pi R h_a C_\gamma/n_g R_g - 1$ and $B_3 = 2\pi h_a^2 C_\gamma/n_g R_g - h_a/R$ are intermediary temperature independent terms assigned and $\mathrm{d}h_m/\mathrm{d}f_\theta = R^3[R^2 + \sqrt[2/3]{3f_\theta R^3 + D}]/[D\sqrt[1/3]{3f_\theta R^3 + D}]$ and

$D = \sqrt{R^6 + 9f_\theta^2 R^6}$.

The simplified form of Eq. (2.20) is as follows

$$T\frac{\mathrm{d}f_\theta}{\mathrm{d}T} + \rho_l(T)\,Q(f_\theta)\frac{\mathrm{d}f_\theta}{\mathrm{d}T} + S(f_\theta) = 0, \tag{2.21}$$

where $Q(f_\theta) = [(A_1 f_\theta^2 + A_2 f_\theta + A_3)\mathrm{d}h_m/\mathrm{d}f_\theta]$ and $S(f_\theta) = (B_1 f_\theta^2 + B_2 f_\theta + B_3)$. Equation (2.21) is a non-linear first-order ordinary differential equation.

Equation (2.21) can be solved using analytical or numerical method. In this chapter, Eq. (2.21) is solved using the fourth-order Runge-Kutta (RK4) numerical method (see Hoffman, 2001 for more details on RK4). On obtaining $f_\theta(T)$ by solving Eq. (2.21), subsequently the capillary pressure is computed as a function of temperature.

At a particular temperature (say T_p), water rises due to capillary effect through the open-end section of the closed-end capillary tube. The calculation of number of moles of gas before and after the capillary rise is as follows. Before the liquid starts to enter into the tube, only air molecules fill up the tube. Initially let the number of moles of air is n_{gi}. After a certain time, liquid meniscus will reach some height and stop and the whole system reaches static equilibrium. Again, let the no. of moles of air in the portion between the water meniscus and top closed-end of the capillary tube to be n_f. It is assumed that there is no loss of air molecules or no air is dissolved in the liquid from the moment of touch of the capillary tube on the surface of water in the infinite reservoir to the time to reach Jurin height. Then the number of moles of air is $n_{gi} = n_{gf} = n_g$. Accordingly, the number of moles of air is:

$$n_g = \frac{(P_a)_i (V_a)_i}{R_g T_p}, \tag{2.22}$$

where $(P_a)_i = P_{\mathrm{ref}} = P_{\mathrm{atm}}$ and $(V_a)_i = V_T = \pi R^2 L$ is the total volume of the capillary tube. Therefore,

$$n = \frac{P_{\mathrm{atm}} V_T}{R_g T_p}. \tag{2.23}$$

Equation (2.8) can be re-written as

$$\begin{aligned} P_c &= \frac{n_g R_g T}{V_a} - P_{\mathrm{atm}} + \rho_l g h, \\ P_c(T) &= \frac{n_g R_g T}{V_a(f_\theta(T))} - P_{\mathrm{atm}} + g\rho_l(T)\left(h_l - h_m(f_\theta(T))\right). \end{aligned} \tag{2.24}$$

The capillary pressure is evaluated from Eq. (2.24) using Eq. (2.13), Eq. (2.18), Eq. (2.23)

and from known fitting relationship of liquid density *vs* temperature ($\rho_l(T)$).

2.3 Results and discussion

The concepts developed in Section-2.2 to determine the capillary pressure for solid - liquid - gas system in a closed-end capillary tube that mimics the dead-end pores in soils, are used to solve some example problems.

2.3.1 Example 1 (Solid: Glass and Liquid: Water)

A glass - water - air (G-W-A) combination is considered as the solid - liquid - gas system in this example for the capillary action. The one end of the cylindrical glass tube is open and the other end is closed. Let the temperature of air in the empty closed-end cylindrical capillary glass tube exists initially at 298.15 K (Fig. 2.1). The Standard Temperature and Pressure (STP) used in this research have the temperature value at 298.15 K and pressure at 101325 Pa. The empty glass tube is placed inverted with the closed-end at the top and the open-end just touching the surface of water in the reservoir (Fig. 2.1). After a certain time, water rises to the Jurin height, $h_\infty = (2\sigma\cos\theta_e)/(R\rho_l g)$ under static equilibrium (De Gennes et al., 2004) (θ_e is the contact angle in static equilibrium or otherwise known as *equilibrium* contact angle). The assumption here is that the Jurin height or capillary rise will be same for the closed-end capillary tube. This assumption is valid by keeping the Bond number (*Bo*) (Hager, 2012) to be much less than 1, i.e. assuring the surface forces will be dominant. Therefore, the condition for the radius of the tube is: $R \ll \sqrt{(\sigma/\rho_l g)}$. The radius of the tube is assumed based on the soil pore size approximately i.e. 50 μm satisfying the above condition of *Bo*. The total height of the capillary tube, which is 0.50 m, is based on the assumption that the total height has to be more than the maximum possible Jurin height (i.e. the capillary height when $\theta_e = 0°$). Table 2.1 gives the necessary values of the parameters of the system. From experimental results of Liechti et al. (1997), and studies from Dean (1999) and Mohr et al. (2016), the parameters for this example analysis are adopted.

Table 2.1: Parameters used for calculation in G-W-A system.

Parameter	Description	Value	Reference
σ	Surface tension of water at 298.15 K	71.99×10^{-3} N m^{-1}	Dean (1999)
ρ_l	Density of water at STP	996.66 kg m^{-3}	Dean (1999)
g	Acceleration due to gravitation	9.81 m s^{-2}	Mohr et al. (2016)
θ_e	Equilibrium contact angle of water on glass	50°	Liechti et al. (1997)
r	Radius of the tube	50×10^{-6} m	Assumed
R_g	Universal gas constant	8.314 N m K^{-1} mol^{-1}	Mohr et al. (2016)
L	Total glass tube height	0.50 m	Assumed

First, the function $f_\theta(T)$ is calculated for the desired temperatures from given reference

temperature (i.e. 298.15 K). To solve Eq. (2.21), the values of the intermediary terms A_1, A_2, A_3, B_1, B_2 and B_3 are needed. For the computation of these five intermediary terms, three parameters i.e. h_a, n_g and C_γ are evaluated from the basic parameters given in Table 2.1. Here are the steps to calculate these three parameters: (a) h_a can be calculated as: $h_a = L - (h_m + h_\infty)$ (h_m can be obtained from Eq. (2.15)), (b) n_g can be obtained from Eq. (2.23) taking T_p as initial temperature 298.15 K, (c) the solid interfacial surface energies are evaluated from the following equations (found from Girifalco and Good, 1957 using Eq. (2.4)) using empirical laws of temperature variation of contact angle, surface tension of liquid and liquid density:

Interfacial energy between glass and air is,

$$\gamma_{ga}(T) = \sigma(T)\left(\frac{(1+\cos\theta(T))^2}{4\Phi(T)^2}\right). \tag{2.25}$$

Interfacial energy between glass and water is,

$$\gamma_{gw}(T) = \sigma(T)\left(\left(\frac{(1+\cos\theta(T))^2}{4\Phi(T)^2}\right) - \cos\theta(T)\right). \tag{2.26}$$

where $\Phi(T) = 4(\mathscr{V}_g\mathscr{V}_w(T))^{1/3}(\mathscr{V}_g^{1/3} + \mathscr{V}_w(T)^{1/3})^{-2}$ and $\mathscr{V}_g$, $\mathscr{V}_w$ are molar volumes of glass and water respectively. Molar volumes: $\mathscr{V}_g = \mathscr{M}_g/\rho_g$ = (60.45 g mol^{-1})/(2.52 g cm^{-3}) = 23.99$\times 10^{-6}$ m^3 mol^{-1} (Seward III and Vascott, 2005) and $\mathscr{V}_w = \mathscr{M}_w/\rho_l(T)$ = (18.00 g mol^{-1})/$\rho_l(T)$, where $\mathscr{M}_g$ and $\mathscr{M}_w$ represent the molar masses of glass and water respectively and ρ_g and $\rho_l(T)$ are densities of glass and water respectively. Thermal sensitivity of glass is neglected and throughout this thesis, the thermal sensitivities of solids in general are neglected because of low thermal coefficient values compared to the liquid counterpart (A11). Data of temperature variations of contact angle, surface tension and density of water are obtained from Neumann (1974), Vargaftik et al. (1983) and Dean (1999), respectively. Using Eq. (2.25) and Eq. (2.26), Fig. 2.2 are drawn for different temperatures depending on available data of the literatures. Linear fit to the data gives the slope values as needed to evaluate C_γ as -8.414×10^{-6} N m^{-1} K^{-1}.

Using the information of slopes from Fig. 2.2 as well as using other input parameters from Table 2.1, the intermediary terms in Eq. (2.21) are obtained. Using the above value and f_θ (T_s = 298.15 K) = $(V_a/\pi r^3 - h_a/r)$ = 0.190021 (from Eq. (2.13)) as initial value in the 4th order Runge-Kutta method, the function $f_\theta(T)$ is calculated for different temperatures. Those values of T and $f_\theta(T)$ along with the density values of water at those temperatures from Dean (1999) are substituted in Eq. (2.17) to calculate the capillary pressure, P_c (Fig. 2.3). Even

though the results are shown as continuous line, the values of P_c at different temperatures are distinct. The subsurface temperature range fluctuates typically, as an example, around 5–10 K throughout the year as measured by Popiel et al. (2001) at Poznan city in Poland. Therefore we have assumed $\Delta T = 10$ K (298.15 K to 308.15 K) to test our theory and comparison purposes only. Temperatures can further be increased or decreased as your chosen preference with known initial value. Here the assumption is that temperature range is always within *certain* ΔT to maintain CLP, as mentioned above during derivation.

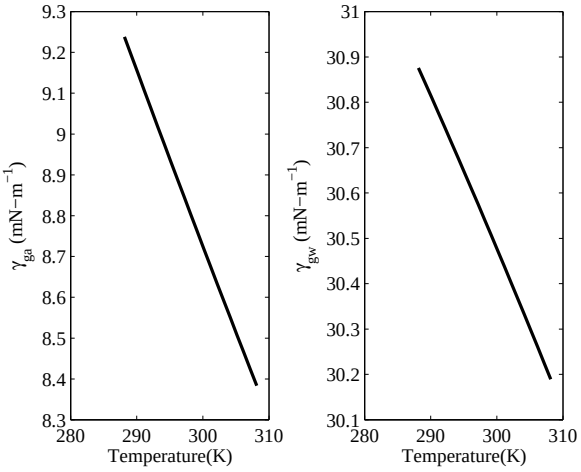

Figure 2.2: Interfacial tension of glass-air and of glass-water *vs.* temperature plots (γ_{ga} *vs.* T and γ_{gw} *vs.* T)

2.3.2 Example 2 (Solid: Polytetrafluoroethylene/PTFE and Liquid: *n*-Hexadecane)

In the second example, a polytetrafluoroethylene - *n*-Hexadecane - air (P-N-A) combination is considered as the gas-liquid-solid system. The physical parameters as well as the ambient conditions and the size of the capillary are kept same as in Example 1 (Fig. 2.1). The relevant basic parameters for this study are given in Table 2.2.

Table 2.2: Parameters used for calculation in P-N-A system.

Parameter	Description	Value	Reference
σ	Surface tension of *n*-Hexadecane at 298.15 K	27.09 $\times 10^{-3}$ N m^{-1}	Vargaftik et al. (1983)
ρ_l	Density of *n*-Hexadecane at STP	771.44 kg m^{-3}	Dean (1999)
g	Acceleration due to gravitation	9.81 m s^{-2}	Mohr et al. (2016)
θ_e	Equilibrium contact angle of *n*-Hexadecane on PTFE	46°	Neumann (1974)
r	Radius of the tube	50 $\times 10^{-6}$ m	Assumed
R_g	Universal gas constant	8.314 N m K^{-1} mol^{-1}	Mohr et al. (2016)
L	Total PTFE tube height	0.20 m	Assumed

Let the temperature of air throughout in the empty closed-end cylindrical PTFE tube exists initially at 298.15 K (Fig. 2.1). Values of surface tension and equilibrium contact angle of

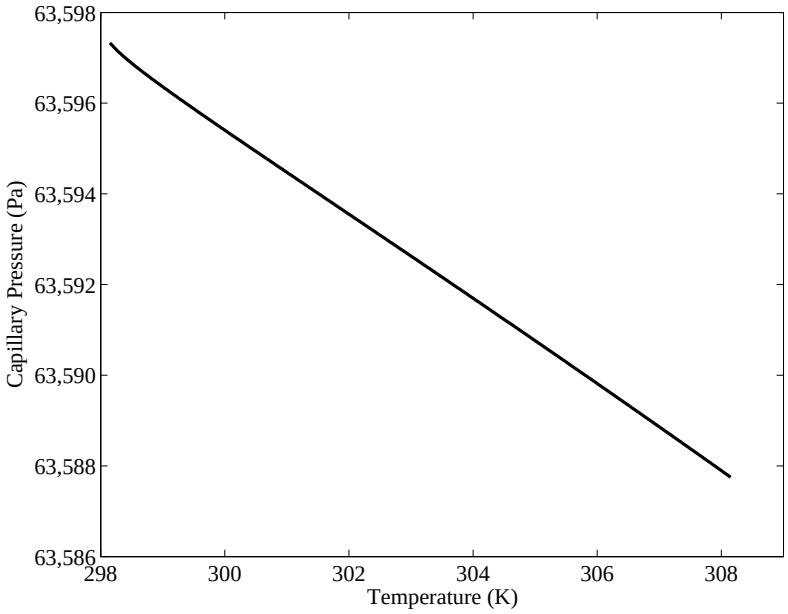

Figure 2.3: Capillary pressure *vs.* temperature plot for G-W-A system (closed-end)

n-Hexadecane on PTFE at STP are taken from Neumann et al. (1971). Density values of *n*-Hexadecane are taken from the internet website of Dortmund Data Bank[‡] (Onken et al., 1989). Values of h_a and n_g are obtained in same way as suggested in Example 1 using the values of basic parameters from Table 2.2. As far as calculation of interfacial tensions $\gamma_{\text{PTFE}-\text{air}}$ and $\gamma_{\text{PTFE}-n\text{-Hexadecane}}$ are concerned, they are directly extracted from the experimental results of Neumann et al. (1971) reproduced in Fig. 2.4. The $\gamma_{\text{PTFE}-\text{air}}$ *vs.* T and $\gamma_{\text{PTFE}-n\text{-Hexadecane}}$ *vs.* T graphs are plotted (Fig. 2.4) and the difference in slopes value ($C_\gamma = -5.643 \times 10^{-5}$ N m^{-1} K^{-1}) are obtained from those plots. Using these values, the intermediary terms of Eq. (2.21) are calculated and putting the initial value of f_θ ($T_s = 298.15$ K) as 0.213005 in RK4 method, Eq. (2.21) is solved for different temperatures. Similarly as before, the capillary pressure is calculated and plotted against temperature (Fig. 2.5) using $f_\theta(T)$ values in Eq. (2.24) through $h_m(T)$, $V_a(T)$ and density data ($\rho_l(T)$).

2.3.3 Discussions

Results show a linear decrease in capillary pressure as temperature rises. This is consistent with experimental results (She and Sleep, 1998; Grant and Bachmann, 2002). Grant (2003) suggested this phenomenon to be a universal one i.e. capillary pressure follows a decreasing linear relationship with temperature for almost every system. In our case, two examples consist of two very different systems and yet follow the same trend. However, the volume of

[‡]Website: http://www.ddbst.com (last accessed on 20.08.2015).

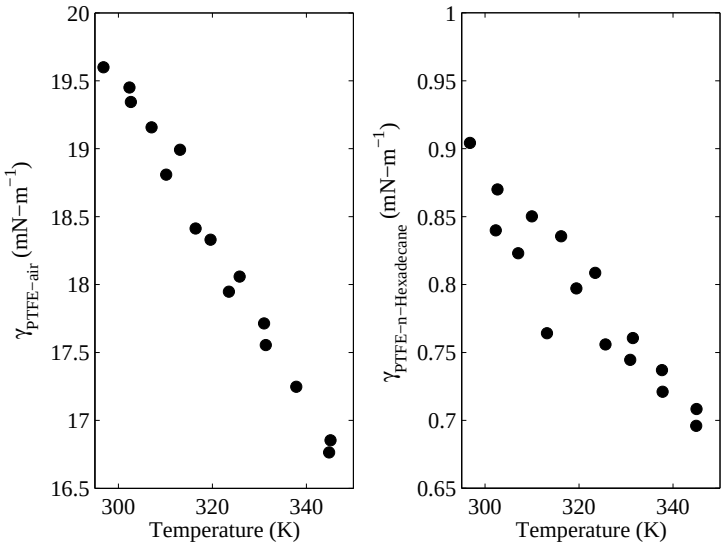

Figure 2.4: Interfacial tension of PTFE−air and of PTFE−*n*-Hexadecane *vs.* temperature plots ($\gamma_{PTFE-air}$ *vs.* T and $\gamma_{PTFE-n\text{-Hexadecane}}$ *vs.* T) reproduced from Fig. 1 of Neumann et al. (1971)

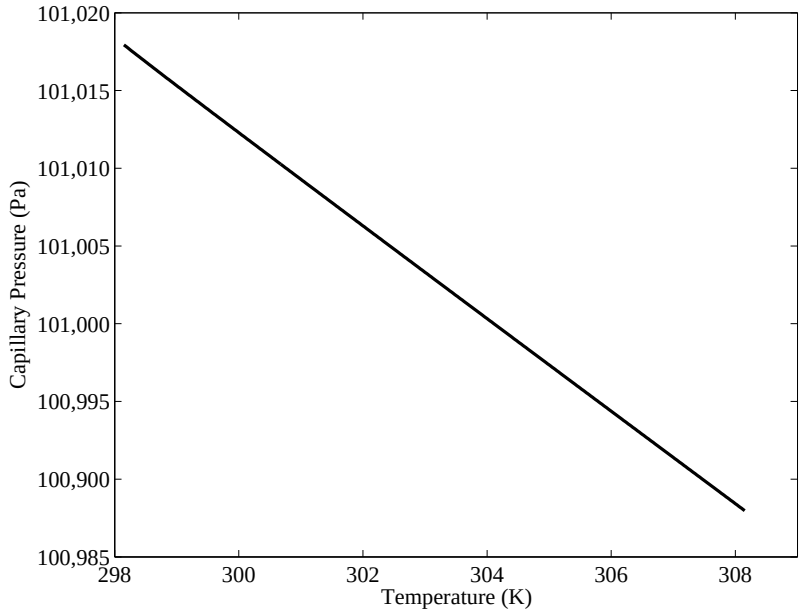

Figure 2.5: Capillary pressure *vs.* temperature plot for P-N-A system (closed-end)

gas in the tube decreases with the raising of liquid. The gas law suggests that the pressure of gas in the capillary should increase during capillary rise of liquid while other state variables remain constant. Therefore, while temperature changes, the gas and liquid pressures change in different way. Densities of liquid and gas i.e. the packing of molecules and intermolecular forces between molecules are different in liquid and in gas or ideal gas (where there are no intermolecular forces and interactions) and they behave differently as temperature changes. To understand these pressures and to get a better view of what is going on, air and liquid pressure for G-W-A and P-N-A systems are shown in Fig. 2.6 respectively. These pressures are just across the air–liquid interface (just below and above the interface).

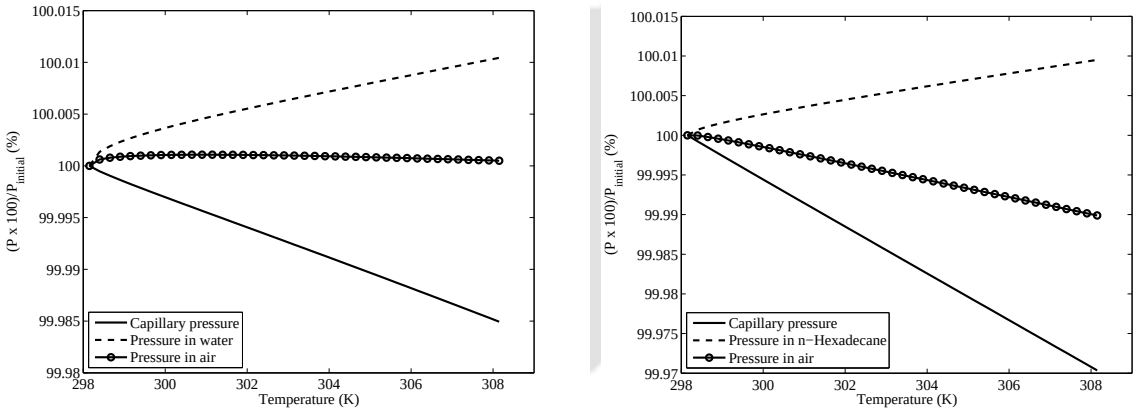

(a) (b)

Figure 2.6: Temperature variations (%) of pressures in (a) air, water and capillary pressures for G-W-A system, (b) air, *n*-Hexadecane and capillary pressures for P-N-A system, are plotted with respect to initial pressures of air, liquid and capillary pressure. P stands for pressure. P_{initial} means the pressure at reference temperature 298.15 K

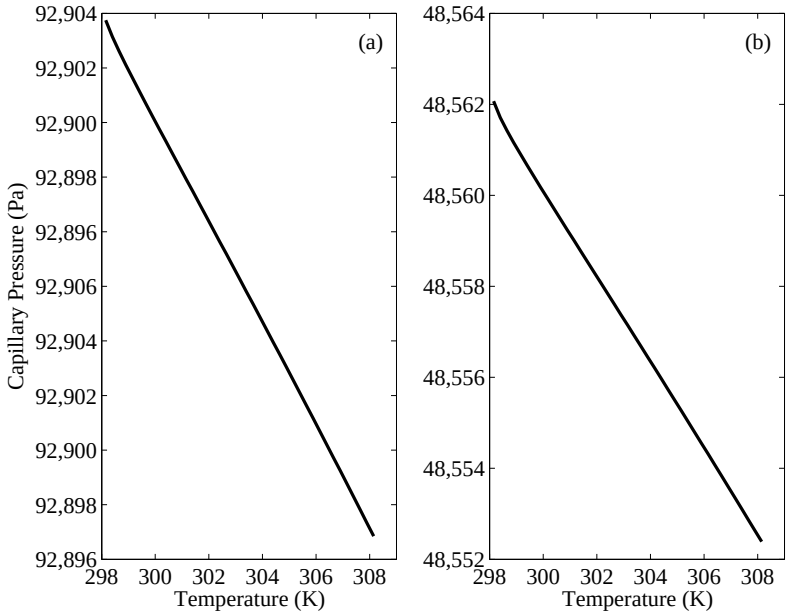

Figure 2.7: Capillary pressure *vs.* temperature plots. Plots for G-W-A system with (a) $L = 0.40$ m and (b) 0.60 m

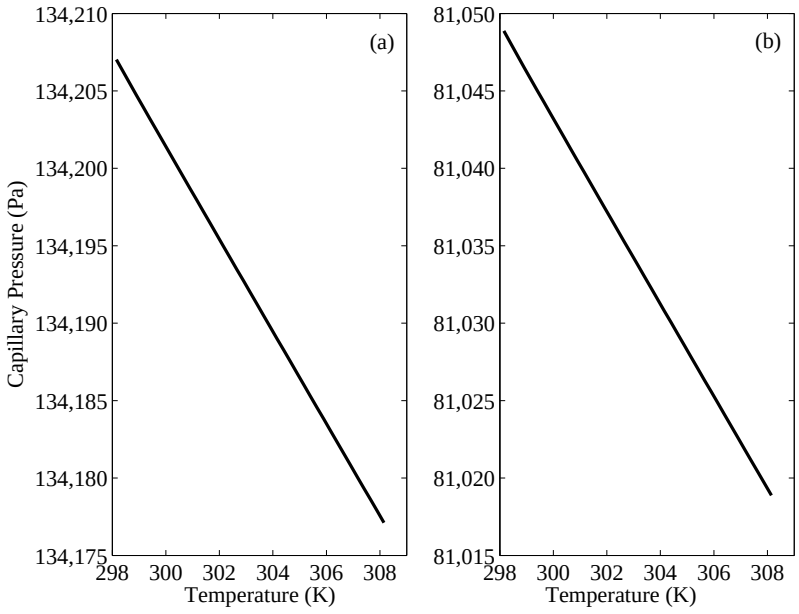

Figure 2.8: Capillary pressure *vs.* temperature plots. Plots for P-N-A system with (a) $L = 0.175$ m and (b) 0.225 m

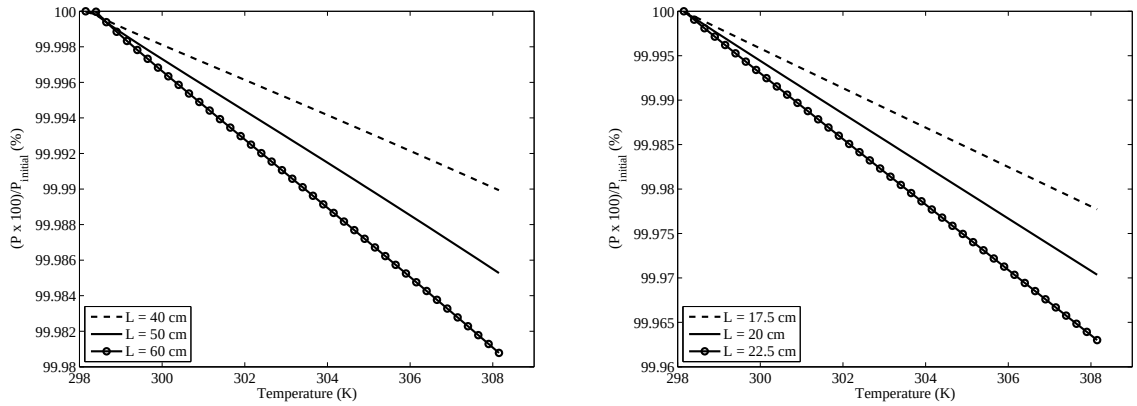

(a) (b)

Figure 2.9: Variation (%) of capillary pressure *vs.* temperature for (a) G-W-A system with $L = 0.40$ m, 0.50 m and 0.60 m and (b) P-N-A system with $L = 0.175$ m, 0.20 m and 0.225 m. P_{initial} means the pressure at reference temperature 298.15 K

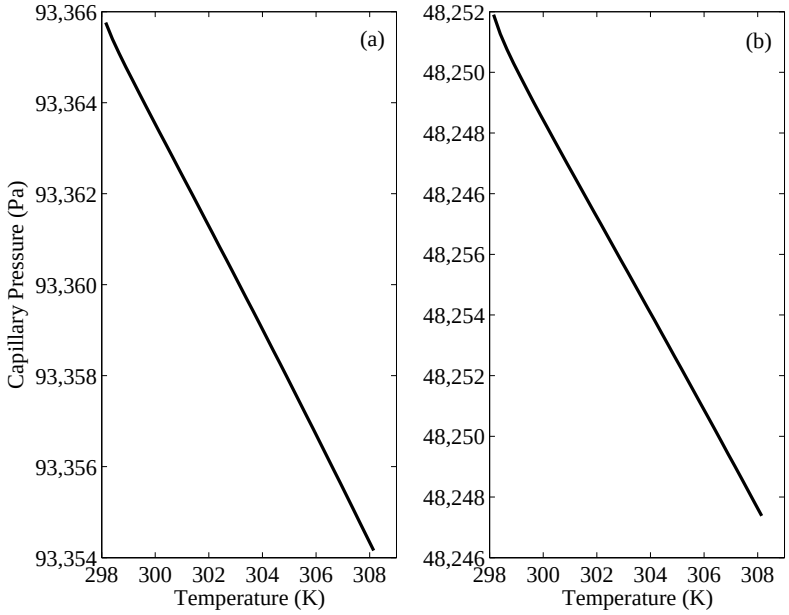

Figure 2.10: Capillary pressure *vs.* temperature plots. Plots for G-W-A system with (a) $R = 40$ μm and (b) 60 μm

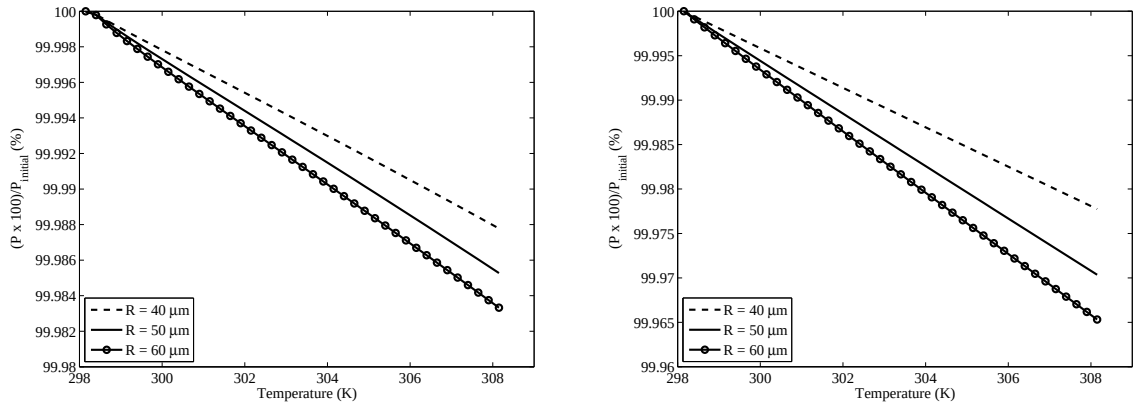

(a) (b)

Figure 2.12: Variation (%) of capillary pressure *vs.* temperature for (a) G-W-A system and (b) P-N-A system with $R = 40\ \mu$m, 50 μm and 60 μm. P_{initial} means the pressure at reference temperature 298.15 K

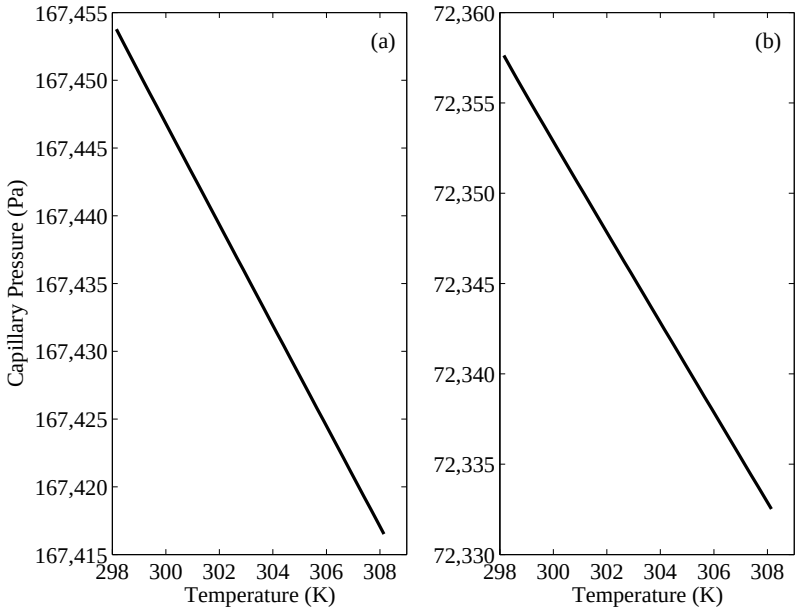

Figure 2.11: Capillary pressure *vs.* temperature plots. Plots for P-N-A system with (a) $R = 40\ \mu$m and (b) 60 μm

Figure 2.6 show that pressure in liquid for both cases changes almost similarly whereas air pressure in P-N-A system changes more with temperature than that of G-W-A system and hence it eventually affects the capillary pressure more. Is there an intrinsic reason for this or is it something extrinsic or combined of these two?

For above examples, the radius (R) and the total height (L) of the capillary tube are assumed.

However, the importance of these parameters on capillary pressure is not ascertained and therefore the exercises are done to evaluate capillary pressures for different values of L and R (Figs. 2.7-2.9 and 2.10-2.12 respectively).

The analyses substantiate that both the factors are important while calculating the capillary pressure from the fact that the magnitudes of capillary pressure drastically changes with radius of the capillary tube as well as the total height of the closed-tube. Since the top end of the capillary tube is closed, and as per the assumption of gas-solubility in liquid as null, the number of gas molecules before the capillary rise and after attaining the Jurin height remains same. Figures 2.7-2.11 reveal one important thing about the entrapment of air and its effects on temperature variation of capillary pressure. As the height of the tube increases, for cases involving same Jurin height and same parameters, the volume for the entrapped air is more. Therefore, the magnitude of air pressure is less for higher tubes as compared to the shorter tubes. Similarly, the capillary pressure is high for shorter tubes as the entrapped space for air is low. For very much longer vertical tubes, the entrapped air gets more space, which decreases the gaseous pressure, and behaves more like as open-end tubes. Figures 2.9-2.12 show that with increasing R and L, capillary pressure becomes sensitive to temperature more and more for both example cases.

2.3.4 Open-end capillary tube

Seeing the effects of vertical length on capillary pressure in closed-end tubes, the researchers investigated the thermal effects of capillary pressures in open-end tubes. With the same explanation provided for the temperature effects on capillary pressure for closed-end tubes, the concept is extended to describe the effects of temperature on capillary pressure in open-end capillary tubes. However, the mathematical expressions (or equations) are modified to take into account the difference in gas pressure at the open-end of the capillary. For example, from Maggi and Alonso-Marroquin (2013), the gas or air pressure is evaluated, neglecting meniscus velocity, as:

$$P_a(T) = P_{\text{atm}} - \rho_a(T)\, gL, \tag{2.27}$$

where P_{atm} is the pressure at the phreatic surface outside the tube (which is atmospheric pressure) and P_a is the pressure in air just at the top of the tube (assumed to be same as inside in the tube). Since, the open-end provides room for escape of gas molecules; the density of air as well as the volume of air differs significantly from that of closed-end tubes. Substituting $P_a(T)$ in lieu of $(n_g R_g T)/V_a(f_\theta(T))$ in Eq. (2.24) and using Eq. (2.27) relation, we have,

$$P_c(T) = -g\rho_a(T)\, L + g\rho_l(T)\,(h_l - h_m(f_\theta(T)))\,. \tag{2.28}$$

The same calculations as performed for the closed-end tubes are repeated to find $f_\theta(T)$ from Eq. (2.21) using same data as used for closed-end capillary tubes (example 1 and 2). After the calculation of $f_\theta(T)$, $h_m(f_\theta(T))$ from Eq. (2.18) are evaluated. Using fitting relationships of temperature and density of liquid (as before) and of air (Golfman, 2012), the capillary pressures are computed for different constant temperatures (Figs. 2.13 and 2.14).

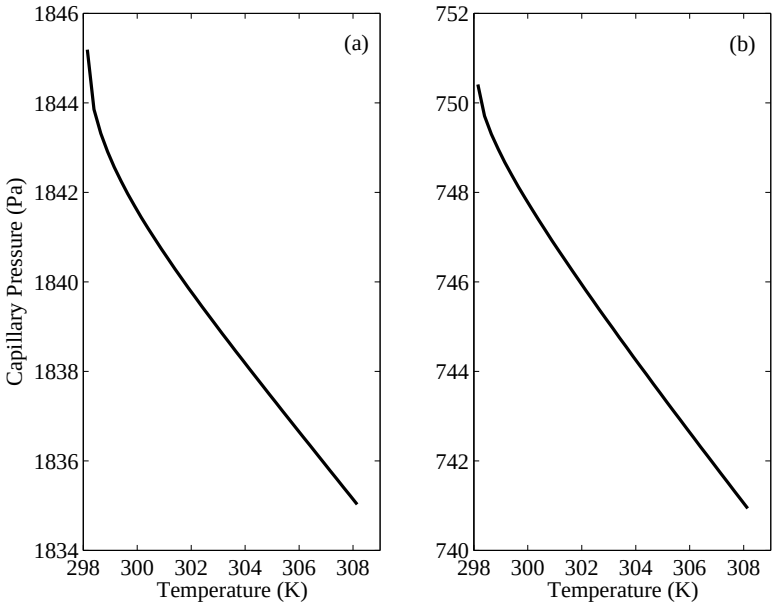

Figure 2.13: Capillary pressure *vs.* temperature plot for (a) G-W-A system (open-end) and (b) P-N-A system (open-end)

In the case of open-end pores, the magnitude of capillary pressure is lower than that of closed-end pores. This is due to the escape of gas molecules through the open-end during the capillary rising of liquid. For both the closed-end as well as the open-end capillary pores, the capillary pressure reduces linearly due to increase in temperature and thus proves the claim of Grant (2003) as mentioned before about the universality of the trend of linear drop of capillary pressure *vs.* temperature relationship (Fig. 2.14). However, one of the reasons may be that the increase in temperature excites the gas-particles and this excitation raises the velocity of air molecules and subsequently the momentum of gas-particles. Consequently, it enforces the solids and liquids and expands the gas volume more compared to the liquid volume. Therefore, the difference between gas-pressure and liquid-pressure gets reduced as temperature rises and thereby causes the reduction in capillary pressure. Another observation is that capillary pressure is more sensitive to temperature in open-end than that of dead-end system.

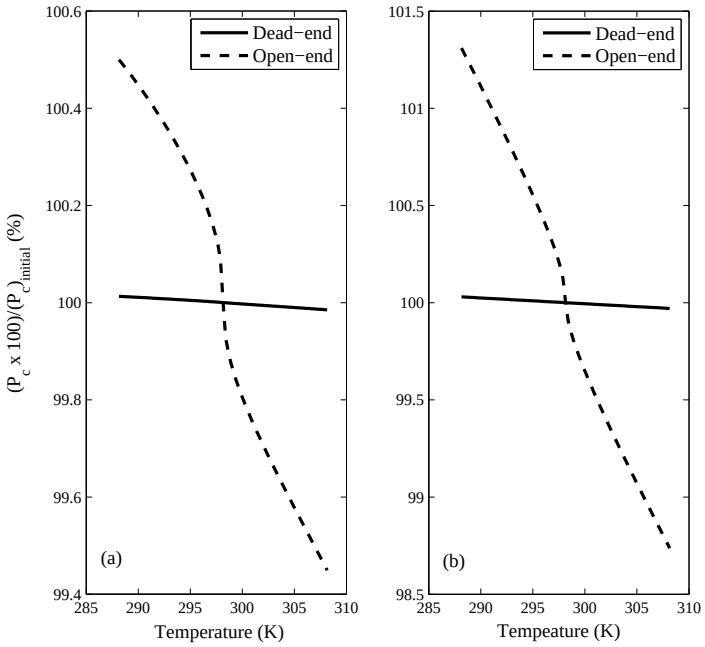

Figure 2.14: Comparison plots of capillary pressures in dead-end and open-end capillary systems. Variation (%) of capillary pressure *vs.* temperature plots for both (a) G-W-A and (b) P-N-A system. P_{initial} means pressure at reference temperature 298.15 K

Figure 2.14 reveals this fact as % drop of P_c from -0.015 % K^{-1} (dead-end) to -0.551 % K^{-1} (open-end) for G-W-A whereas -0.030 % K^{-1} (dead-end) to -1.263 % K^{-1} (open-end) for P-N-A. It can be hypothesized following the Figs. 2.7-2.12 that the capillary pressures in very long closed-end capillary tubes may behave almost the same way as in open-end tubes. Entrapment length of air or h_a (see Fig. 2.1) takes an important role in capillary pressure magnitude. Equilibrium contact angle also has an effect on $P_c(T)$. Slope values of P_c-*vs.*-T while changing θ_e in dead-end cases, can vary from -1.04 Pa K^{-1} (with $\theta_e = 40°$) to -0.824 Pa K^{-1} (with $\theta_e = 60°$) for G-W-A, and from -3.102 Pa K^{-1} (with $\theta_e = 36°$) to -2.855 Pa K^{-1} (with $\theta_e = 56°$) for P-N-A. Soil pore size (radius) can range from ~ 0.05 μm ('cryptopores') to 2500 μm ('macropores') (Soil Science Society of America, 2008). Dimension of capillary tube along with θ_e can give an idea of approximate range of slope values for dead-end case. Pore radius changing from 1 (with $\theta_e = 10°$) to 1000 μm (with $\theta_e = 80°$) with $L = 150$ m while keeping other terms constant in the case of G-W-A, slope changes from ~ -57.9 Pa K^{-1} to -4 Pa K^{-1} and similarly in the case of P-N-A but only with $L = 7.5$ m, slope changes from ~ -162.4 Pa K^{-1} to -1.2 Pa K^{-1}. Therefore 10 K change in temperature can drop the capillary pressure from 12–40 Pa to 579–1624 Pa. Limitation that can be questioned here, is that usual capillary pressure measuring sensors of the present

age may not be able to capture this *small* change. However, the lack of accuracy in current measuring devices (e.g. accuracy of even recent standard tensiometers like T5 Tensiometer[§], is only $\pm$ 0.5 kPa) need not hinder the progress of theory in this research field. Nevertheless, for both cases, the linear drop of capillary pressure with temperature is observed, even though both are very different system. This validates the equation derived in this chapter qualitatively if not quantitatively (Grant and Bachmann, 2002) as only a single capillary tube is considered and dealt with. Grant (2003) mentioned that relative drop in capillary pressure at 298 K is *typically* around -1 % K^{-1}, and as early results show the relative drop at 298.15 K to be around -0.551 % and -1.263 % K^{-1} for G-W-A and P-N-A respectively.

As P_c is found to linearly vary with T, Eq. (2.17) can be replaced with a simple linear relation: $P_c = a + bT$, where a [Pa], b [Pa K^{-1}] are fitting parameters. Following the Figs. 2.3 and 2.5, a , b can be obtained: (1) for G-W-A system, $a = 63877.437$ Pa (standard error[¶] or SE: 0.515), $b = -0.939$ Pa K^{-1} (SE: 0.002); (2) for P-N-A system, a = 101909.086 Pa (SE: 0.466), $b = -2.989$ Pa K^{-1} (SE: 0.002). This simple relation may hold for most systems but does miss out some intricate physics underneath. Empirical relationships of physical parameters and temperature are now-a-days easily available or can be obtained through standard experiments. Equation (2.17) gives much broader picture than that of a one-parameter or two-parameter model. Here, two generic cases are solved as the data of these materials are available. With regards to heterogeneous soils, depending upon soil chemistry and thermal experiments upon soil, the temperature dependency of physical properties like ρ_l *vs.* T, σ_l *vs.* T (as in Dean, 1999), $\theta_{\text{liquid on soil}}$ *vs.* T (as in Bachmann et al., 2002) etc., can be obtained and then utilized as input parameters in the similar example problems described earlier. ead-end pores can be identified by some conventional methods (electric logging formation factor, mercury injection capillary pressure and miscible displacement etc.) as mentioned by Jackson and Klute (1967) or as mentioned by Fatt et al. (1966) and most recently by Phirani et al. (2018) and these methods can provide with an effective size as well as volumetric fraction of dead-end pores. The method proposed here can be modified or extended to deal with the more generic cases like the liquid flux. Thermal component of the total gradient of capillary head contributes to the liquid flux in unsaturated soil as $-K_w \frac{\partial \psi}{\partial T}|_\eta \nabla T$ (Philip and De Vries, 1957), where K_w is the unsaturated hydraulic conductivity[‖]. The non-isothermal term can be decomposed into three parts as

$$\left.\frac{\partial \psi}{\partial T}\right|_\eta = \underbrace{\omega_D \left.\frac{\partial \psi}{\partial T}\right|_{\text{dead-end}} + \omega_O \left.\frac{\partial \psi}{\partial T}\right|_{\text{open-end}}}_{\text{unsaturated}} + \underbrace{\omega_S \times 0;}_{\text{saturated}} \tag{2.29}$$

[§]Please refer: https://www.metergroup.com/environment/products/t5-tensiometer-water-potential/

[¶]Please refer the web-book: *Experimental Design and Analysis* by Dr. Howard Seltman, CMU, USA.

[‖]From Eq. (1.7): $K_{wij} = 0$; $i \neq j$ (isotropic) and as well $K_{wij} = K_w$; $i = j$; $i, j = 1, 2, 3$ (homogeneous).

$$\text{with } \omega_D + \omega_O + \omega_S = 1 \text{ and } \omega \in [0,1].$$

Here three weighting factors (ω), subscripted as D, O and S, represent volumetric fraction of dead-end pore (ω_D) (saturated or unsaturated), of open-end unsaturated pores (ω_O) and of open-end saturated pore (η_S) relative to total void in an averaging volume of soil. Researchers (Coats and Smith, 1964; Jackson and Klute, 1967; Wirner et al., 2014; Phirani et al., 2018, and others) gave methods to measure the immobile or stagnant or dead-end pore volume and they always distinguished two domains – mobile and immobile zone, but only in the terms of fully saturated soil. As per Eq. (2.29), mobile zone comprises of whole open-end pores (saturated as well as unsaturated ones) and immobile zone is of dead-end pore. If the dead-end pore is only the unsaturated part of the soil, then the term $\partial\psi/\partial T\big|_{\text{open-end}}$ turns into zero and $\partial\psi/\partial T\big|_{\text{dead-end}}$ term only survives and then this term will have *small* effect on $\partial\psi/\partial T\big|_{\eta}$ and thus on the liquid flux. Therefore, the impact of dead-end is relative to physical condition of the soil or any other porous medium and depends on equilibrium contact angle of liquid over the solid matrix, weighting fraction and physical dimension of dead-end pores in that particular porous medium. When whole soil is saturated, the temperature derivative term becomes zero and contribute none to actual liquid flux. However, we limit the present study as described here and suggest the generic cases as future scope along with sophisticated experimentations.

2.4 Summary

The dead-end pores are assumed as capillary tubes with one end closed and the effect of temperature on liquid-gas meniscus is analyzed. Main assumptions during derivation are: 1. meniscus is spherical, 2. capillary forces are dominant ($Bo << 1$), 3. temperature dependence of interfacial tensions is linear, 4. displacement of meniscus is neglected due to sticking of liquid to the same position at the solid surface known as CLP and 5. air-diffusivity into liquid is null. The effect of temperature on capillary pressure is worked out by first identifying the change in meniscus curvatures due to incremental variation in temperature and thereby the changes in the interfacial tensions that consequently causes change in capillary pressures. This whole concept is represented using a differential equation in this chapter, in which the dependent variable is a new term called temperature function. The differential changes in meniscus height (h_m) were evaluated. Thus capillary pressure is calculated from meniscus height values and density values at different temperatures with respect to a chosen reference temperature. For both the G-W-A and P-N-A systems, the results show linear drop of capillary pressure with temperature. An important observation in dead-end pores or closed-end tubes is that of significance of entrapped air as well as the dimensions of R and h_a as well as the value of θ_e in computations of capillary pressure at different constant temperatures.

The effect of temperature on liquid-gas meniscus curvature in the open-end capillary tube also showed linear drop of capillary pressure with temperature. However, the magnitudes of capillary pressures are much lower compared to the dead-end pore cases. As both the closed-end and open-end capillary tubes show linear drop in capillary pressures with rise in temperatures, the phenomena is critical in designing the subsurface drainage of irrigated fields. The drainage of water may increase more than intended during temperature rise as the capillary pressure reduces. Closed-end capillary tubes with very large air column at the top behave approximately like the open-end tubes with respect to capillary pressure-*vs.*-temperature. The results presented here are consistent with the experimental data qualitatively. In addition, the chapter, for the first time, provides a conceptual insight into the dead-end pores' significance on temperature effects on capillary pressure or on capillary pressure-*vs.*-saturation relationship at a particular liquid saturation.

2.4.1 Questions?

Some questions remain to be answered and those are the practicability or validity of the above assumptions. Capillary force ($\sim \sigma$) are dominant than gravity force ($\sim (\rho_l - \rho_a)gL^2$) and this assumption is true for capillary tubes (De Gennes et al., 2004). Our main focus being capillary pressure in porous media, this assumption is vital in this thesis. We discuss the plausibility of CLP in the next chapter. Linearity assumption of interfacial tension (γ) *vs.* temperature (T) is valid, cause of, almost linear trend between γ and T. Quadratic relation can be fitted as: $\gamma = a + bT + cT^2$. The experimental results (see Neumann et al., 1971; Neumann, 1974) show that the quadratic coefficient $|c|$ has a very low value than $|b|$ ($(|c|/|b|) << 1$) and thus, proves to be negligible without losing any loss of generality. Air-diffusivity into liquid is null and this means that there is an equilibrium between liquid and air phases. This is only possible when air is saturated with liquid vapor. *However, phase equilibrium always exists at the interface of two phases of a species* (from Çengel and Boles, 2015, p. 823). Therefore, our assumption is an extension of phase-equilibrium criterion. We assume that within this small close-end capillary tube, this criterion exists. Last but not the least, the shape of the meniscus is *assumed* being of spherical, even when CLP of meniscus exists. This assumption puts limits on temperature range (see Appendix-A2.1). Plausibility of this range may be questioned. Assumption of meniscus shape is taken mostly as spherical, mainly because of lesser effect of gravity in capillary tubes (viz. raindrop will be of perfect sphere shape under no gravity). We argue and question this assumption in the next chapters. We try to understand how meniscus shape has an effect on changes in contact angle and thus, eventually on capillary pressure.

A2 Appendix

A2.1 Limitation of temperature based on meniscus height

The values of meniscus height (h_m) with different temperatures are shown in the following Fig. A2.1 for two example cases (G-W-A and P-N-A systems). It is pretty clear that h_m increases with temperature. Our assumption is that meniscus shape is spherical even if meniscus sticks to same place while temperature changes.

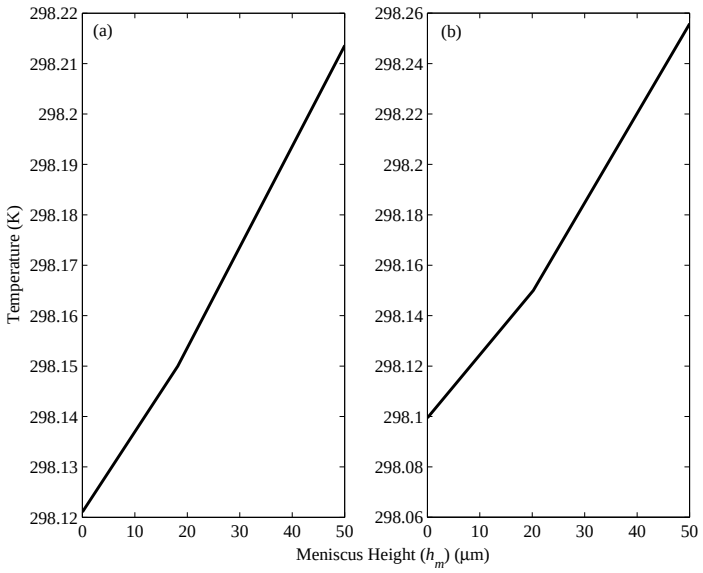

Figure A2.1: T-*vs.*-h_m plots for: (a) G-W-A system and (b) P-N-A system from $R = 0$ to 50 μm

As a consequence the contact angle decreases with the increase of h_m. Contact angle is calculated using following equation:

$$\theta_e(T) = \tan^{-1}\left(\frac{R^2 - h_m(T)^2}{2Rh_m(T)}\right) \text{ within } \left[0, \frac{\pi}{2}\right] \tag{A2.1}$$

Equation (A2.1) suggests that contact angle (θ_e) becomes 0° while h_m reaches the R i.e. in our case 50 μm. Similarly with decrease in temperature, contact angle eventually becomes 90° while h_m is zero. This puts a limitation on h_m and that is: $h_m \in [0, R]$. Figure A2.1 shows that θ_e and h_m become zero and R respectively at same temperature. Now limitation on h_m or θ_e gives the highest or lowest temperatures. These temperatures can be obtained from fitting relationship $T(h_m)$ at $h_m = 0$ and R for lowest and highest temperatures respectively (say, T_{lowest} and $T_{highest}$). Here, the fitting relationship with $T(h_m = R)$ and $T(h_m = 0)$ provide:

(a) for G-W-A system, $T_{highest} = 298.21$ K and $T_{lowest} = 298.12$ K and (b) for P-N-A system, $T_{highest} = 298.26$ K and $T_{lowest} = 298.1$ K, respectively.

CHAPTER 3

Temperature Effects on Contact Angle with New Meniscus

3.1 Introduction

Contact angle is defined as the angle made by free air-liquid surface (i.e. meniscus or a *zero*-width line with intrinsic properties, especially of the liquid, like surface tension) on the solid surface (Lee and Lee, 2007). The above definition of contact angle gives a microscopic view of contact angle and therefore, can be called, henceforth, *microscopic* contact angle (MCA). In this thesis, whenever we mention contact angle (CA, θ), we mean MCA, if not meant otherwise. Ambient solid surfaces or natural surfaces are rarely smooth or chemically homogeneous. Therefore, unique CA on a particular surface, as described by Youngs' equation, is merely a theoretical expression (Yuan and Lee, 2013). Meniscus gets pinned at crevices of the surface and depending on the location, meniscus can move only after crossing some *energy barrier* or *activation barrier* (Marmur, 1994; Gao and McCarthy, 2006). Within that barrier any *vibrational energy* only changes the static CA (SCA) and exhibits metastable states (Johnson Jr and Dettre, 1964). The SCA ranges from maximum (θ_{max}) to minimum value (θ_{min}) at the pinned position depending upon two extremes of energy barrier (Marmur, 1994). The difference between these angles is known as contact angle hysteresis (CAH, $C_{\mathscr{H}} = |\theta_{max} - \theta_{min}|$). Quéré (2008) mentioned that defects or roughness need to be of molecular dimension (nanometric) to overcome energy barrier by thermal energy (of the order of $k_B T$, where k_B is Boltzmann constant and T is temperature [K]). Their (defects) effect will still be visible macroscopically as a hysteresis of CA (Bonn et al., 2009). Recently, Kuchin and Starov (2016) theorized that CAH can *even* be present in a smooth, chemically homogeneous solid surface due to liquid films. As we have already discussed in Chapter-2 that while capillary pressure changes for various reasons, the meniscus adjusts itself, to some extent, due to contact line pinning (CLP) and prevents any translation movement of the fluid. Even if the system is in static equilibrium, the capillary pressure can change due to various reasons (like temperature, solute concentrations, electricity, magnetism, etc.) that should have initiated the movement of fluids. However, the CLP resists the movement and creates the hysteresis effects on SCAs. This hysteretic behavior affects the SCA and contradicts the assumption that SCA

is same for all temperatures (e.g. as assumed by Maggi and Alonso-Marroquin, 2013).

The aim of this chapter is to investigate the temperature effects on SCA and hysteresis of SCA, considering a new meniscus shape rather than as always *assumed* spherical shape.

3.2 Mathematical modeling

Capillary rise occurs in a *thin* cylindrical capillary tube dipped in an infinite source of liquid. The liquid reaches the stable equilibrium height (or Jurin's height, h_∞) at a particular temperature, T (Fig. 3.1a). Equilibrium height in a capillary tube is obtained by minimizing the surface energy and gravitational energy (De Gennes et al., 2004):

$$h_\infty = \frac{2\sigma\cos\theta_e}{R\rho_l g}, \tag{3.1}$$

where θ_e is the SCA [°] and R the radius of the tube [m].

However, the equilibrium height (Eq. (3.1)) does not include the meniscus information. It is a general assumption that the meniscus is of *nearly* spherical shape in a cylindrical capillary tube (Rand, 1978). However, the near wall image of meniscus could be lost due to the critical angle of refraction (Hoffman, 1975; Lee and Lee, 2007) and therefore true shape is not known. As R gets bigger within the limitation of $R << \sqrt{(\sigma/\rho_d g)}$ (from Bond number (Hager, 2012)), the spherical form of the meniscus may no longer be a valid approximation. Phenomenologically, the meniscus can be thought of like a hanging chain linked/pinned at a solid wall. In 1691, Gottfried Leibniz, Christiaan Huygens, and Johann Bernoulli proved independently on a challenge posed by James Bernoulli that hanging chain under uniform force field takes the shape of a catenary curve or hyperbolic cosine function (Lockwood, 1961). We introduce, in this research, catenary curve in $z-r$ plane (as our domain is z-axis symmetric) and the surface of revolution around the z-axis will give the meniscus shape (Fig. 3.1b). If the 2-D form is rotated 360° along z-axis, meniscus shape in 3-D* emerges in more like upside down Igloo form (Handy, 1973). The equation of c/s of the meniscus can be written as:

$$z(r) = h_\infty + a\cosh\left(\frac{r}{a}\right) - a. \tag{3.2}$$

Slope at boundary i.e. $\mathrm{d}z/\mathrm{d}r|_{r=R}$ is $\cot(\theta_e)$ and this boundary condition gives the value of the parameter: $a = R/\sinh^{-1}(\cot(\theta_e))$.

*This is *different* from catenoid shape, which is the surface of revolution around r-axis, and mean curvature of the catenoid shape is zero.

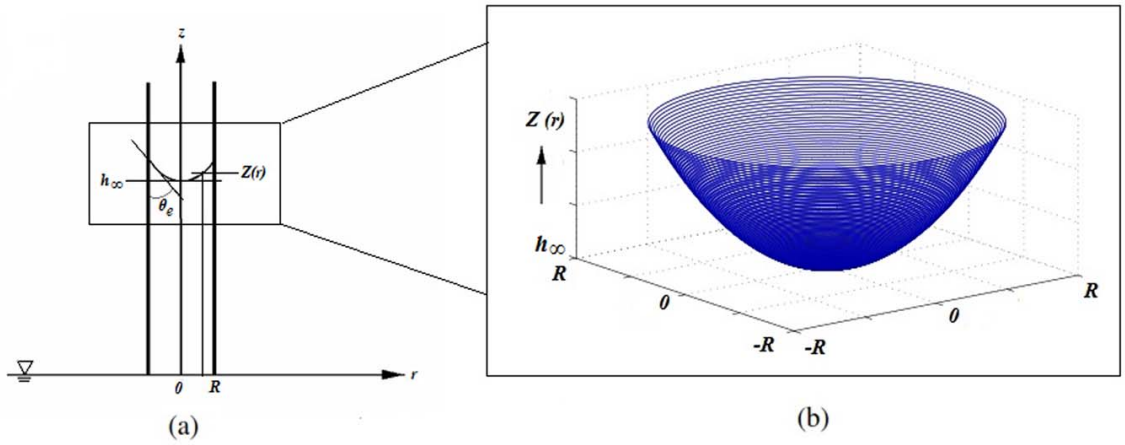

Figure 3.1: (a) Schematic of capillary tube and (b) Sample meniscus shape

The equilibrium height after meniscus correction is:

$$\bar{z} = \frac{1}{R}\int_0^R z(r)\mathrm{d}r = (h_\infty - a) + \frac{a^2}{R}\cot\theta_e. \tag{3.3}$$

As per Laplace's theorem, the pressure difference across the interface between liquid and air is equal to the product of the surface tension and mean curvature of the interface (De Gennes et al., 2004).

$$P_c = \sigma\left(\frac{1}{R_1} + \frac{1}{R_2}\right), \tag{3.4}$$

where P_c is the capillary pressure [Pa] and R_1, R_2 are the principal radii of the meniscus surface [m].

Radius of the meniscus (Eq. (3.2)) is (see Piskunov, 1969, p. 217):

$$\frac{\left[1 + (\mathrm{d}z/\mathrm{d}r)^2\right]^{3/2}}{|\mathrm{d}^2z/\mathrm{d}r^2|} = a\cosh^2\left(\frac{r}{a}\right). \tag{3.5}$$

The mean radius of the meniscus is (taking average along the r-axis):

$$R_m = \frac{1}{R}\int_0^R a\cosh^2\left(\frac{r}{a}\right)dr = \frac{a^2}{4R}\sinh\left(\frac{2R}{a}\right) + \frac{a}{2}. \tag{3.6}$$

This radius is equal in two principal axes and therefore, $R_1 = R_2 = R_m$.

Multiphase effect is introduced in the weight function considering weight of gas:

$$w(\bar{z}) = \rho_d g\bar{z} + \rho_a gL, \tag{3.7}$$

where L is the total height of the capillary tube (m) and $\rho_d = \rho_l - \rho_a$ where ρ_l is the density of liquid and ρ_a density of air.

At static or quasi-static equilibrium, P_c equals total weight per unit area or gravitational pressure ($w(\bar{z})$) on the meniscus (Rand, 1978; Lu and Likos, 2004):

$$\frac{2\sigma}{R_m} = \rho_d g\bar{z} + \rho_a gL. \tag{3.8}$$

Temperature changes surface tensions, densities, and as well as pressures in fluids. Incremental changes in P_c across the meniscus due to the temperature difference, try to initiate the translation of the whole liquid system. However, CLP causes meniscus to move or adjust itself rather than translate the entire liquid system (Poynting and Thomson, 1902; Elliott and Riddiford, 1967; Slattery and Flumerfelt, 1982; Hassanizadeh and Gray, 1993). Meniscus adjustment causes a change in SCA. Two values of temperatures can be tied to the two extremes of energy barrier or metastable equilibrium states of CAH before the system becomes unstable i.e. the meniscus starts moving and thus CLP holds within the range of temperatures say temperature, $T \in [T_{lc}, T_{uc}]$ (where, T_{lc} is lower critical temperature and T_{uc} is upper critical temperature). The analysis of meniscus shape in the static or quasi-static equilibrium situation (as there is no vertical translation) is performed to interpret the temperature effects and CLP on the meniscus.

The derivative of Eq. (3.8) with respect to temperature T is:

$$F(\kappa)\frac{\mathrm{d}\kappa}{\mathrm{d}T} + G(\kappa) = 0, \tag{3.9}$$

where,

$$\begin{aligned}
\kappa &= \sinh^{-1}(\cot\theta_e), \\
F(\kappa) &= g\rho_d f_1(\kappa) + \frac{2\sigma f_2(\kappa)}{{R_m}^2}, \\
G(\kappa) &= g\bar{z}\left(\frac{\mathrm{d}\rho_d}{\mathrm{d}T}\right) + gL\left(\frac{\mathrm{d}\rho_a}{\mathrm{d}T}\right) + g\rho_d f_3(\kappa) - \frac{2}{R_m}\left(\frac{\mathrm{d}\sigma}{\mathrm{d}T}\right), \\
f_1(\kappa) &= \frac{2\sigma\,\mathrm{sech}^2\kappa}{R\rho_l g} + \frac{R}{\kappa^2} + \frac{R\cosh\kappa}{\kappa^2} - \frac{2R\sinh\kappa}{\kappa^3},
\end{aligned}$$

$$f_2(\kappa) = \frac{R\cosh 2\kappa}{2\kappa^2} - \frac{R\sinh 2\kappa}{2\kappa^3} - \frac{R}{2\kappa^2}, \quad \text{and}$$
$$f_3(\kappa) = \frac{2\tanh\kappa}{R\rho_l g}\left(\frac{d\sigma}{dT}\right) - \frac{2\sigma\tanh\kappa}{R{\rho_l}^2 g}\left(\frac{d\rho_l}{dT}\right).$$

Equation (3.9) is a first-order non-linear ordinary differential equation in terms of $\kappa(T)$. In this paper, this equation is solved by the fourth-order Runge-Kutta method (RK4) for different constant temperatures starting from a reference temperature, T_{eq} (at which $\kappa(T_{eq})$ is a known quantity). The assumption is that temperature variation of $\rho_l(T)$, $\rho_a(T)$, $\sigma(T)$ are known quantities, and so subsequently temperature derivatives are known. These temperature derivative values of $\rho_l(T)$, $\rho_a(T)$ and $\sigma(T)$, are obtained from empirical relationships or fitting relationships to the published data (e.g. Fig. 3.2). Within the small range of temperatures ($T \in [T_{lc}, T_{uc}]$) or metastable states at adiabatic condition, it is assumed that Marangoni effects are negligible.

The solution of Eq. (3.9) provides $\kappa(T)$, which straightway is used to calculate SCA (θ_e).

$$\theta_e(T) = \begin{cases} \cot^{-1}\left(\sinh\left(\kappa(T)\right)\right);\ \theta_e(T) \in \left(0, \frac{\pi}{2}\right] \ \forall\, T \in [T_{lc}, T_{uc}]. \\ \pi + \cot^{-1}\left(\sinh\left(\kappa(T)\right)\right);\ \theta_e(T) \in \left[\frac{\pi}{2}, \pi\right) \ \forall\, T \in [T_{lc}, T_{uc}]. \end{cases} \tag{3.10}$$

Due to CLP, meniscus line will be contracted or stretched depending on the dominance of upward or downward forces respectively within the temperature range $T \in [T_{lc}, T_{uc}]$. Range of temperatures i.e. T_{lc} and T_{uc} can be evaluated from a fitting relationship of θ_e-*vs.*-T plot, if the CAH is known a priori. Assuming the CAH is known to be $(\alpha_1 + \alpha_2)$ i.e. $(\theta_e + \alpha_1)$ and $(\theta_e - \alpha_2)$, then from θ_e-*vs.*-T plot, a polynomial relationship can be obtained as $T = \sum_{i=0}^{n}\left(b_i {\theta_e}^i\right) = f_t(\theta_e)$ (n is a positive integer; b_n, b_{n-1},..., b_0 are the curve-fitting parameters and $b_n \neq 0$). Therefore, the range of temperatures will be: $T_{uc} = f_t\left(\theta_e(T_{eq}) - \text{sgn}(b_n)\alpha_1\right)$ and $T_{lc} = f_t\left(\theta_e(T_{eq}) + \text{sgn}(b_n)\alpha_2\right)$, where $\text{sgn}(x)$ is the sign function of x. The above formulations can be extended to multicomponent system as well as to dynamic situation as discussed briefly in Appendix-A3.1-A3.2.

3.3 Results and discussion

Capillary rise occurs in a cylindrical capillary tube inserted in a pool of liquid at a standard temperature of 298.15 K. After a particular time, the liquid reaches an equilibrium height and meniscus makes SCA. The liquid is assumed to stick to the solid wall if the change in temperature occurs within *some* temperature range (i.e. $T \in [T_{lc}, T_{uc}]$). Henceforth, SCA of the meniscus will change only within the temperature range before the meniscus moves up

or down (translation). The radius and the length of the capillary tube are taken as 50 μm and 0.50 m, respectively for the numerical simulations. Initial SCAs for different liquids on solids (Table 3.1) are considered at 298.15 K i.e. θ_e ($T_{eq} = 298.15$ K). The temperature, $T_{eq} = 298.15$ K is the reference value, and the parameter, κ at this initial or reference temperature is $\kappa(T_{eq}) = \kappa_{eq}$. Equation (3.9) is, thereafter, numerically solved using κ_{eq} as the initial value to obtain $\kappa(T)$ for the intended range of temperature. In addition, the temperature-dependent values of liquid densities $\rho_l(T)$, air density $\rho_a(T)$, and surface tensions $\sigma(T)$ are collected from various literature sources (as shown in Fig. 3.2) and are fitted with polynomial relationships. From the initial conditions like κ_{eq} and $\theta_e(T_{eq})$ (see Table 3.1), the parameter $\kappa(T)$ is calculated for different constant temperatures (say, $T >$ or < 298.15 K) at the adiabatic condition. Therefore, SCAs ($\theta_e(T)$) for these constant temperatures are calculated from Eq. (3.10). Figure 3.3 shows the variation of SCA for the temperature range of $T_{eq} \pm 20$ K. Even if the figure shows the continuous line, in theory, $\theta_e(T)$ values are distinct at constant temperatures within $T_{eq} \pm 20$ K. This range of temperatures is selected arbitrarily just to test the proposed model.

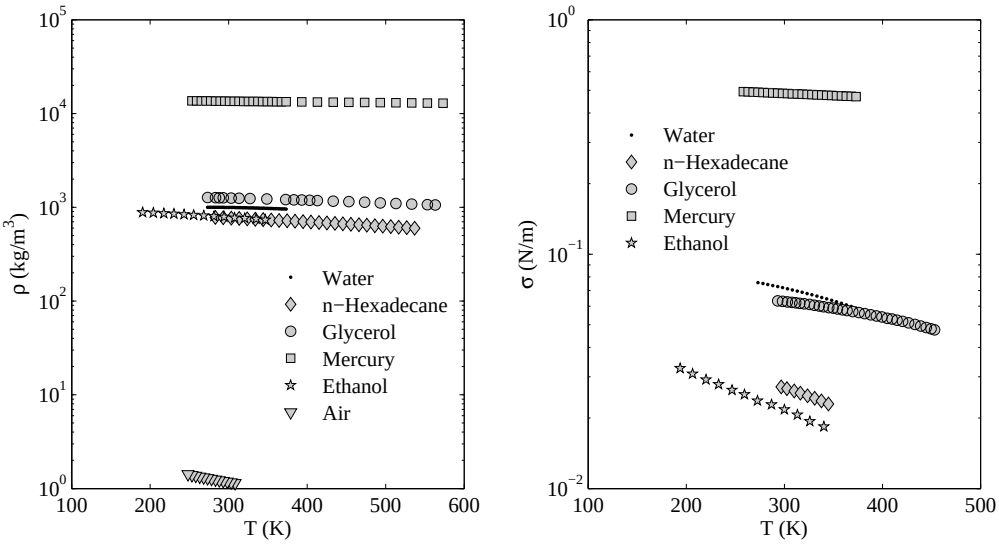

Figure 3.2: Temperature-dependent densities of liquid, air and surface tension i.e. $\rho_l(T)$, $\rho_a(T)$ and $\sigma(T)$ respectively. Data sources of densities: water (Dean, 1999), *n*-hexadecane (Onken et al., 1989), glycerol (Glycerine Producers' Association, 1963), mercury (Dean, 1999), ethanol (Maggi and Alonso-Marroquin, 2013), air (Golfman, 2012). Data sources of surface tension: water (Vargaftik et al., 1983), *n*-hexadecane (Neumann et al., 1971), glycerol (Glycerine Producers' Association, 1963), mercury (Dean, 1999), ethanol (Maggi and Alonso-Marroquin, 2013).

The SCA decreases with T in the case of $\theta_e < 90^\circ$ (i.e. wetting fluids, e.g. water, *n*-hexadecane and glycerol), however, it increases with temperature in the event of $\theta_e > 90^\circ$ (i.e. non-wetting fluids, e.g. mercury) (Fig. 3.3). Non-dimensional θ_e with non-dimensional T is, therefore, plotted for all the liquids mentioned above for comparison purposes (Fig. 3.4). This trend of

Table 3.1: Initial SCAs for different liquids

Liquid on Solid	θ_e (T_{eq} =298.15 K)	Reference
Water on Glass	50°	Liechti et al. (1997)
n-Hexadecane on Polytetrafluoroethylene	46°	Neumann et al. (1971)
Glycerol on Glass	48.5°	Liechti et al. (1997)
Mercury on Glass	133°	Ellison et al. (1967)

SCA of wetting and non-wetting fluids is qualitatively analogous to Wenzel state, as surface becomes more hydrophilic and more hydrophobic in the presence of surface roughness, which is defined by Wenzel (1936) as the ratio of real surface to the projected one (Das et al., 2012, and see references therein). In this analysis, this trend is, however, happening due to temperature and other CAH-inducing surface parameters like roughness.

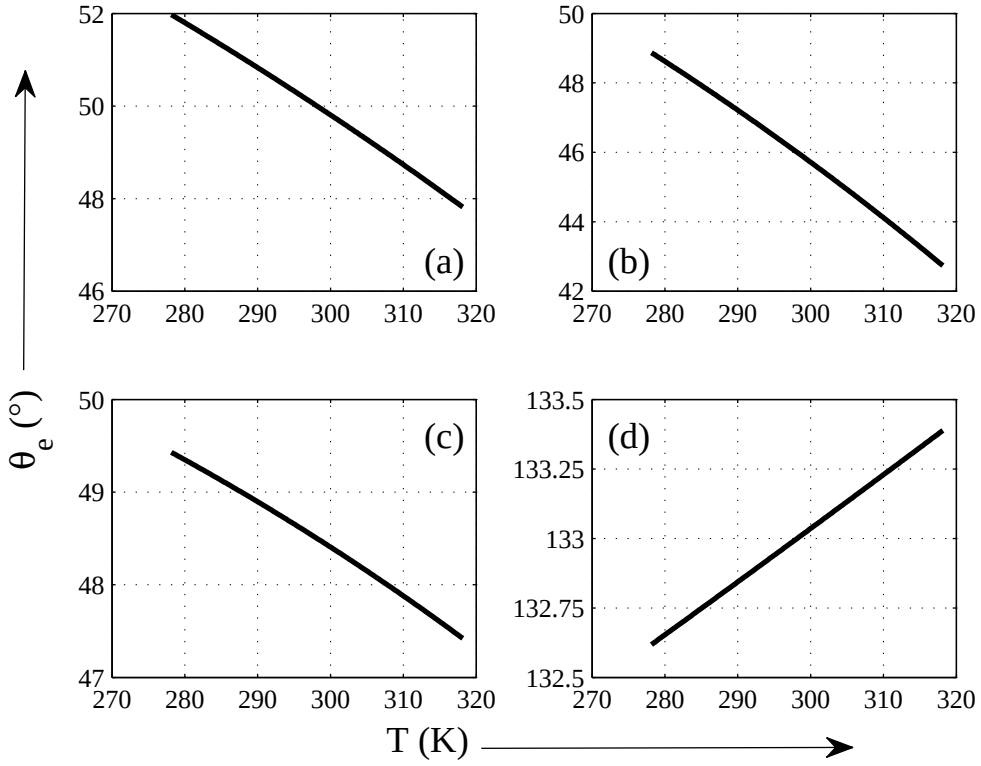

Figure 3.3: Temperature-dependent SCAs for (a) water, (b) *n*-hexadecane, (c) glycerol and (d) mercury for temperature ranges of 298.15 K ± 20 K.

CAH ($C_{\mathscr{H}}$) can be construed as the slope of the graph between SCA and temperature at T_{eq} i.e. for a small and fixed ΔT $\left(=\max(|T_{uc}-T_{eq}|,|T_{lc}-T_{eq}|)\right)^{\dagger}$, $C_{\mathscr{H}} = |\theta_{max}-\theta_{min}| \approx \left(\mathrm{d}\theta_e/\mathrm{d}T|_{T=T_{eq}}\right)|\Delta T|$. The temperature variation of θ_e is susceptible to density, as it is

$^{\dagger}\max(r,s)$ = maximum value among r and $s = \frac{1}{2}(r+s+|r-s|)$ (see Kalman's (1984) paper).

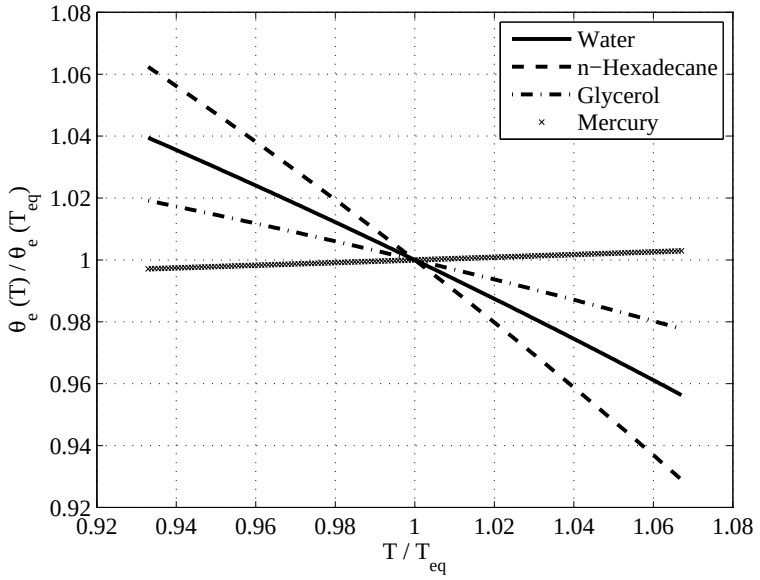

Figure 3.4: Non-dimensional SCAs versus non-dimensional temperatures with respect to reference temperature $T_{eq} = 298.15$ K for water, *n*-hexadecane, glycerol and mercury.

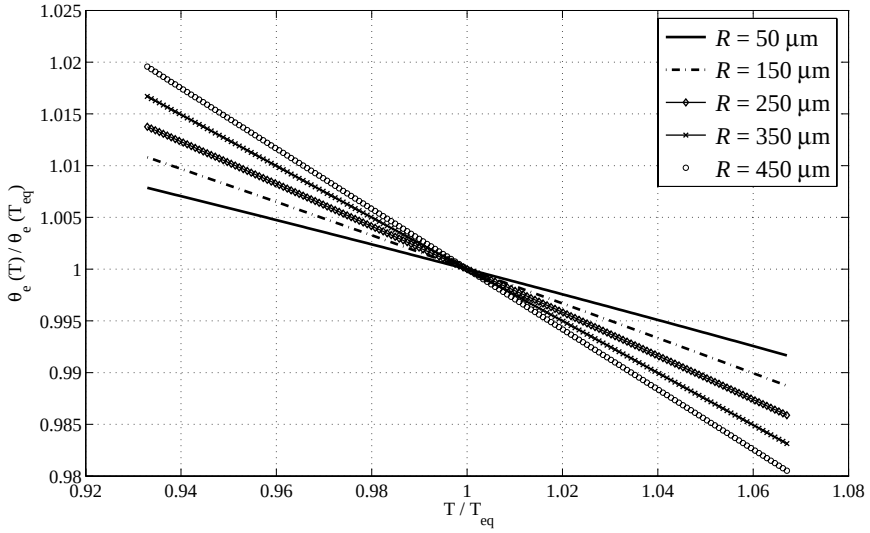

Figure 3.5: Non-dimensional SCAs-*vs.*-non-dimensional temperatures with respect to reference temperature $T_{eq} = 298.15$ K for water, assuming different R and keeping other parameters constant.

observed that the lighter fluid like *n*-hexadecane has more slope than other heavier fluids like water or glycerol or mercury (Figs. 3.5-3.6). The thermal variation of SCA is more for the lighter liquids. Magnitudes of slope, $|(\mathrm{d}\theta_e/\mathrm{d}T)|$ ($\equiv C_{\mathscr{H}}$) in decreasing order are: (1) *n*-hexadecane: 0.14461° K^{-1} and $\rho_l(T_{eq}) = 771.44$ kg m^{-3}, (2) water: 0.088505° K^{-1} and $\rho_l(T_{eq}) = 996.66$ kg m^{-3}, (3) glycerol: 0.043374° K^{-1} and $\rho_l(T_{eq}) = 1258.18$ kg m^{-3} and (4) mercury: 0.016932° K^{-1} and $\rho_l(T_{eq}) = 13533.13$ kg m^{-3}. This shows a dependency of densities of liquids on CAH. Thermal variation of θ_e depends only on $\theta_e(T_{eq})$ and the radius (R) of the capillary tube and does not depend on L. It is evident from Eq. (3.9) that $C_{\mathscr{H}}(T)$ is directly proportional to R for wetting fluids (see Fig. 3.5) and vice versa for non-wetting fluids (see Fig. 3.6) (if all other parameters remain constant). As $\theta_e(T_{eq})$ reduces in the case of wetting liquid (e.g. water from 89° to 10°) or increases in the case of non-wetting liquid (e.g. mercury from 91° to 170°), $|(\mathrm{d}\theta_e/\mathrm{d}T)|$ varies from 0.002° K^{-1} to 0.514° K^{-1} for water and 0.0002° K^{-1} to 0.145° K^{-1} for mercury (Fig. 3.7).

Another interesting observation is that $C_{\mathscr{H}}(T)$ tends to zero, or the curve of $\theta_e(T)$ becomes asymptote (Fig. 3.8) as $\theta_e(T)$ tends to 0° or 180° (from Eq. (3.10)). Hitherto, if the initial SCA ($\theta_e(T_{eq})$) is closer to the value of 0° or 180°, then the chances of $\theta_e(T)$ reaching asymptotic value are high, within small temperature ranges (especially for lighter liquids as they are much susceptible to temperature).

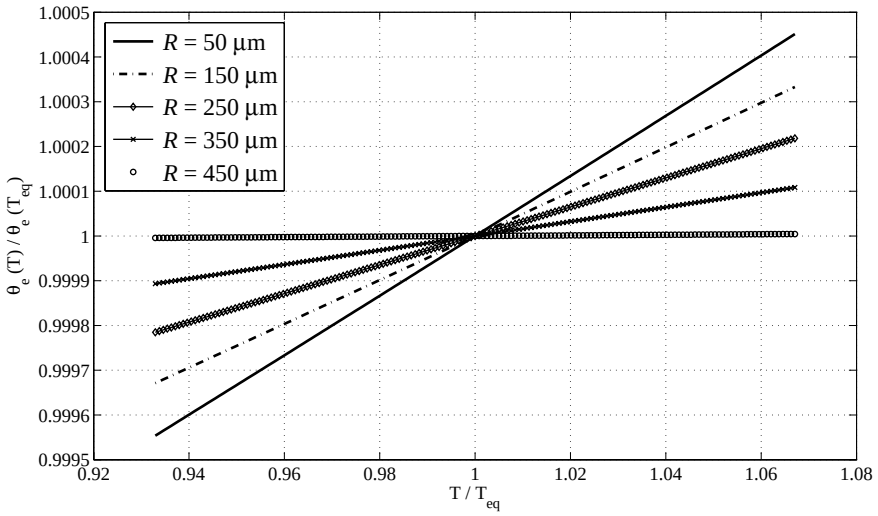

Figure 3.6: Non-dimensional SCAs-*vs.*-non-dimensional temperatures with respect to reference temperature $T_{eq} = 298.15$ K for mercury, assuming different R and keeping other parameters constant.

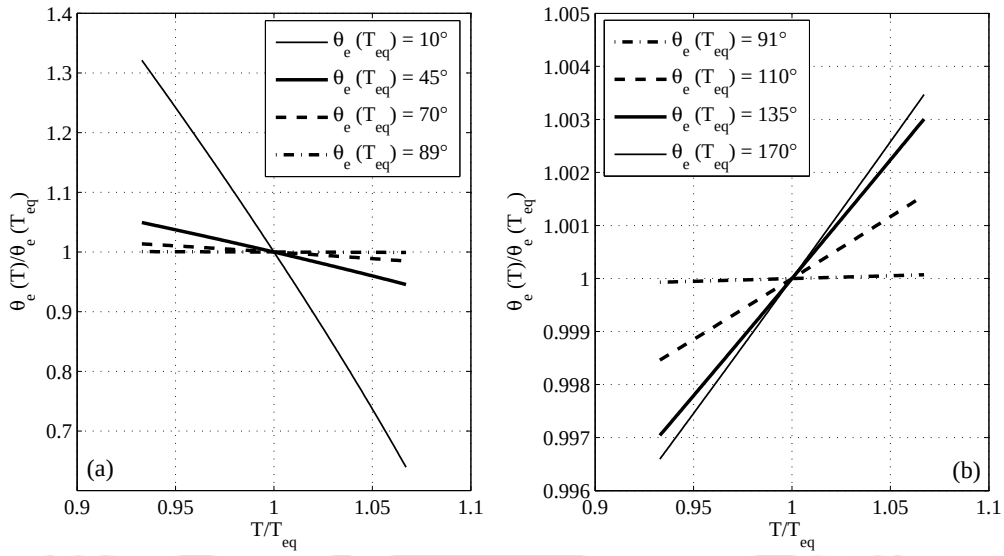

Figure 3.7: Non-dimensional SCAs versus non-dimensional temperatures with respect to reference temperature $T_{eq} = 298.15$ K for (a) water and (b) mercury, assuming different $\theta_e(T_{eq})$ and keeping other parameters constant.

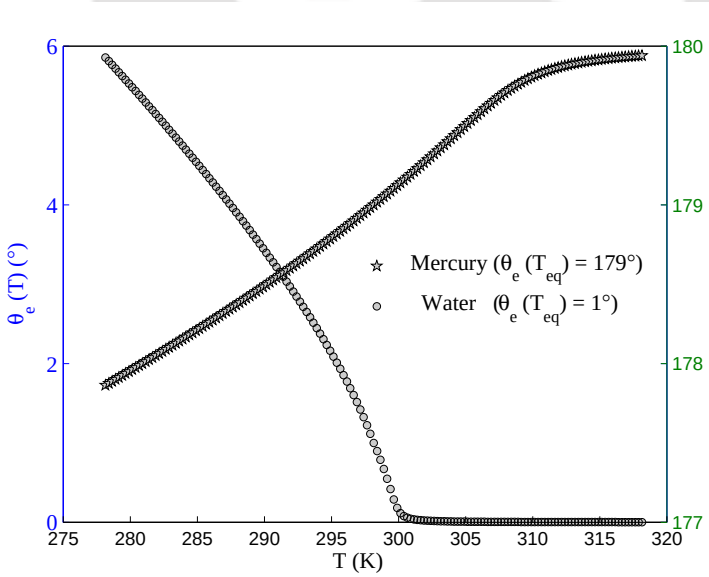

Figure 3.8: Temperature-dependent SCAs for mercury and water for temperature ranges of 298.15 K $\pm$ 20 K with $\theta_e(T_{eq}) = 179^\circ$ and 1° (i.e. closer values to stable angles) respectively.

3.3.1 Validation against published results

We have compared our results with the experimental values of Neumann et al. (1971) and with Adamson's potential distortion model (PDM) (Adamson, 1973) (see Fig. 3.9). We calculate our results for a particular liquid with known $\theta_e(T_{eq})$, $\sigma(T)$ and $\rho_l(T)$ (see Table 3.2). Our

model matches with experimental data quite well. Large range of temperatures shows that contact angle changes not exactly in linear fashion, also predicted by PDM (Adamson, 1973). This large range is just to show the non-linearity of θ_e-*vs.*-T relation. Adamson (1973) showed that contact angle will be zero at a critical temperature (T_c) . This is not true in our case as our model predicts that at stable angles (i.e. 0° or 180°), $\theta_e(T)$ becomes asymptotic with increasing temperature (see Fig. 3.8). This may be because we have not included interfacial energies of solid-air or solid-liquid that could be one of the reasons to reduce the asymptotic behavior near stable angles. Our model is specifically targeted to CAH due to CLP phenomenon. We assume in deriving the Eq. (3.9) that CLP happens within small range of T. Within small range of T, our model matches quantitatively with PDM and experimental result of Neumann et al. (1971) satisfactorily.

Table 3.2: Temperature-dependent properties required for verification purpose

Liquid on teflon	$\sigma(T)^{(1)}$	$\rho_l(T)^{(2)}$	θ_e ($T_{eq} = 288.15$ K)
n-octane	$0.04949 - 0.00009509T$	$703.1224 - 0.8099T - 0.0003471T^2$	$29.91°^{(3)}$
n-decane	$0.050792 - 0.00009197T$	$730.1536 - 0.7678T - 0.001962T^2$	$38.13°^{(4)}$
n-undecane	$0.05107 - 0.0000901T$	$740.7080 - 0.7064T - 0.0002179T^2$	$41.70°^{(4)}$

Data sources: $^{(1)}$: Jasper and Kring (1955), $^{(2)}$: Egloff (1939), $^{(3)}$: Sutula et al. (1967), $^{(4)}$: Neumann et al. (1971)

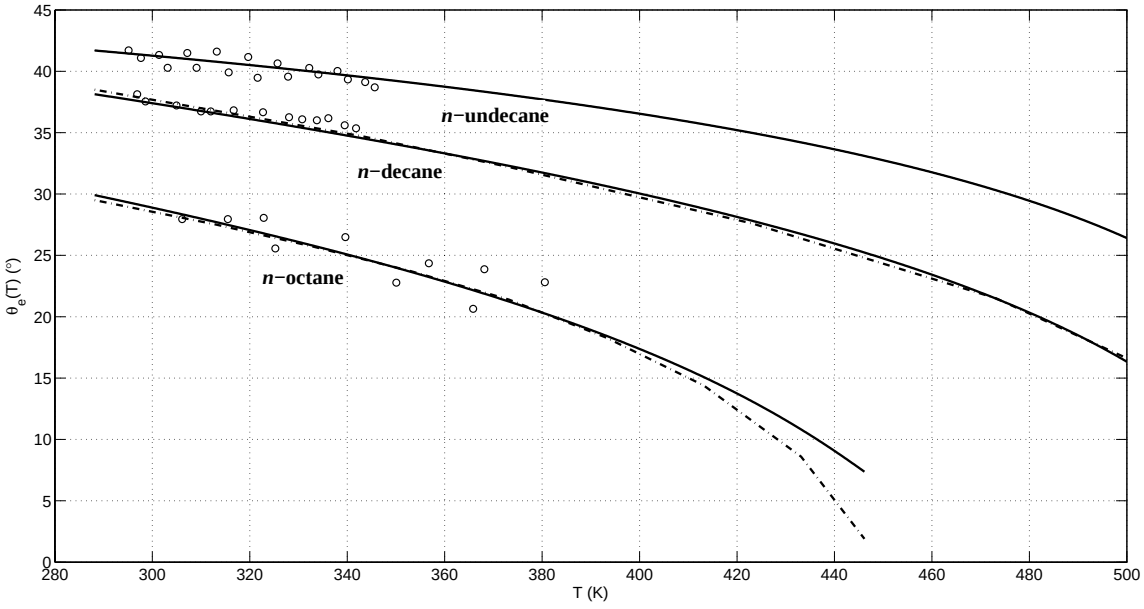

Figure 3.9: SCAs-*vs.*-T on teflon for liquids: *n*-octane ($R = 800$ μm), *n*-decane ($R = 400$ μm) and *n*-undecane ($R = 40$ μm) with L being 0.5 m and $\rho_a(T)$ being same as in Fig. 3.2. Here symbols - circle (○), dash-dot ($-\cdot$), and solid line ($-$) represent the results of experiment, PDM, and our model respectively. Experimental data of *n*-octane are taken from Sutula et al. (1967) (through Adamson, 1973), and *n*-decane and *n*-undecane from Neumann et al. (1971).

3.4 Summary

Spherical shape of meniscus is assumed based on the fact that effects of surface forces overrides the effects of gravity and further extension of this logic gives that gravitational effect is negligible on meniscus shape. Hyperbolic nature of meniscus within two parallel plates (Hauksbee, 1710), inspired us to represent meniscus in the catenary form in a cylindrical capillary tube. The inclusion of meniscus shape in Jurin height helps to accommodate the temperature sensitive SCA. The thermal derivative of static or quasi-static equilibrium equation gives a non-linear ordinary differential equation, which is solved with the numerical RK4 method. The SCAs decrease with temperature for wetting liquids and increase for non-wetting liquids. The SCAs ($\theta_e(T)$) of lighter liquids are more susceptible to changes in temperature. Initial SCA and radius of the tube has an impact on CAH (from different model, Kuchin and Starov (2016) also concludes that $C_{\mathscr{H}}$ is dependent upon R). If the value of $\theta_e(T_{eq})$ is near to 0° or 180°, the CAH is more prominent. This theoretical model investigates CAH due to small temperature perturbations. The variations in fluid properties like pressure, surface tension, and density, etc. are more of a resultant of temperature differentials. Therefore, we conclude that temperature is an intrinsic reason for CAH. Validation with published data shows the potential of inclusion of meniscus shape and then eventual effect on SCA with temperature. We have tried an extended form of Eq. (3.2) and P_c as presented in Appendix-A3.3, which fails to validate the experimental P_c results using the proposed steps and algorithm to calculate P_c in the next chapter. However this model validates the experimental results of θ_e with the meniscus and show a promise. Thus, we start with a more general form of the shape in the next shape and effects of temperature on SCA and capillary pressure.

A3 Appendix

A3.1 Dynamic contact angle

In dynamic equilibrium, the dynamic CA (DCA, θ_d), which depends on the meniscus velocity (i.e. $u = \mathrm{d}\bar{z}/\mathrm{d}t$), is used in capillary dynamics rather than the SCA. Accordingly, the equation of DCA is:

$$\cos(\theta_d) = \cos(\theta_e) - \mathrm{sgn}(u) f_u(u), \tag{A3.1}$$

where $f_u(u)$ is a function of meniscus velocity derived by many researchers (Blake and Haynes, 1969; Mumley et al., 1986; Chebbi, 2007; Hilpert, 2009, and others). At this juncture,

$\cos(\theta_e)$ can be replaced by $\tanh(\kappa(T))$. Therefore, the new form for DCA will be:

$$\cos(\theta_d(T)) = \begin{cases} \tanh(\kappa(T)) \ \forall \ T \in [T_{lc}, T_{uc}]. \\ \tanh(\kappa(T_{uc})) - \mathrm{sgn}(v) f_v(v) \ \forall \ T > T_{uc}. \\ \tanh(\kappa(T_{lc})) - \mathrm{sgn}(v) f_v(v) \ \forall \ T < T_{uc}. \end{cases} \tag{A3.2}$$

This work can be thought of as a precursor of study on capillary dynamics.

A3.2 Multicomponent fluid system

An example of a multiphase, multicomponent liquid system involving water-ethanol mixture with multi-component air is analysed in this research. Following the approach described by Maggi and Alonso-Marroquin (2013), density and surface tension of mixture are assumed to be linear or non-linear combination of densities and surface tensions of pure components (in this case, water and ethanol, subscripted as w and el on parameters respectively):

Density of the mixture is:

$$\rho_{w-el} = x_w \rho_w + x_{el} \rho_{el}, \tag{A3.3}$$

where, x_i and ρ_i represent the mass fraction and density of i-component of the mix respectively.

Surface tension of the mixture is:

$$\sigma_{w-el} = \left(\vartheta_{sw} (\sigma_w)^{1/4} + \vartheta_{sel} (\sigma_{el})^{1/4} \right)^4, \tag{A3.4}$$

where, σ_i and ϑ_{si} are the surface tension and the superficial volume fraction of i-component that is obtained by solving the Eqs. (A3.5a)-(A3.5b) (Tamura et al., 1955):

$$\log\left(\frac{\vartheta_{sw}}{\vartheta_{sel}}\right) = \log\left(\frac{\vartheta_w}{\vartheta_{el}}\right) + \frac{0.441q}{T}\left(\frac{\sigma_{el}\mathcal{V}_{el}^{2/3}}{\eth} - \sigma_w \mathcal{V}_w^{2/3}\right), \tag{A3.5a}$$

$$\vartheta_{sw} + \vartheta_{sel} = 1, \tag{A3.5b}$$

where, $\vartheta_j = x_j \mathcal{V}_j / (x_w \mathcal{V}_w + x_j \mathcal{V}_j)$ and $\vartheta_w = x_w \mathcal{V}_w / (x_w \mathcal{V}_w + x_j \mathcal{V}_j)$; $\mathcal{V}_w$, $\mathcal{V}_j$ are molar volumes of water and j-component [m^3 mol^{-1}] respectively; $\eth$ is the number of carbon atoms in j-component; and T is the temperature [K].

In addition, the initial SCA for the mixture is also assumed as a linear combination of the initial SCAs of pure components (Table 3.1). That is:

$$\theta_e(T_{eq}) = x_w \theta_w(T_{eq}) + x_{el} \theta_{el}(T_{eq}). \tag{A3.6}$$

The thermal variation of SCA of the mixture is deduced here for different constant temperatures. The temperatures are included explicitly in thermal dependent properties of water and ethanol (Fig. 3.2) and the properties of the mixture at those temperatures are computed from the equations as mentioned earlier of the mix (Eqs. (A3.3)-(A3.6)). For four mass fraction values of ethanol (f $= x_{el}$) with $R = 0.03296 \times 10^{-3}$ m and $L = 0.25$ m, Eq. (3.9) is solved for $\theta_e(T)$ at constant temperatures for the water-ethanol mixture with air (Fig. A3.1).

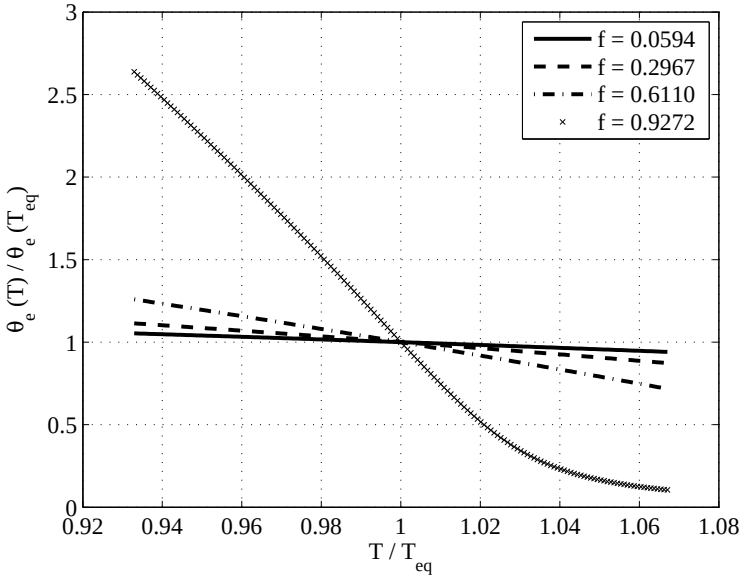

Figure A3.1: Non-dimensional SCAs versus non-dimensional temperatures with respect to reference temperature $T_{eq} = 298.15$ K for water-ethanol mixture at different mass fractions of ethanol (f).

A3.3 Extension of meniscus form

We extend Eq. (3.2) in a general form (subscripted as 'gf'):

$$z_{\mathrm{gf}}(r) = \sum_{k=0}^{n-1} A_i \cosh\left(\frac{ir}{A_i}\right). \tag{A3.7}$$

Coefficients, A_i can be evaluated depending on n numbers of boundary conditions. Two conditions need to be satisfied for any analytic form to be considered:

Condition I.

$$|z(r) - z_{\mathrm{gf}}(r)| \approx 0 \;\forall\; r \in [0, R]. \tag{A3.8a}$$

Condition II. (Boundary conditions):

$$\text{Primary conditions: } z_{\text{gf}}(r=0)=h_\infty,\ z_{\text{gf}}(r=R)=h_l, \tag{A3.8b}$$

$$\text{Auxilary condition: } \left.\frac{\mathrm{d}z_{\text{gf}}}{\mathrm{d}r}\right|_{r=R}=\cot(\theta). \tag{A3.8c}$$

Equation (A3.7) becomes (based on Eqs. (A3.8b) i.e. $n=2$):

$$z_{\text{gf}}(r)=A_0+A_1\cosh\left(\frac{r}{A_1}\right). \tag{A3.9}$$

Condition II (Eqs. A3.8b-A3.8c) gives:

$$A_0+A_1=h_\infty,\ A_0+A_1\cosh\left(\frac{R}{A_1}\right)=h_l, \tag{A3.10a}$$

$$\sinh\left(\frac{R}{A_1}\right)=\cot(\theta). \tag{A3.10b}$$

Primary conditions (Eqs. (A3.8b)) are not enough to solve coefficients A_i. Therefore, auxilary condition is invoked and Eqs. (A3.10) result in:

$$\sinh\left[\frac{R\left(\sqrt{1+\mathscr{A}_u{}^2}-1\right)}{h_m}\right]=\mathscr{A}_u, \tag{A3.11}$$

where $h_m=h_l-h_\infty$ and $\mathscr{A}_u=\cot(\theta)$. If you know h_m, you have to solve a non-linear equation of $\mathscr{A}_u$ (Eq. (A3.11)). Consequently, we can find:

$$A_1=\frac{R}{\sinh^{-1}(\mathscr{A}_u)}\ \text{and}\ A_0=h_\infty-A_1. \tag{A3.12}$$

The final form of the expression will be:

$$z(r)\approx h_\infty+\frac{R}{\sinh^{-1}(\mathscr{A}_u)}\left[\cosh\left(\frac{r\sinh^{-1}(\mathscr{A}_u)}{R}\right)-1\right]. \tag{A3.13}$$

This analytic expression can be used to calculate the capillary pressure from the following

form (using Eq. (3.4), (3.5) and (3.6)):

$$P_c = \frac{2\sigma}{\left[\frac{A_1^2}{4R}\sinh\left(\frac{2R}{A_1}\right) + \frac{A_1}{2}\right]}. \tag{A3.14}$$

CHAPTER 4

Temperature Effects on Capillary Pressure with Generalized Meniscus

4.1 Introduction

Flow in pore spaces like soil has been studied by substituting the pore space as bundles of cylindrical capillary tubes. Flow in capillary tube can be thought of, as an equivalent system to study the flow in porous media with proper assumptions. The flow problem in capillary tube (i.e. study of dynamics) started with the studies of flow in capillary spaces by Bell and Cameron (1906). Mathematical theory of capillary dynamics is first described by Lucas (1918) and then independently by Washburn (1921). The Lucas-Washburn theory (LWT), which is also called capillary model theory in porous media, was used to model the porous media as bundle of cylindrical capillary tubes. Laplace (1805) gave the first formal description of capillary pressure in terms of mean curvature of meniscus. Inclusion of this theory into curved surface of liquid-air interface or meniscus in a capillary tube and extension to soil pores is studied by many researchers (Collins, 1961; Dullien et al., 1977; Or and Tuller, 1999; Bear et al., 2011, and others).

In this chapter, first we introduce a new approach to calculate meniscus shape considering both liquid and air for the static case. In subsequent sections, we calculate the effects of temperature on meniscus shape. Finally, we calculate the capillary pressure for different soils.

4.2 Equation of meniscus shape

We start with an assumption that the surface tension (σ, N m^{-1}) as constant throughout the radius r [m], of the capillary cylinder, and assuming the phreatic surface as datum and the center-line as z-axis, the combined weight of liquid and air inside the tube is a function of this capillary radius:

$$w(r) = \rho_l g z(r) + \rho_a g\,(L - z(r)) = \rho_d g z(r) + \rho_a g L \;\forall\; r \in [0, R], \tag{4.1}$$

where ρ_l is the density of liquid [kg m^{-3}], ρ_a is the density of air [kg m^{-3}], $\rho_d = \rho_l - \rho_a$, $z(r)$ is the meniscus height above datum line at perpendicular distance r from z-axis.

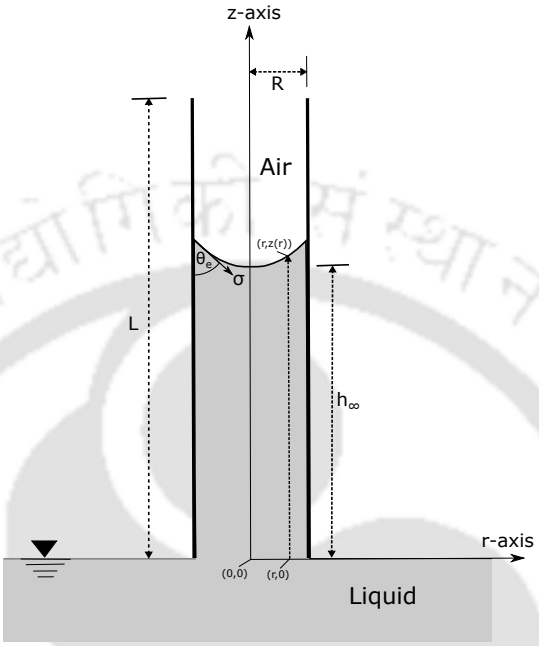

Figure 4.1: Schematic diagram of a capillary tube

Phenomenologically it can be said that the slope of the meniscus is resultant of vertical and horizontal forces acting over the meniscus. This assumption generates a differential equation of $z(r)$ (lets call this equation *phenomenological meniscus equation*, PME) (see Appendix-A4.1):

$$\frac{\mathrm{d}^2 z(r)}{\mathrm{d}r^2} = \frac{w(r)}{\sigma}\sqrt{1+\left(\frac{\mathrm{d}z(r)}{\mathrm{d}r}\right)^2} + \frac{\rho_d g}{w(r)}\left(\frac{\mathrm{d}z(r)}{\mathrm{d}r}\right)^2, \tag{4.2}$$

with boundary conditions as: $\mathrm{d}z/\mathrm{d}r|_{r=0} = 0$ and $z(r=0) = h_\infty$ (Eq. (3.1)).

We trial with known values from literature (Maggi and Alonso-Marroquin, 2012; Extrand and Moon, 2013) to investigate the new form of meniscus shape (Eq. (4.2)). Using the liquid properties of Table 4.1, Equation (4.2) is numerically solved using the 4$^{\text{th}}$ order Runge-Kutta method (RK4) for different liquids (taking $L = 0.08$ m, $\theta_e = 0^\circ$ and $\rho_a = 1.2$ kg m^{-3}) and results are shown in Fig. 4.2. Interplay of surface tension and gravity is visible in every meniscus shape. Slopes or contact angle values show the limitations of the approach.

Table 4.1: Properties of liquid used in Eq. (4.2) for $z(r)$ calculation

Liquid	R [mm]	σ [mN m^{-1}]	ρ_l [kg m^{-3}]	Reference
Ethanol	0.295	22	789	Maggi and Alonso-Marroquin (2012)
Water	0.295	72	998	Maggi and Alonso-Marroquin (2012)
Ethylene Glycol	0.250	48	1110	Extrand and Moon (2013)
Glycerol	0.600	65	1260	Extrand and Moon (2013)

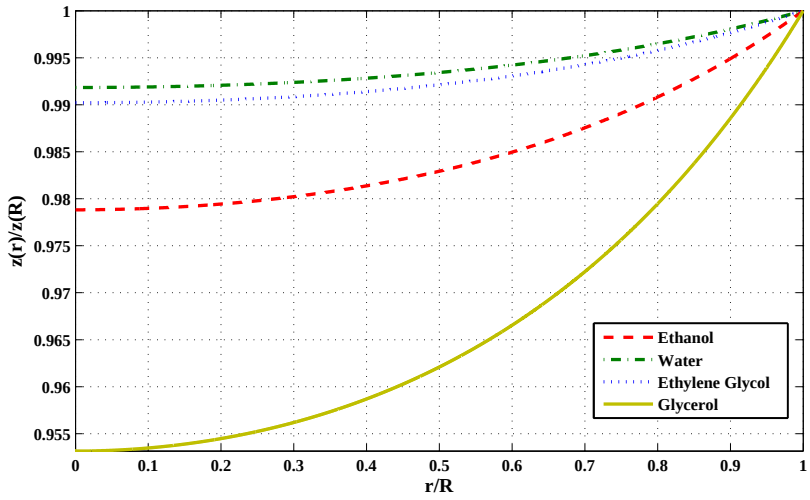

Figure 4.2: Dimensionless meniscus shapes i.e. $z(r)/z(R)$ versus r/R for liquids: (a) ethanol, (b) water, (c) ethylene glycol and (d) glycerol

Caveat: The initial SCA value is used as 0° as an input through h_∞. From $\mathrm{d}z/\mathrm{d}r|_{r=R}$, we can calculate $\theta_a = \cot^{-1}(\mathrm{d}z/\mathrm{d}r|_{r=R})$. Here θ_a is the *apparent contact angle* (ACA), as defined by Lee and Lee (2007) (p. 957) as "...a macroscopic angle formed by the solid wall and the tangent plane to the free surface at a *certain* distance from the contact line ...often used as an auxiliary concept in interpreting the experimental observations" and not equal to the theoretical value of SCA (θ_e). This part also is discussed The results are: (a) $\theta_a = 14.83°$ for ethanol, (b) $\theta_a = 15.23°$ for water, (c) $\theta_a = 15.17°$ for ethylene glycol and (d) $\theta_a = 14.31°$ for glycerol. These disparities of θ_e and θ_a come from the fact that liquid experiences some forces near the solid wall. These forces are long range forces ($\propto 1/(R-r)^n$, n is an integer and $n \geq 2$) like van der Waals forces (where n is 6, see p. 94 of De Gennes et al., 2004). These forces are not included in Eq. (4.2) and so does exist the disparity. Long-range forces dominate over a certain distance and after that become weak. Lets say this distance be some δ [m] from the tube wall. It can be said that within this length our approach will not work. Equation (4.2) is valid up to the range: $r \in [0, R-\delta)$. As an example, we take van der Waals force as a long-range force. Now maximum dominancy limit of van der Waals force is $\sim$ 1000 Å (De Gennes et al., 2004, p. 101). Hansen and Toong (1971) also showed in their

paper that the classical concepts of interface behaviour is inapplicable at distances less than $100-1000$ Å. Equation (4.2) is valid for $r \in [0, R_e)$ (where $R_e = R - \delta$). Let's state R_e as *effective* radius. Assumption is that within this indiscernible length (δ), meniscus will reach from θ_a to $\theta_e = 0^\circ$ value. This disparity may be remedied including a molecular component of disjoining pressure. We give a plausible form of the equation including the component in Appendix-A4.2.

4.2.1 Modified PME

We modify the highly non-linear ordinary differential equation PME to make the problem more tractable and solvable. To do so, we neglect the air column density* term being two to three orders of magnitude less denser than the liquid column density based on the following analysis of the order of magnitudes† of the terms of $w(r)$:

$$\begin{aligned}
\rho_l \sim \mathcal{O}\left(10^2\right) \text{ or } \mathcal{O}\left(10^3\right),\ \rho_a \sim \mathcal{O}\left(10^0\right),\\
z(r) \sim \mathcal{O}\left(10^{-1}\right),\ L \sim \mathcal{O}\left(10^{-1}\right).\\
\rho_l - \rho_a = \rho_d \sim \mathcal{O}\left(10^2\right) \text{ or } \mathcal{O}\left(10^3\right).\\
\rho_d z(r) \sim \mathcal{O}\left(10^1\right) \text{or } \mathcal{O}\left(10^2\right),\ \rho_a L \sim \mathcal{O}\left(10^{-1}\right).\\
\frac{\rho_d z(r)}{\rho_a L} \sim \mathcal{O}\left(10^2\right) \text{or } \mathcal{O}\left(10^3\right).
\end{aligned}$$

This infers that $w(r) = \rho_d g z(r) + \rho_a g L \approx \rho_d g z(r)$ and replacing this expression of $w(r)$ in Eq. (4.2), PME becomes *modified* PME (*m*PME) as

$$\frac{\mathrm{d}}{\mathrm{d}r}\left(\frac{1}{z(r)}\frac{\mathrm{d}z(r)}{\mathrm{d}r}\right) - \sqrt{\xi\left(1+\left(\frac{\mathrm{d}z(r)}{\mathrm{d}r}\right)^2\right)} \approx 0, \tag{4.3}$$

where $\sqrt{\xi} = (\rho_d g)/\sigma$.

*Column fluid density or area density [kg m^{-2}] is obtained from integrating volumetric density over a column (see p. 470 of Visconti, 2001).

†Magnitude of a physical variable $x := \mathtt{mag}(x)$. Let's say the order of $\mathtt{mag}(x)$ is y, i.e. $x \sim \mathcal{O}(10^y)$, where $y = \lfloor \log_{10}(\mathtt{mag}(x)) \rfloor$. Example, for $\rho_{\text{ethanol}} = 789$ kg m^{-3}, $\rho_{\text{glycerol}} = 1260$ kg m^{-3}, and $\rho_{\text{air}} = 1.2$ kg m^{-3}, orders of $\mathtt{mag}(\rho)$ will be: $\rho_{\text{ethanol}} \sim \mathcal{O}(10^2)$, $\rho_{\text{glycerol}} \sim \mathcal{O}(10^3)$, and $\rho_{\text{air}} \sim \mathcal{O}(10^0)$.

Series solution of *m*PME using H2LTM method

We solve the modified version of PME in this section. We use the transformation of $k(r) = \ln(z(r))$ in Eq. (4.3) and square both sides. Equation (4.3) becomes

$$\left(\frac{\mathrm{d}^2k}{\mathrm{d}r^2}\right)^2 - \xi e^{2k}\left(\frac{\mathrm{d}k}{\mathrm{d}r}\right)^2 - \xi \approx 0, \tag{4.4}$$

with modified boundary conditions of $k(0) = \ln(h_\infty)$ and $\mathrm{d}k/\mathrm{d}r|_{r=0} = 0$.

Taking the Laplace transform of Eq. (4.4), we have,

$$\mathscr{L}\left\{\left(\frac{\mathrm{d}^2k}{\mathrm{d}r^2}\right)^2\right\} - \xi\mathscr{L}\left\{e^{2k}\left(\frac{\mathrm{d}k}{\mathrm{d}r}\right)^2\right\} - \frac{\xi}{s} \approx 0, \tag{4.5}$$

where $\mathscr{L}\{f(t)\}(s) = \int_0^\infty f(t)\,e^{-st}dt$ is the Laplace transform of a function $f(t)$ defined for $t \geq 0$ and s is a *complex number* frequency parameter with $s = s_{\text{real}} + is_{\text{imaginary}}$ and $i = \sqrt{-1}$ (see Abramowitz and Stegun, 1972 for more details). We are going to apply H2LTM method (Fatoorehchi and Abolghasemi, 2016) to tackle the non-linear terms by Laplace transform method (LTM). Fatoorehchi and Abolghasemi gave three novel theorems to handle non-linear terms in LTM using well-known Adomian polynomials (one may refer Adomian, 1994).

Applying Theorems 3.3 and 3.4 of Fatoorehchi and Abolghasemi (2016) to Eq. (4.5), we have,

$$\sum_{i=0}^{\infty} A_i(d_0,\ldots,d_i)\frac{i!}{s^{i+1}} - \xi\sum_{i=0}^{\infty}\mathscr{L}\left\{A'_i\left(c_0,\ldots,c_ir^i\right)\right\} - \frac{\xi}{s} \approx 0, \tag{4.6}$$

where $d_i = (i+1)(i+2)c_{i+2}$; and A_i and A'_i are the Adomian polynomials. Assuming $k(r) = \sum_{i=0}^{\infty} c_ir^i$, the two modified boundary conditions give $c_0 = \ln(h_\infty)$ and $c_1 = 0$.

Decomposing the non-linearity $N(k) = \left(\mathrm{d}^2k/\mathrm{d}r^2\right)^2$ (first part of the left hand side of Eq. (4.6)) with the simple algorithm of calculating Adomian polynomials proposed by Biazar and Shafiof (2007), we have,

$$\begin{aligned}
&A_0(d_0) = {d_0}^2 = 4{c_2}^2,\ A_1(d_0,d_1) = 2d_0d_1 = 24c_2c_3,\\
&A_2(d_0,d_1,d_2) = 2d_0d_2 + {d_1}^2 = 36{c_3}^2 + 48c_2c_4,\\
&A_3(d_0,d_1,d_2,d_3) = 2d_0d_3 + 2d_1d_2 = 144c_3c_4 + 80c_2c_5,\\
&A_4(d_0,d_1,d_2,d_3,d_4) = {d_2}^2 + 2d_1d_3 + 2d_0d_4 = 144{c_4}^2 + 240c_3c_5 + 120c_2c_6,\\
&\vdots
\end{aligned}$$

We compute the Adomian polynomials related to the non-linearity $N(k) = e^{2k}(\mathrm{d}k/\mathrm{d}r)^2$ (second part of the left hand side of Eq. (4.6)) as

$$
\begin{aligned}
&A'_0(c_0) = 0,\ A'_1(c_0, c_1 r) = 0,\ A'_2\left(c_0, c_1 r, c_2 r^2\right) = 0,\ A'_3\left(c_0, c_1 r, c_2 r^2, c_3 r^3\right) = 0,\\
&A'_4\left(c_0, c_1 r, c_2 r^2, c_3 r^3, c_4 r^4\right) = 4e^{2c_0} {c_2}^2 r^2 = 4{h_\infty}^2 {c_2}^2 r^2,\\
&A'_5\left(c_0, c_1 r, c_2 r^2, c_3 r^3, c_4 r^4, c_5 r^5\right) = 12{h_\infty}^2 c_2 c_3 r^3,\\
&A'_6\left(c_0, c_1 r, c_2 r^2, c_3 r^3, c_4 r^4, c_5 r^5, c_6 r^6\right) = \frac{{h_\infty}^2}{15}\left(40{c_2}^3 + 135{c_3}^2 + 240 c_2 c_4\right) r^4,\\
&\vdots
\end{aligned}
$$

Putting the above expansions of Adomian polynomials in Eq. (4.6), we have,

$$
\begin{aligned}
&\left(A_0\frac{0!}{s} + A_1\frac{1!}{s^2} + A_2\frac{2!}{s^3} + \cdots\right) - \xi\mathscr{L}\left(A'_4 + A'_5 + A'_6 + \cdots\right) - \frac{\xi}{s} \approx 0,\\
&\left(A_0\frac{0!}{s} + A_1\frac{1!}{s^2} + A_2\frac{2!}{s^3} + A_3\frac{3!}{s^4} + A_4\frac{4!}{s^5} + \cdots\right)\\
&-\xi\left(\begin{array}{l}\left(4{c_2}^2{h_\infty}^2\right)\dfrac{2!}{s^3} + \left(12 c_2 c_3 {h_\infty}^2\right)\dfrac{3!}{s^4}\\ +{h_\infty}^2\left(\dfrac{8}{3}{c_2}^3 + 9{c_3}^2 + 16 c_2 c_4\right)\dfrac{4!}{s^5} + \cdots\end{array}\right) - \frac{\xi}{s} \approx 0.
\end{aligned}
\tag{4.7}
$$

Comparing the both sides of Eq. (4.7) for coefficients of s, we get,

$$
\begin{aligned}
&c_2 = \frac{\xi^{1/2}}{2}, c_4 = \frac{{h_\infty}^2\xi^{3/2}}{24},\\
&c_6 = \frac{{h_\infty}^2\xi^2\left(4 + {h_\infty}^2\xi^{1/2}\right)}{720}, c_8 = \frac{{h_\infty}^4\xi^3\left(9 + {h_\infty}^2\xi^{1/2}\right)}{41040},\\
&c_{10} = \frac{{h_\infty}^4\xi^{7/2}\left(-6384 + 8304{h_\infty}^2\xi^{1/2} + 55{h_\infty}^4\xi\right)}{147744000},\\
&c_{12} = -\frac{{h_\infty}^6\xi^{9/2}\left(-1052160 + 327376{h_\infty}^2\xi^{1/2} + 869{h_\infty}^4\xi\right)}{42904857600},\\
&\vdots
\end{aligned}
\tag{4.8}
$$

and $c_i = 0$ (where $i = 3, 5, 7, \ldots$).

The solution of Eq. (4.4) is:

$$
k(r) = \sum_{i=0}^{\infty} c_{2i} r^{2i} = c_0 + c_2 r^2 + c_4 r^4 + \cdots,
$$

$$= \ln(h_\infty) + k_s(r), \text{ where } c_0 = \ln(h_\infty) \text{ and } k_s(r) = \sum_{i=1}^{\infty} c_{2i} r^{2i}, \tag{4.9}$$

and thus the solution of Eq. (4.3) becomes (subscripted as 'mP' for *m*PME solution),

$$z(r) \approx z_{\mathrm{mP}}(r) = e^{k(r)} = h_\infty \left[\cosh(k_s(r)) + \sinh(k_s(r))\right]. \tag{4.10}$$

Figure 4.3 shows the result of above equation taking varied degree of r starting from 2. We show in this figure of meniscus with taking up to 14^{th} degree power of r in $k_s(r)$ and all these shapes overlap on each other. As it can be seen that as the degree of r goes from lower to higher in Eq. (4.10), the meniscus shape converges to a stable shape. With different radii (R), terms of series may vary to converge to a stable shape, but it does not go more than 12^{th} degree power. We are not showing any of these results to keep the thesis uncluttered.

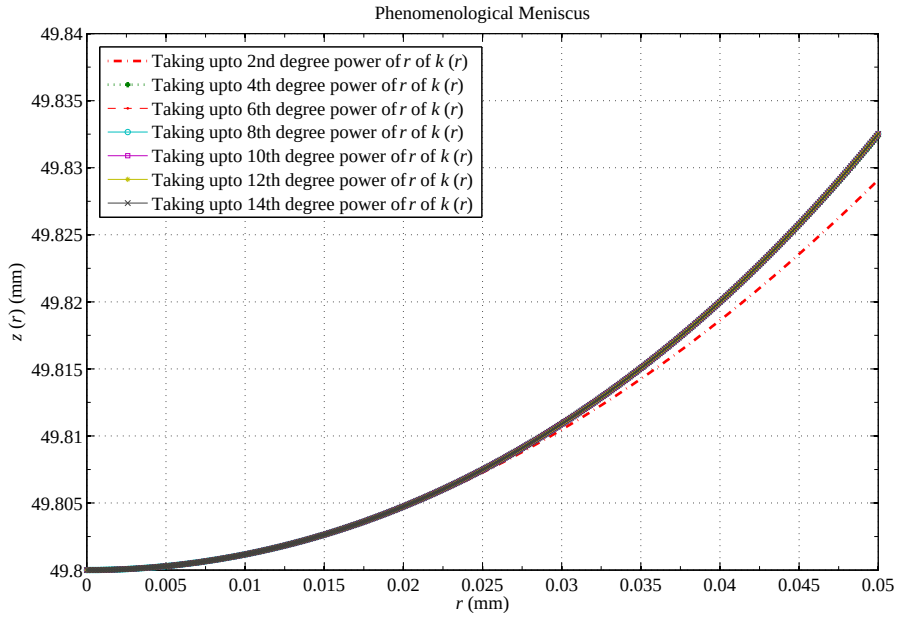

Figure 4.3: Meniscus shape $z_{\mathrm{mP}}(r)$ of water-air in a cylindrical tube with assumed values of $\rho_d = 1000$ kg m^{-3}, $\sigma = 72$ mN m^{-1}, $R = 50$ μm, $h_\infty = 49.8$ mm taking up to 2^{nd} till 14^{th} degree of r in $k(r)$

A comparison between numerical solution by RK4 (achieved by making $L = 0$ in the numerical code of PME) and analytical solution of *m*PME, is done for ethanol-air meniscus and the result is given in Fig. 4.4. This validates our numerical code. We checked the numerical code with different Δr values (10^{-6} m to 10^{-10} m) and numerical and analytical solution match well.

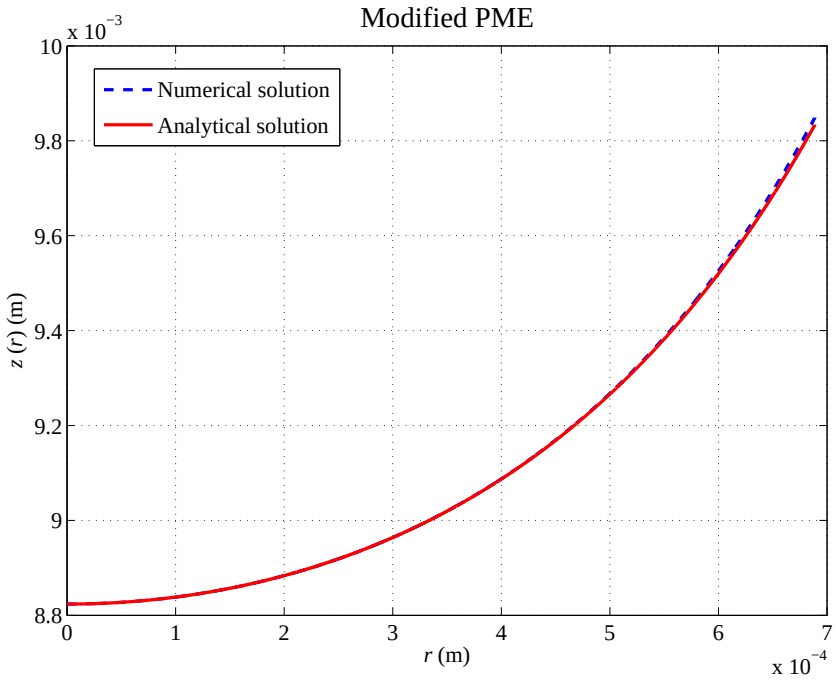

Figure 4.4: Comparison between numerical RK4 and analytical solution of Eq. (4.3) for meniscus shape of ethanol-air in a cylindrical tube with assumed values of $\rho_d = 782.65$ kg m^{-3}, $\sigma = 23.4$ mN m^{-1}, $R = 0.689$ mm, $\theta_e = 0^\circ$

4.3 Temperature effects on capillary pressure

As per Laplace's theorem (De Gennes et al., 2004), capillary pressure (P_c) across the liquid-air interface (meniscus) is product of surface tension of liquid and mean curvature of the meniscus. Equation (4.2) describes the meniscus shape i.e. $z(r)$. Mean curvature (K_m [m^{-1}]) denotes the average of inverses of two principle radii of the curvature (R_1, R_2).

$$\text{Capillary pressure, } P_c = \sigma\left(\frac{1}{R_1} + \frac{1}{R_2}\right) = \sigma \times K_m. \tag{4.11}$$

We introduce temperature T [K] in capillary pressure relation (Eq. (4.11)) through surface tension, $\sigma(T)$ and mean curvature, K_m, i.e. through densities of air and of liquid. These effects of temperature are intrinsic to the fluid properties.

Calculation of mean curvature (K_m): Mean curvature can be evaluated from mean radius (R_m) and mean radius from the radius of meniscus (see Piskunov, 1969, p. 217) averaged over the r-axis (see Eq. (4.12)). Mean radius will be equal in two principal axes and therefore,

$R_1 = R_2 = R_m$:

$$K_m = \left(\frac{1}{R_1} + \frac{1}{R_2}\right) = \frac{2}{R_m};\ R_m = \frac{1}{R}\int_0^R \frac{\left[1 + \left(\frac{\mathrm{d}z}{\mathrm{d}r}\right)^2\right]^{\frac{3}{2}}}{\left|\frac{\mathrm{d}^2 z}{\mathrm{d}r^2}\right|}\mathrm{d}r. \tag{4.12}$$

From the series solution of *m*PME (Eq. (4.10)), we have,

$$K_m = \frac{2M}{R\sqrt{1+(M)^2}};\ M = 2z_{\mathrm{mP}}(R)\sum_{i=1}^{\infty} i c_{2i} R^{2i-1}, \tag{4.13}$$

where $z_{\mathrm{mP}}(R) = h_\infty e^{k_s(R)}$, $k_s(R) = c_2R^2 + c_4R^4 + c_6R^6 + \cdots$. Numerical value of mean curvature can be found by summing the above series in M up to some finite terms (let's say n no. of terms). So, we can write K_m as

$$K_m \approx K_{m(n)} \text{ where } K_{m(n)} = \frac{2M_{(n)}}{R\sqrt{1+\left(M_{(n)}\right)^2}}; \tag{4.14}$$

$$M_{(n)} = 2z_{\mathrm{mP}(n)}(R)\sum_{i=1}^{n} i c_{2i} R^{2i-1},\ z_{\mathrm{mP}(n)}(R) = h_\infty e^{k_{s(n)}(R)}, \tag{4.15}$$

$$\text{and } k_{s(n)}(R) = c_2R^2 + c_4R^4 + \cdots + c_{2n}R^{2n}.$$

Numerically we have $z(r)$ values at $(n+1)$ locations solving Eq. (4.2) using RK4 with *small* enough $\Delta r = R/n$. Equation (4.12) can be approximated using finite difference equations and we have:

$$K_m \approx \frac{2}{n}\sum_{i=0}^{n} \frac{\left|\frac{z_i - 2z_{i-1} + z_{i-2}}{(\Delta r)^2}\right|}{\left[1 + \left(\frac{z_i - z_{i-1}}{\Delta r}\right)^2\right]^{3/2}}, \tag{4.16}$$

where $z_i = z(i \times \Delta r)$ (i-th component of $z(r_i)$ is calculated at $(n+1)$ numbers of locations, i.e., n segments of radius R from $r = 0$ to $r = R$) and $z_0 = h_\infty$. The symmetry of the problem w.r.t. z-axis, provides $z_{-1} = z_1$ and $z_{-2} = z_2$.

Therefore, we can calculate capillary pressure - analytically (from Eq. (4.13)) or numerically (from Eq. (4.16)) from Eq. (4.11).

4.3.1 Steps to calculate capillary pressure in a porous media (soil)

In this paper, we illustrate our theory in the domain of soil or any porous media structurally similar to soil. To identify soil, we need to know the *soil texture*. Soil texture refers to the size range of particles in the soil and particle sizes in soils is traditionally characterized by dividing the array of possible particle sizes into some separate size ranges known as *soil separates*, namely, sand (0.05-2 mm), silt (0.002-0.05 mm), and clay ($<$ 0.002 mm) (Knight, 1938; Hillel, 1980). We model the 2-D pore-space in between three spherical particles equivalent to size of soil separates extracted from the whole population of soil particles. This approach has similarities with Jaafar and Likos's (2011) pore model (see references therein). Their model describes a framework to calculate capillary pressures at the entire saturation range (in the form of water films, pendular water and completely water-filled pores) by considering different sized spherical four-particle (loose packing) and three-particle (dense packing) assemblies randomly selected from a particle population to match the actual particle-size distribution. Our study is within a framework of three soil particles only, to encompass both relatively loose and dense packing introducing a parameter adjusted to meet the porosity of the medium. In the following steps, we introduce some *new* methods (to best of our knowledge) to quantify pore space and then eventually to calculate capillary pressure.

Step 1: ***Calculation of no. of particles*** Let us say that there are n different types of soil separates (e.g. silt, clay, fine sand etc.) with radii $r_1, r_2, r_3, \ldots, r_s, \ldots, r_n$ in a representative volume of porous media. Here every soil particle is assumed to be of spherical form of equivalent diameter to its size. The soil sample comprises of $x_1, x_2, x_3, \ldots, x_s, \ldots, x_n$ percentages of total weight with n soil separates of radii $r_1, r_2, r_3, \ldots, r_s, \ldots, r_n$ and of particle densities $\rho_1, \rho_2, \rho_3, \ldots, \rho_s, \ldots, \rho_n$ respectively. Percentages of soil separates can be known from particle size distribution (PSD) (using sieve analysis etc.) or soil texture triangle (STT) of Soil Conservation Service (1975).

Table 4.2: Particle size distribution

% weight	x_1	x_2	...	x_n
Particle dia.	$D_1 = 2r_1$	$D_2 = 2r_2$	...	$D_n = 2r_n$

One can find out the number (N_s) of spherical particles out of 100 of a particular separate (say, it is 's') as:

$$N_s(\%) = \lfloor N_{a\text{-}s} \rceil \tag{4.17}$$

where,

$$N_{a\text{-}s}(\%) = 100 \left(\sum_{m=1}^{n} \frac{x_m \rho_s r_s^3}{x_s \rho_m r_m^3} \right)^{-1}$$

and $\lfloor x \rceil$ represents the nearest integer value of x (Hastad et al., 1989).

Step 2: ***Algorithm to calculate mean value in a representative porous medium*** Cell for a particular arrangement can be thought of as triangular prism cell with triangular-face $\triangle A_1A_2A_3$ with height L as shown in Fig. 4.5d. Three particles from any type of soil separates can make a pore. There are $\mathsf{T}_n = \binom{n+2}{3}$ possible combinations of specific pore space inside a particular cell while taking three out of n soil separates.

We present an algorithm of averaging (AoA) to calculate mean value of any property associated with soil (or any structurally similar to soil porous media) from the triangular prism cell value made out of each and every arrangement (say, t-th arrangement, which is one of T_n combinations), based on the percentages of different separates, which compose the porous media.

STEPS involved in AoA are:

1$^{\text{ST}}$. Enter the number of a particular 's' soil separate in the t-th arrangement:

$$\mathsf{n}(t_s) = l;\ l \in \{0,1,2,3\}. \tag{4.18}$$

2$^{\text{ND}}$. Calculate the no. of combinations for the t-th arrangement for n types of soil separates out of N_s as:

$$\mathsf{N}_{C(t_s)} = \begin{pmatrix} N_s \\ \mathsf{n}(t_s) \end{pmatrix} = \begin{pmatrix} N_s \\ l \end{pmatrix}. \tag{4.19}$$

3$^{\text{RD}}$. Calculate the total no. of possibilities of t-th arrangement as:

$$\mathsf{P}_t = \prod_{s=1}^{n} \mathsf{N}_{C(t_s)}. \tag{4.20}$$

4$^{\text{TH}}$. The probable outcome of t-th arrangement is:

$$\mathsf{w}_t = \frac{\mathsf{P}_t}{\sum\limits_{m=1}^{\mathsf{T}_n} \mathsf{P}_m}, \tag{4.21}$$

with the property of $\sum_{t=1}^{\mathsf{T}_n} \mathsf{w}_t = 1$.

5$^{\text{TH}}$. Calculate the mean value of Q in the representative volume knowing cell values for t-th

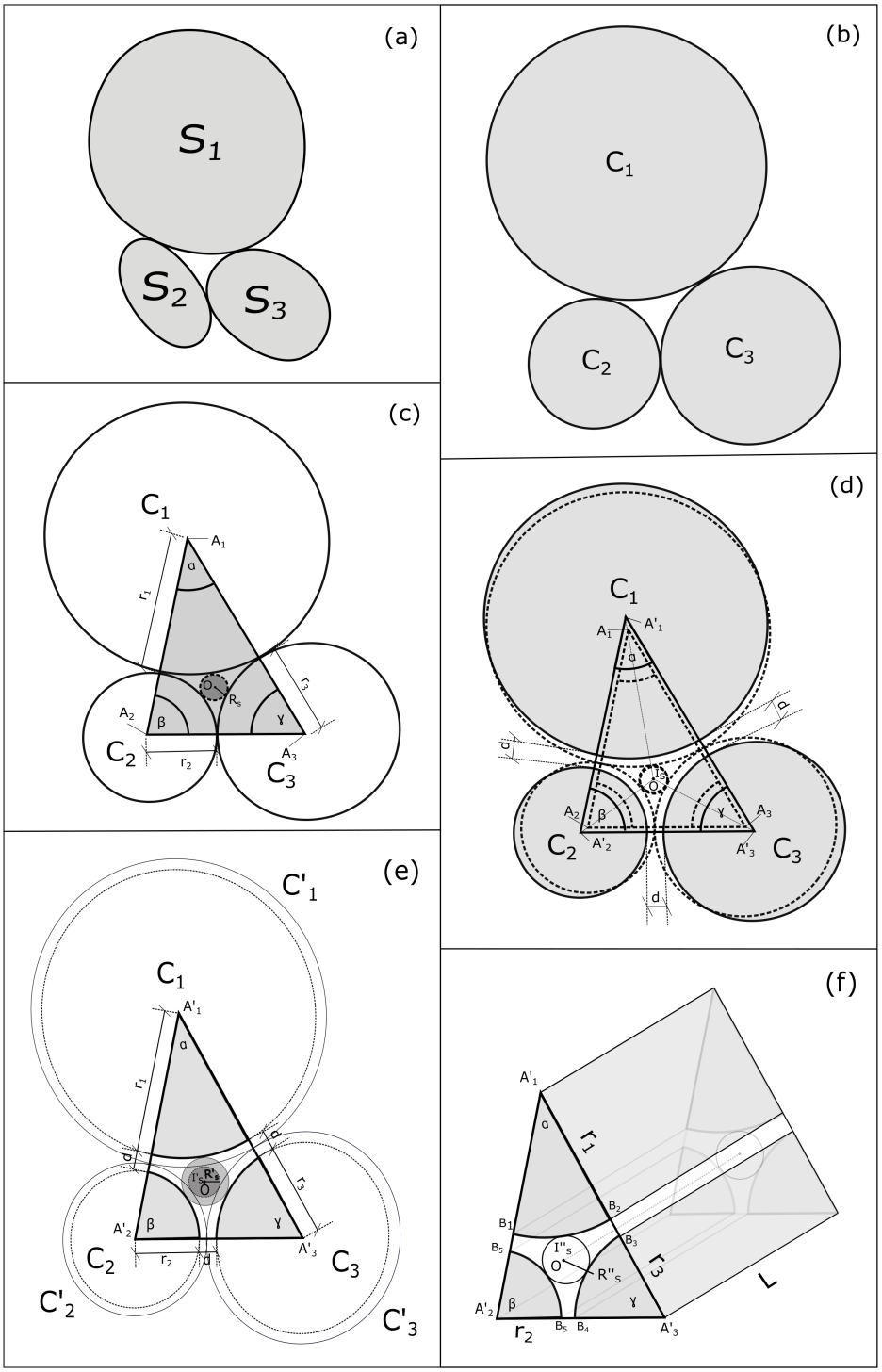

Figure 4.5: (a) Plan view of densest real porous media of three different soil separates (say, S_1, S_2, S_3), (b) Soil separates are idealized as circles (say, C_1, C_2, C_3) of radii (say, r_1, r_2, r_3) as size of particular separate, (c) Minimum area in the pore space is a circle with radius, R_s, (d) Plan view of sparse porous medium idealized as circles: $C_1(A_1', r_1)$, $C_2(A_2', r_2)$, $C_3(A_3', r_3)$, found by spacing the circles: $C_1(A_1, r_1)$, $C_2(A_2, r_2)$, $C_3(A_3, r_3)$, along OA_1, OA_2, OA_3 respectively such that $A_1A_1' = A_2A_2' = A_3A_3'$, (e) New sparse configuration of the porous medium with new inner Soddy circle, $I_s'(O, R_s')$, and (f) Representative cell (triangular prism) with length L

arrangement through w_t as:

$$\langle Q \rangle = \sum_{t=1}^{\mathsf{T}_n} \mathsf{w}_t \times (Q_{\text{cell}})_t \,. \tag{4.22}$$

where $\langle(\cdot)\rangle$ suggests statistical mean or just, mean of $(\cdot)$.

In case some property (say, G) is different for three separates involved in a particular arrangement and then mean value of function f of G can be implemented:

$$G_t = \frac{1}{3} \sum_{s=1}^{n} (\mathsf{n}(t_s) \times G_s)\,, \tag{4.23a}$$

$$\langle f(G) \rangle = \sum_{t=1}^{\mathsf{T}_n} \mathsf{w}_t \times f(G_t). \tag{4.23b}$$

As an example, SCA can be different for soil separates. We simplify this problem by using single value of SCA as

$$\langle \theta_e \rangle = \sum_{t=1}^{\mathsf{T}_n} \mathsf{w}_t \times \left(\frac{1}{3} \sum_{s=1}^{n} \mathsf{n}(t_s) \times (\theta_e)_s \right) \tag{4.24}$$

in the calculation of $(h_\infty)_t$.

Step 3: *Calculation of pore radius* Three soil particles can be idealized as three circles as shown in Fig. 4.5a-b. Now, these circles are moved equally from mid-point O of inner Soddy circle as in Fig. 4.5c. This movement geometrically makes these circles equally distant apart from each other (say, at d distance apart). The parameter d can be termed as *spacing parameter* and can be chosen based on required porosity. This new arrangement forms a new triangle $\triangle \mathrm{A}_1'\mathrm{A}_2'\mathrm{A}_3'$ from $\triangle \mathrm{A}_1\mathrm{A}_2\mathrm{A}_3$ (Fig. 4.5d). Eppstein (2001) mentioned that any triangle can uniquely determines three mutually tangent circles on the triangle vertices with radii being $(-a+b+c)/2$, $(a-b+c)/2$ and $(a+b-c)/2$ (where a,b,c are side lengths of the triangle). Here the triangle is $\triangle \mathrm{A}_1'\mathrm{A}_2'\mathrm{A}_3'$ and three mutually tangent circles are C_1', C_2' and C_3' on the triangle vertices A_1', A_2' and A_3' with radii $r_1'(=r_1+0.5d)$, $r_2'(=r_2+0.5d)$ and $r_3'(=r_3+0.5d)$ respectively (see Fig. 4.5b).

Pore radius (R_p) can be calculated by imposing radial-construct to the pore space. One is minimum and other is maximum radius. Minimum is the radius of circle $\mathrm{I}_s''(\mathrm{O}, R_s'')$ (i.e., circle I"$_s$ is of center O and radius R_s'') as in Fig. 4.5f. Following Fig. 4.5e, R_s'' can be found from the inner Soddy circle $\mathrm{I}_s'(\mathrm{O}, R_s')$ (Soddy, 1936; Coxeter, 1969), which is touching the outer

three mutually tangent circles $C'_1(A'_1, r'_1)$, $C'_2(A'_2, r'_2)$ and $C'_3(A'_3, r'_3)$, as:

$$R'_s = \frac{r'_1 r'_2 r'_3}{2\sqrt{r'_1 r'_2 r'_3 (r'_1 + r'_2 + r'_3)} + (r'_1 r'_2 + r'_2 r'_3 + r'_1 r'_3)}, \tag{4.25}$$

$$R''_s = R'_s + 0.5d, \tag{4.26}$$

and maximum is the radius equalizing void area, i.e., area of $B_1B_2B_3B_4B_5$ (A_v) (see Fig. 4.5f) to a circular area:

$$R_a = \sqrt{\frac{A_v}{\pi}}, \tag{4.27}$$

where,

$$A_v = \triangle - \frac{\alpha r_1^2 + \beta r_2^2 + \gamma r_3^2}{2}, \ \triangle = \sqrt{r'_1 r'_2 r'_3 (r'_1 + r'_2 + r'_3)}, \tag{4.28a}$$

$$\alpha = \arcsin\left(\frac{A_{(123)}}{2A_{(12)}A_{(13)}}\right), \ \beta = \arcsin\left(\frac{A_{(123)}}{2A_{(12)}A_{(23)}}\right), \ \gamma = \arcsin\left(\frac{A_{(123)}}{2A_{(23)}A_{(13)}}\right); \tag{4.28b}$$

$$A_{(12)} = r_1 + r_2, \ A_{(23)} = r_2 + r_3, \ A_{(13)} = r_1 + r_3; \tag{4.28c}$$

$$A_{(123)} = \sqrt{2\left(A^2_{(12)}A^2_{(23)} + A^2_{(23)}A^2_{(13)} + A^2_{(12)}A^2_{(13)}\right) - A^4_{(12)} - A^4_{(23)} - A^4_{(13)}}. \tag{4.28d}$$

We calculate the pore radius $(R_p)_t$ for a particular arrangement t from minimum $(R''_s)_t$ to maximum $(R_a)_t$ to encompass and to understand the entire range of radial effect over capillary pressure.

Step 4: ***Calculation of length of representative cell*** Pore radius is used as radius of the cylinder to calculate pressure value. Our choice of cylindrical pore space justifies that volumteric porosity or porosity will be same as areal porosity (as in Eq. 1.3.8 of Bear, 1972). Equivalence of porosity and liquid content in soil with total volume of cylinder and of liquid inside the cylinder generates a constant length value (L), for all T_n arrangements:

$$L = \frac{1}{\eta}\sum_{t=1}^{\mathsf{T}_n} (\mathsf{w}_t \times \phi_t) \max_t \left(|h_\infty|_t\right), \tag{4.29}$$

where η is liquid content, w_t is the statistical *weight* as per Eq. (4.21) for t-th arrangement, $\phi_t = (A_v)_t / \triangle_t$ is the volumetric porosity of the cell of t-th arrangement, $(A_v)_t$ and $\triangle_t$ are the area of void space and total area of the t-th arrangement respectively (see the expressions in (4.27)), $\max_t(.)$ represents the maximum value of $(.)$ among all T_n arrangements and

$(h_\infty)_t = (2\sigma\cos\theta_e)\,/\,(\rho_l g (R_p)_t)$ (through h_∞ (Eq. (3.1))).

Step 5: *Capillary pressure in soil* Capillary pressure in representative soil volume can be evaluated summing up all weighted-cell values of pressures. Capillary pressure in triangular prism cell of the t-th arrangement $(P_c)_t$ (or more precisely the cylindrical pore of radius $(R_p)_t$ and length L inside the prism cell) can be evaluated through Eqs. (4.13)-(4.16) from Eq. (4.11), replacing R as $(R_p)_t$ (i.e., pore radius for t-th arrangement = $(R_s'')_t$ or $(R_a)_t$).

$$\text{Capillary pressure, } \langle P_c \rangle = \sum_{t=1}^{\mathsf{T}_n} \mathsf{w}_t \times (P_c)_t \,. \tag{4.30}$$

where,

$$(P_c)_t = ((P_c)_{\mathrm{mP}})_t \text{ or } ((P_c)_{\mathrm{P}})_t$$

$$((P_c)_{\mathrm{mP}})_t \approx \frac{2\sigma M_t}{(R_p)_t\sqrt{1+(M_t)^2}}, \text{ [solving } m\text{PME]} \tag{4.31a}$$

$$\text{and } ((P_c)_{\mathrm{P}})_t \approx \frac{2\sigma}{n}\sum_{i=0}^{n} \frac{\left|\dfrac{z_i - 2z_{i-1} + z_{i-2}}{(\Delta r)^2}\right|}{\left[1+\left(\dfrac{z_i - z_{i-1}}{\Delta r}\right)^2\right]^{3/2}}, \text{ [solving PME]} \tag{4.31b}$$

where $M_t = 2z_{\mathrm{mP}}((R_p)_t)\sum_{i=1}^{\infty} i c_{2i} (R_p)_t^{2i-1}$. The value of z at i-th location is $z_i = z(i\times\Delta r) = z(i\times(R_p)_t/n)$, where $i = \{0,1,2,\ldots,n\}$. The subscripts 'P' and 'mP' are indicative of the solutions from 'PME' (P) and 'mPME' (mP) respectively. Here, we calculate M_t of Eq. (4.31a) taking up to 22^{nd} degree power of the coefficients c_{2i} to keep the results in a safer side (as we have used different pore sizes) and Δr of Eq. (4.31b) as 10^{-10} m.

4.4 Results and discussion

4.4.1 Effect of temperature on capillary pressure

In this section, we calculate the capillary pressures for different constant temperatures from published results and compare to understand our method and underlying physics of the problem. First lets describe how to calculate capillary pressure at temperature T in soil or soil-like porous media. Capillary pressure (Eqs. (4.31a)-(4.31b)) is informed by the values of basic porous media forming separates characteristics - volumetric porosity η, separate weight percentage x_s, separate density ρ_s, separate diameter $D_s = 2r_s$ and SCA of liquid at each solid

separate $(\theta_e)_s$ at a temperature T. Table 4.3 presents altogether the basic parameters and their calculations from the basic inputs to eventual calculation of $\langle P_c(T)\rangle$.

Table 4.3: Step-wise calculation of all parameters involved in $\langle P_c(T)\rangle$

Parameters	Calculation steps
$\rho_l(T)$	Fitting relationship of ρ_l-*vs.*-T; e.g. density of water: $\rho_l = -0.0035361T^2 + 1.8555T + 757.78$ (Table 5.14 of Dean, 1999).
$\rho_a(T)$	Fitting relationship of ρ_a-*vs.*-T; $\rho_a = 10^{-5}T^2 - 0.0118T + 3.5612$ (Maggi and Alonso-Marroquin, 2013).
$\sigma(T)$	Fitting relationship of σ_l-*vs.*-T; e.g. surface tension of water: $\sigma_l = -0.00017398T + 0.12384$ (Vargaftik et al., 1983).
$\xi(T)$	$\left(\frac{\rho_d(T)g}{\sigma(T)}\right)^2$ and $\rho_d(T) = \rho_l(T) - \rho_a(T)$.
$(R_p)_t$	Minimum $(R_s'')_t$ (Eq. 4.26) to maximum $(R_a)_t$ (Eq. 4.27) using separate radius r_s and spacing parameter d.
w_t	Equation (4.21) with Eq. (4.17) using % weight of separate x_s, separate density ρ_s and r_s.
$\langle\theta_e\rangle$	Equation (4.24) using w_t and $(\theta_e)_s$.
$(h_\infty(T))_t$	Equation (3.1) using $\sigma(T)$, $\langle\theta_e\rangle$, $\rho_l(T)$, $\rho_a(T)$ and $(R_p)_t$.
$\langle\phi\rangle$	$\sum_{t=1}^{\mathsf{T}_n} \mathsf{w}_t \times \phi_t$; $\phi_t = (A_v)_t/\Delta_t$ using r_s and d^* (Eq. 4.28a).
L	Equation (4.29) using η, w_t, ϕ_t and $\max_t (h_\infty(T))_t$.
$\langle P_c(T)\rangle$	Equations (4.31a)-(4.31b) using $\xi(T)$, $w(r,T)$ from $\rho_d(T)$ and L with boundary conditions being $z(r=0) = (h_\infty(T))_t$ and $z'(r = (R_p)_t) = 0$; $r \in [0, (R_p)_t]$.

*Value of d is so assumed that $\langle\phi\rangle$ becomes equal to the porosity of soil.

Whenever the results of capillary pressure-vs-temperature at some constant moisture content are not given directly, we have fitted van Genuchten model (van Genuchten, 1978) to the available published data of dynamic capillary pressures-vs-liquid content at different constant temperatures to interpolate and extract information of saturated liquid content (η_s i.e. maximum η) and residual saturation (η_r i.e. liquid content when liquid becomes discontinuous (Bear et al., 2011)). Saturated liquid content (η_s) is taken as porosity for our calculation, if not given. If PSD of the soil is not given in the literature but only name of the soil texture is given, PSD for that particular soil texture is taken from other literature or using STT of Soil Conservation Service (1975) taking diameter of sand as particles in between 2 mm to 0.05 mm, of silt being in between 0.05 mm to 0.002 mm and of clay being in between 0.002 mm to lower.

Following the above steps shown in Table 4.3, we have found capillary pressure at constant temperatures. These results indicate a decreasing linear relationship and this is in accordance

with Grant's (2003) claim of universality of the relation:

$$P_c(T,\eta)|_\eta = a(\eta) + b(\eta)T, \tag{4.32a}$$

$$\left.\frac{\partial P_c}{\partial T}\right|_\eta = b(\eta), \tag{4.32b}$$

where a [Pa] and b [Pa K^{-1}] are fitting parameters. Equation (4.32b) represents relative changes of P_c with T (as shown in Eq. (1.19) of chapter 1 that relative changes directs soil-water flow). We present experimental and corresponding predicted values of b for six varied porous media (or PM) in Table 4.4 (column 12-14), using input variables (column 2-7) and taking all density of separate as same. Pore radius from maximum ($= R_a$) to minimum ($= R_s''$) is evaluated to calculate b and those values are given in the table for both radii solving PME (column 13) and *m*PME (column 14) equations. Slope values increase with radius. Pore radii from R_a to R_s'' put a range over the slope value - minimum to maximum respectively. Five experimental slope values out of six PM fall inside the predicted PME ones and three out of them are within predicted *m*PME ones.

4.4.2 Effect of temperature on ACA

ACA (θ_a) is evaluated from the slope value at solid wall. We present the relative changes of ACA values with temperatures in the columns 15 and 16 in Table 4.4. ACA increases with temperature for PME and decreases with temperature for *m*PME. Pore radius has very little effect over the values of $\frac{\Delta(\theta_a)_{\text{mP}}}{\Delta T}$ for both PME and *m*PME results (see column 15 and 16 that maximum difference between $\frac{\Delta(\theta_a)_{\text{mP}}}{\Delta T}$ values obtained through R_a and R_s'' is ± 0.00001). The radius of meniscus curvature (R_c) can be evaluated as $R_p/\cos\theta_a$ (with spherical assumption). Thus P_c is proportional to $\cos\theta_a$. Decreasing relation of P_c with T, infers theoretically an increasing relation of θ_a with T when $\theta_a < 90^\circ$ and vice versa, when $\theta_a > 90^\circ$. The PME results of $\frac{\Delta\theta_a}{\Delta T}$ (column 15) confirm the above theoretical explanation and so does experimental results of King (1981) and Figure 10 of Grant and Bachmann (2002); and with *m*PME results, values of $\frac{\Delta\theta_a}{\Delta T}$ are just reverse, which is again consistent with most experimental results as per Grant and Bachmann (2002). All experimental θ_a are decreasing or increasing with increasing T irrespective of θ_a being $< 90^\circ$ or $> 90^\circ$. This fact differs from our predicted linear slope values. Experimental magnitudes of $\frac{\Delta\theta_a}{\Delta T}$ as conducted on wettable and water-repellent soils by Bachmann et al. (2002), range from 0.03° K^{-1} to 0.26° K^{-1}, whereas the predicted ones are much less smaller for *m*PME results (0.00003° K^{-1} to 0.00018° K^{-1}) and for PME results (0.00007° K^{-1} to 0.00112° K^{-1}). If we take pore radius as R_s'' or R_a from one texture to another, $\frac{\Delta\theta_a}{\Delta T}$ results show that radius does have weak effect on θ_a-*vs*-T relation. Difference of results of PME and *m*PME methods infers primarily to the effect of the weight of column of

Table 4.4: Comparison of experimental and calculated values of $P_c(T)$ and $\theta_a(T) \pm$ (standard deviation)

1	2	3	4	5	6	7	8	9	10	11	12	13	14	15	16	17
	Input Variables						van Genuchten Parameters				Exp. Results	Calculated $b(\eta)$		Calculated		
PM	Separate values		η	$\langle\phi\rangle$	d	$\langle\theta_e\rangle$	$\langle\eta_s\rangle$	$\langle\eta_r\rangle$	$\langle\alpha_{vG}\rangle$	$\langle n_{vG}\rangle$	$\frac{\partial(P_c)_{exp}}{\partial T}\|_\eta$	$\frac{\partial(P_c)_P}{\partial T}\|_\eta$	$\frac{\partial(P_c)_{mP}}{\partial T}\|_\eta$	$\frac{\Delta(\theta_a)_P}{\Delta T}$	$\frac{\Delta(\theta_a)_{mP}}{\Delta T}$	Reference
	D_s [mm]	x_s [%]	[%]	[%]	[mm]	[°]	[%]	[%]	[kPa^{-1}]	–	[kPa K^{-1}]	[kPa K^{-1}]	[kPa K^{-1}]	[° K^{-1}]	[° K^{-1}]	
	PSD: STT															
Sandy loam (SL)	0.4 0.02	60 40	14.9	32.7	0.0033	0	–	N-	-A	–	−0.82229 (0.00000)	R_a : −0.06619 R''_s : −0.18421	R_a : −0.06862 R''_s : −0.19095	R_a : 0.00022 R''_s : 0.00021	R_a : −0.00017 R''_s : −0.00017	Gardner (1955)
104-149 μm sand (SD)	0.104	100	5	38	0.0218	0	38	3.55	0.15	8.36	−0.01210 (0.00000)	R_a : −0.01168 R''_s : −0.03458	R_a : −0.01208 R''_s : −0.03576	R_a : 0.00112 R''_s : 0.00112	R_a : −0.00018 R''_s : −0.00017	Wilkinson and Klute (1962)
	0.149	100	5	38	0.0313	0	38	3.55	0.15	8.36	−0.01210 (0.00000)	R_a : −0.00815 R''_s : −0.02413	R_a : −0.00843 R''_s : −0.02495	R_a : 0.00112 R''_s : 0.00112	R_a : −0.00018 R''_s : −0.00017	
Glass beads (GB)	0.181	100	10	30	0.025	0	30	5.09	0.54	4.95	−0.02222 (0.00451)	R_a : −0.00802 R''_s : −0.02107	R_a : −0.00831 R''_s : −0.02184	R_a : 0.00033 R''_s : 0.00034	R_a : −0.00018 R''_s : −0.00017	Nimmo and Miller (1986) [Imbibition]
	PSD: Likos (2013)															
F-75 silica Sand (SS)	0.07 0.17 0.37 0.70	7 77 15 1	36	41	0.0253	0	41	4.8	0.44	7.88	−0.03031 (0.00137)	R_a : −0.01055 R''_s : −0.03423	R_a : −0.01095 R''_s : −0.03550	R_a : 0.00007 R''_s : 0.00009	R_a : −0.00016 R''_s : −0.00015	She and Sleep (1998) [Drainage]
Hydrophobic sand (HS)	1.3 0.4 0.13 0.03	0.4 90.5 8.5 0.6	7	34.8	0.0074	97.2 (5.6)	34.8	2.73	0.42	8.84	−0.01431 (0.00799)	R_a : −0.00762 (0.00605) R''_s : −0.02426 (0.01929)	R_a : −0.03145 (0.00000) R''_s : −0.10022 (0.00000)	R_a : −0.00044 (0.00035) R''_s : −0.00041 (0.00032)	R_a : 0.00008 (0.00006) R''_s : 0.00008 (0.00006)	Bachmann et al. (2002) [13.5 cm deep]
Hydrophobic humic soil (HH)	1.315 0.415 0.1315 0.0415 0.013 0.004 0.0013	3 60.1 28.7 4.3 1.6 0.5 1.8	5.1	29	0.000198	92.6 (5.2)	29	0.22	0.98	1.51	−0.38935 (0.03080)	R_a : −0.14979 (0.10145) R''_s : −0.42645 (0.28883)	R_a : −0.99019 (0.00000) R''_s : −2.82062 (0.00000)	R_a : −0.00027 (0.00054) R''_s : −0.00015 (0.00031)	R_a : 0.00003 (0.00006) R''_s : 0.00003 (0.00006)	Bachmann et al. (2002) [4.5 cm deep]

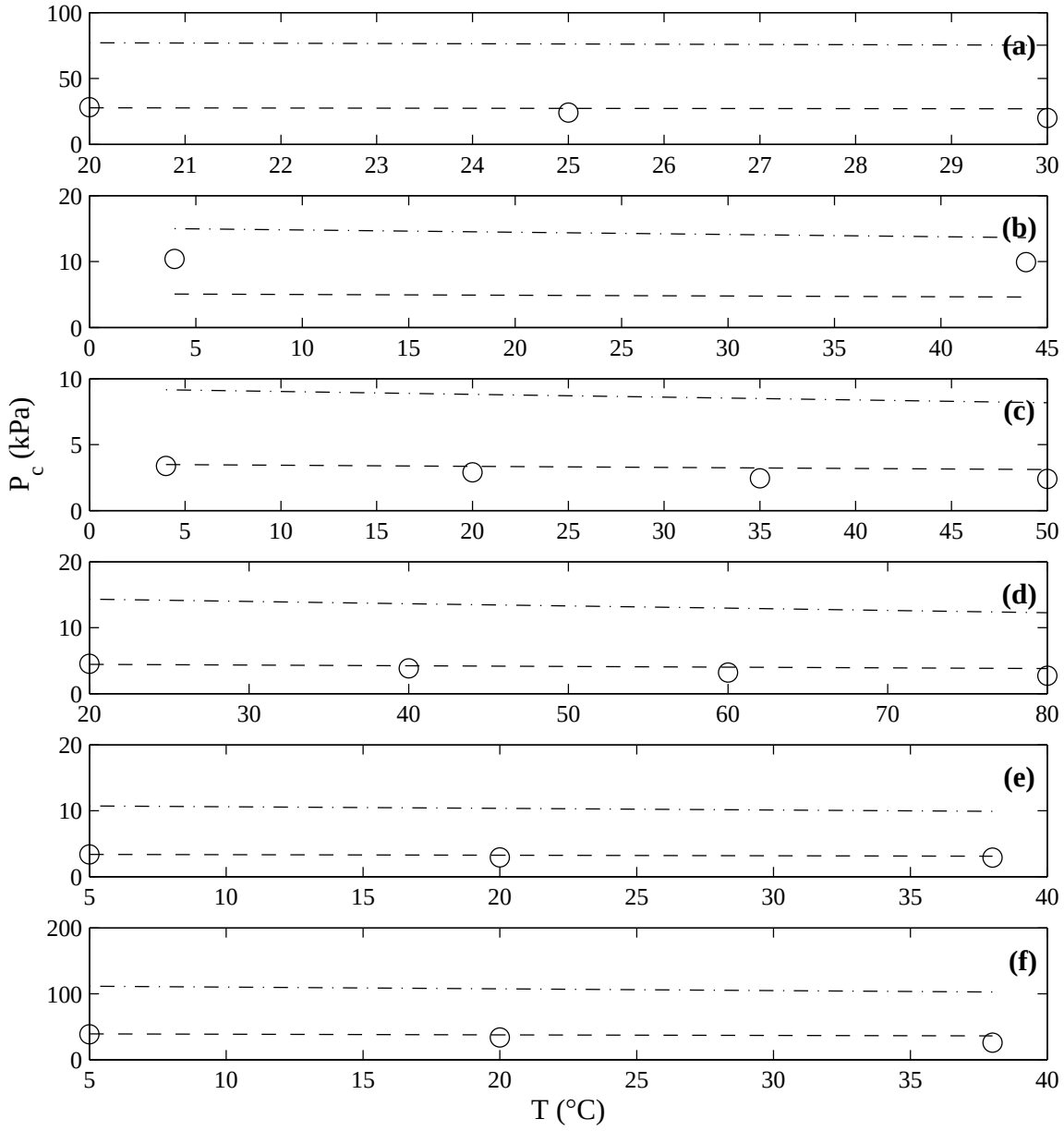

Figure 4.6: P_c-vs-T results - experimental (`circle`), PME results using R_p from minimum R_s'' (`dash-dot`) to maximum R_a (`dash`) for (a) SL, (b) SD, (c) GB, (d)SS, (e) HS and (f) HH

air over meniscus. Higher magnitudes of $\frac{\Delta\theta_a}{\Delta T}$ of PME results than that of *m*PME results for almost every texture, thus show the influence of air effect. Still discrepancy is there between experimental and predicted ones. Now the question is why? One reason may be that $\sigma_{\text{soil water}}$ is more sensitive with T than that of σ_{water} (quantitatively, $\frac{\Delta\sigma_{\text{soil water}}}{\Delta T} \approx 2\frac{\Delta\sigma_{\text{water}}}{\Delta T}$) (Grant and Bachmann, 2002). We use in our analysis the surface tension of liquid (σ_l) as of pure water (σ_{water}) instead of surface tension of soil water ($\sigma_{\text{soil water}}$).

Another way to understand how exactly ACAs are changing with temperature for experimental results, is to trial with some assumed θ_e value for each temperature till experimental P_c value exactly matches with predicted P_c value, for each soil texture. This may give us some idea about *actual* θ_a values for soil textures. All values are evaluated from PME, as *m*PME results are insensitive towards any given θ_e value (we discuss the relation of PME and *m*PME results later in details). Figure 4.7 shows the results of assumed θ_e with correspondingly calculated P_c, which are matched with experimental P_c values and calculated θ_a values. These values are all averaged with statistical weights as mentioned before. ACA-vs-T for all soil textures except SD follow the same trend as calculated from PME in Table 4.4. Magnitudes of $\Delta\theta_a/\Delta T$ show a range from 0.03050° K^{-1} to 2.89334° K^{-1}. The assumed values of θ_e (as in Fig. 4.7) of hydrophobic humic soil (HH) and sand (HS) are within the whole range of Bachmann et al.'s (2002) experimental values $92.6^\circ \pm 5.2^\circ$ and $97.2^\circ \pm 5.6^\circ$ respectively (see Table 4.4) and values of $\Delta\theta_a/\Delta T$ are also from -0.03° K^{-1} to -0.26° K^{-1}. This confirms (if not definitely) that this model has the capability to calculate average θ_e value indirectly for a soil texture.

4.4.3 Effect of liquid and air Content

During derivation of *m*PME, the effects of air in terms of its weight (through '$\rho_a L$') is excluded. The length is calculated from the liquid content (η) (see Eq. 4.29). As liquid content is getting less and less, air-column will be more and more over the capillary liquid. Thus air-effect can be understood analyzing PME and *m*PME capillary pressure results differing liquid contents while keeping other parameters constant. Table 4.5 presents the results. As liquid content is getting from $0.05\eta_s$ to $0.95\eta_s$, air content (lets say, η_a) goes from $0.95\eta_s$ to $0.05\eta_s$. This implies that air-effect will be less. Figure 4.8 shows that curvature gets less from $0.05\eta_s$ to $0.95\eta_s$ for both F-75 silica sand (SS) and hydrophobic humic soil (HH) and thus capillary pressure values get less as well (see Table 4.5). This result is consistent with typical P_c-*vs.*-η relationship. Our results are for static condition and this mean, we calculate capillary pressure at a particular liquid content and a temperature while whole system is in static equilibrium. Figure 4.8 also shows that with liquid content from $0.05\eta_s$ to $0.95\eta_s$, ACA gets more for hydrophilic cases (i.e. $\theta_e < 90^\circ$) (SL,SD,GB,SS) and gets less for hydrophobic cases (i.e. $\theta_e > 90^\circ$) (HS,HH). Capillary pressure and ACA do not exactly follow linear pattern. But to understand better the relative changes of P_c and θ_a due to relative changes in liquid content, we

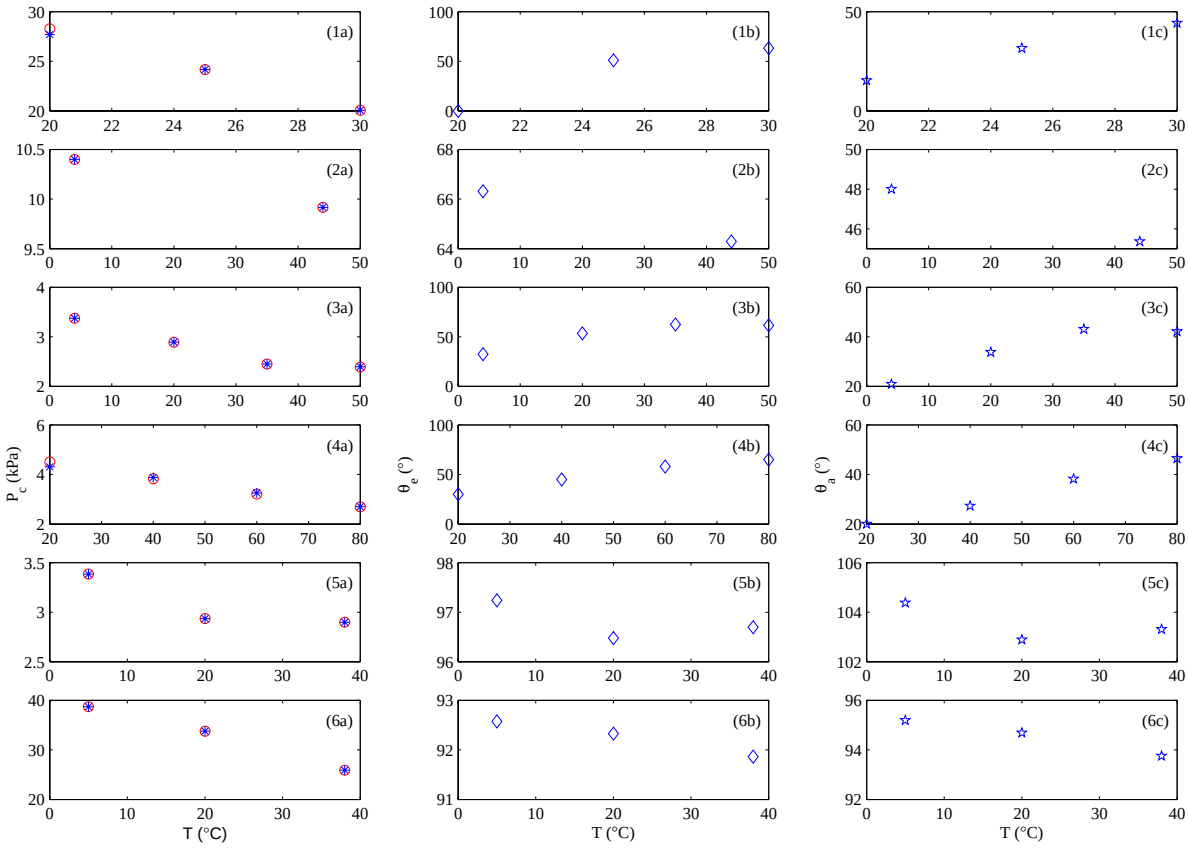

Figure 4.7: Calculated P_c (`asterisk`) with experimental P_c (`circle`) (column a), assuming θ_e (`diamond`) (column b) and calculated θ_a (`star`) (column c) at different constant temperatures. Soil textures for row 1: SL, row 2: 104 μm SD, row 3: GB, row 4: SS, row 5: HS, row 6: HH. Relative changes of θ_a with T are for different soil textures - SL: 2.89334° K^{-1}, SD: $-0.066030°$ K^{-1}, GB: 0.48124° K^{-1}, SS: 0.45079° K^{-1}, HS: $-0.03050°$ K^{-1} and HH: $-0.04377°$ K^{-1}

present $\frac{\Delta P_c}{\Delta \eta}$ and $\frac{\Delta \theta_a}{\Delta \eta}$ in Table 4.5. Capillary pressures change from minimum -8.30311 kPa to maximum -0.01940 kPa, while ACA changes - (I) for hydrophilic cases, from minimum 1.27502° to maximum 1.86307° and (II) for hydrophobic cases, from minimum -0.91510° to maximum -0.41266°, due to changes in η. As pore radius goes from maximum R_a to minimum R_s'', the magnitude of relative changes get steeper. This is a direct consequence of $P_c \propto 1/R_p$. The ACA also changes with R_p. Now, as we surmise $\eta \sim \frac{1}{K_m}$, we can establish a relation between η, θ_a and R_p as $\eta \sim R_p \propto \frac{1}{\cos\theta_a}$ $(\theta_a < 90^\circ)$ or $\frac{1}{-\sin(\theta_a - 90^\circ)}$ $(\theta_a > 90^\circ)$. This relation confirms the PME results. But *m*PME results show that η has no effect over P_c and θ_a. We compare in the later section the results of PME and *m*PME and discuss about η.

Table 4.5: Effect of liquid content on capillary pressures and ACAs

PM (T°C)	R_a or R_s''		Capillary pressure $\mathsf{R}_{(P_c)_P}(\eta)$ E(η) 0.05	0.35	0.65	0.95	$\frac{\Delta(P_c)_P}{\Delta\eta}$ (kPa)	$\mathsf{R}_{(P_c)_{mP}}(\eta)$ E(η) 0.05-0.95	ACA $\mathsf{R}_{(\theta_a)_P}(\eta)$ E(η) 0.05	0.35	0.65	0.95	$\frac{\Delta(\theta_a)_P}{\Delta\eta}$ (°)	$\mathsf{R}_{(\theta_a)_{mP}}(\eta)$ E(η) 0.05-0.95
SL (30°C)	R_a		1	0.99777	0.99760	0.99753	−0.20953	1	1	1.03250	1.03504	1.03598	1.67554	1
	R_s''		1	0.99779	0.99761	0.99753	−0.58374	1	1	1.03177	1.03426	1.03518	1.63942	1
SD (44°C)	104 μm	R_a	1	0.99798	0.99782	0.99776	−0.02779	1	1	1.02863	1.03086	1.03169	1.27502	1
		R_s''	1	0.99798	0.99782	0.99776	−0.08223	1	1	1.02863	1.03086	1.03169	1.27508	1
	149 μm	R_a	1	0.99798	0.99782	0.99776	−0.01940	1	1	1.02867	1.03091	1.03173	1.27649	1
		R_s''	1	0.99798	0.99782	0.99776	−0.05745	1	1	1.02866	1.03090	1.03173	1.27659	1
GB (20°C)	R_a		1	0.99768	0.99749	0.99742	−0.02955	1	1	1.03318	1.03578	1.03673	1.86292	1
	R_s''		1	0.99768	0.99749	0.99742	−0.07766	1	1	1.03318	1.03577	1.03673	1.86307	1
SS (60°C)	R_a		1	0.99773	0.99755	0.99748	−0.02521	1	1	1.03347	1.03609	1.03705	1.37401	1
	R_s''		1	0.99761	0.99741	0.99734	−0.08622	1	1	1.03641	1.03927	1.04033	1.49069	1
HS (38°C)	R_a		1	0.98281	0.98149	0.98100	−0.17625	1	1	0.99731	0.99710	0.99702	−0.91510	1
	R_s''		1	0.98328	0.98199	0.98152	−0.54595	1	1	0.99744	0.99725	0.99717	−0.86862	1
HH (5°C)	R_a		1	0.98027	0.97873	0.97815	−3.06424	1	1	0.99821	0.99807	0.99802	−0.66640	1
	R_s''		1	0.98123	0.97973	0.97922	−8.30311	1	1	0.99889	0.99880	0.99877	−0.41266	1

$\mathsf{R}_X(\eta) = \frac{X|_{@E(\eta)}}{X|_{@E=0.05}}$, $\mathsf{E}(\eta) = \frac{\eta}{\eta_s}$, η_s is the saturated liquid content (saturated water content, as for our case).

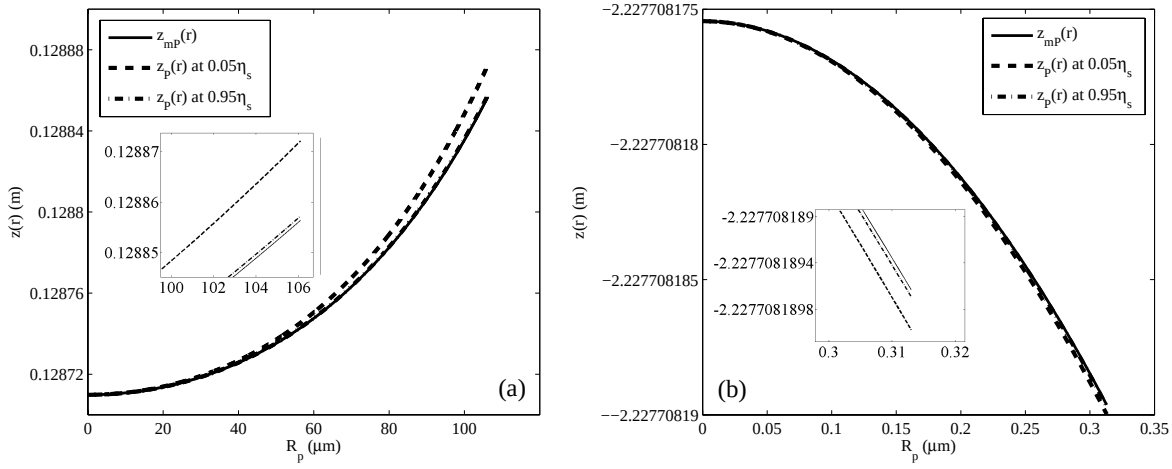

Figure 4.8: Meniscus $z_{\mathrm{mP}}(r)$(using *m*PME) (`line`; $-$) and $z_{\mathrm{P}}(r)$(using PME) in a pore of (a) F-75 silica sand (60°C) and (b) Hydrophobic humic soil (5°C), at $0.05\eta_s$(`dash`; $--$) and $0.95\eta_s$(`dot-dash`; $-\cdot$)

4.4.4 Comparison of PME and *m*PME results

The difference of PME and *m*PME in calculating P_c is visible as one tracks the results from one soil texture to texture. However, there is an interesting similarity with P_c by *m*PME (Eq. 4.31a) and P_c value assuming spherical meniscus with $\theta_e = 0°$ (i.e. $((P_c)_{sp})_t = 2\sigma/(R_p)_t$) and these results are same. Here if we also add contact angle effect with $((P_c)_{sp})_t$ i.e. $((P_c)_{sp})_t \times \cos((\theta_a)_P)_t$, this has similarity with $((P_c)_P)_t$. Results in Table 4.6 show that $\langle(P_c)_{mP}\rangle = \langle(P_c)_{sp}\rangle$ (within $< 10^{-6}$% error) and $\langle(P_c)_P\rangle = \langle(P_c)_{sp}\cos(\theta_a)_P\rangle$ (within < 0.15% error).

Table 4.6: Connection between PME and *m*PME results

PM (T°C)	R_a or R_s''		$\langle(R_p)\rangle$ (μm)	$\langle(P_c)_P\rangle$ (kPa)	$\langle(P_c)_{mP}\rangle$ (kPa)	$\langle(\theta_a)_P\rangle$ (°)	$\langle(P_c)_{sp}\rangle$ (kPa)	$\langle(P_c)_{sp}\cos(\theta_a)_P\rangle$ (kPa)	$\langle\Delta(P_c)_P\rangle^*$ (%)
SL (20°C)	R_a		5.1903	27.6994	28.7268	15.3772	28.7268	27.6982	0.0042
	R_s''		1.8347	77.0901	79.9424	15.3795	79.9424	77.0795	0.0136
SD (4°C)	104 μm	R_a	28.7973	5.0683	5.2520	15.2016	5.2520	5.0682	0.0009
		R_s''	9.7307	14.9993	15.5429	15.2032	15.5429	14.9989	0.0025
	149 μm	R_a	41.2982	2.3537	2.4405	15.3303	2.4405	2.3537	0.0005
		R_s''	13.9463	10.4654	10.8447	15.2026	10.8447	10.4652	0.0016
GB (50°C)	R_a		41.8799	3.1138	3.2292	15.3622	3.2292	3.1138	0.0006
	R_s''		15.9342	8.1840	8.4872	15.3655	8.4872	8.1838	0.0015
SS (80°C)	R_a		32.7403	3.7851	3.9261	15.4027	3.9261	3.7851	0.0007
	R_s''		10.3819	12.2758	12.7329	15.4025	12.7329	12.2755	0.0022
HS (38°C)	R_a		12.2392	3.1070	12.5996	104.2839	12.5996	3.1070	0.0012
	R_s''		3.7506	9.9001	40.1522	104.2795	40.1522	9.8997	0.0038
HH (5°C)	R_a		0.5710	39.0835	429.4036	95.2420	429.4036	39.0685	0.0356
	R_s''		0.1311	111.3505	1223.1777	95.2179	1223.1777	111.1948	0.1365

$^*\Delta(P_c)_P(\%) = 100\left(\frac{(P_c)_{sp}\cos(\theta_a)_P}{(P_c)_P} - 1\right)$.

These results show that PME results encompass whole effect of pore radius, contact angle and surface tension of liquid, whereas *m*PME results lack the information of contact angle. That shows impact of both air and liquid weights over meniscus formation. The above results of P_c, θ_a, air and liquid content due to T already confirm the effectiveness of PME over *m*PME results with respect to experimental observations.

4.5 Summary

In this final chapter, we have proposed a new generalized form (PME) and applied in Laplace's theorem to calculate P_c. To get the capillary pressure value in the soil or porous media, we have proposed an algorithm (AoA) based on unit-cell approach. Temperature effect is introduced through temperature-dependent parameters and we have tracked the changes from one to another temperature. We have ignored the effect of air phase or L in the PME and get into simpler version of PME or *m*PME, which is solved analytically. Results of PME and *m*PME are shown to be distinctive in sense of that *m*PME presents P_C values similar to P_c values if meniscus assumed to be of spherical form. All results of PME shows effective results over

*m*PME results. We have validated our model against experimental results of varied texture of porous media (PM) from synthetic to natural soils and from water-wet to water-repellent PMs.

A4 Appendix

A4.1 Derivation of PME

Symmetry of our problem domain makes the three dimensional problem to a two-dimensional one. Surface of the meniscus becomes a curved line in the $z-r$ plane. Here we consider the meniscus from a mechanical point of view rather than chemical or physio-chemical view though chemical forces are involved in microscopic level. So, we take their average effect on macroscopic level just like any other physical forces and continue our calculation. Phenomenologically, we can write the slope of the meniscus at every point as a resultant of two forces – vertical and horizontal i.e.

$$\frac{\mathrm{d}z(r)}{\mathrm{d}r} = \frac{\sum F_{\text{vertical}}}{\sum F_{\text{horizontal}}}, \tag{A4.1.1}$$

where F stands for the force component acting over the meniscus. Following Fig. 4.1 and Eq. (A4.1.1) for a small elemental length of meniscus, $s(r)$ we get:

$$\frac{\mathrm{d}z(r)}{\mathrm{d}r} = \frac{w(r)s(r)}{\sigma}. \tag{A4.1.2}$$

Differentiating Eq. (A4.1.2) with respect to r, we have,

$$\frac{\mathrm{d}^2z(r)}{\mathrm{d}r^2} = \frac{1}{\sigma}\left[s\frac{\mathrm{d}w(r)}{\mathrm{d}r} + w\frac{\mathrm{d}s(r)}{\mathrm{d}r}\right] \tag{A4.1.3}$$

Now $s(r) = \frac{\mathrm{d}z(r)}{\mathrm{d}r}\frac{\sigma}{w(r)}$ (from Eq. (A4.1.2)), $\frac{\mathrm{d}w(r)}{\mathrm{d}r} = (\rho_d g)\frac{\mathrm{d}z(r)}{\mathrm{d}r}$ (from Eq. (4.1)) and $\frac{\mathrm{d}s(r)}{\mathrm{d}r} = \sqrt{1+\left(\frac{\mathrm{d}z(r)}{\mathrm{d}r}\right)^2}$ (from Pythogorean theorem). Replacing these terms in Eq. (A4.1.3), we get,

$$\frac{\mathrm{d}^2z(r)}{\mathrm{d}r^2} = \frac{w}{\sigma}\sqrt{1+\left(\frac{\mathrm{d}z(r)}{\mathrm{d}r}\right)^2} + \frac{\rho_d g}{w}\left(\frac{\mathrm{d}z(r)}{\mathrm{d}r}\right)^2 \tag{A4.1.4}$$

A4.2 Inclusion of disjoining pressure

The molecular component of disjoining pressure arises from van der Waals bonds between condensed bodies (Lebeau and Konrad, 2010). Inclusion of this component of thin planar

film in vertical component of force as an opposing force to gravity generates the following equation:

$$\frac{\mathrm{d}^2 z(r)}{\mathrm{d}r^2} = \frac{F(r)}{\sigma}\sqrt{1+\left(\frac{\mathrm{d}z(r)}{\mathrm{d}r}\right)^2} + \frac{\rho_d g\left(\frac{\mathrm{d}z(r)}{\mathrm{d}r}\right)^2}{F(r)} - \frac{3C\left(\frac{\mathrm{d}z(r)}{\mathrm{d}r}\right)}{F(r)(R-r)^2} \tag{A4.1.5}$$

where $F(r) = w(r) - C/(R-r)^3$, $C = \mathrm{a}^2\sigma$, a = molecular length (see p. 95 of De Gennes et al., 2004). Equation (A4.1.5) is valid for $r \in [0, R-\varepsilon)$ (ε = thickness of thin film). Taking $\mathrm{a} = 1$Å and $\varepsilon \sim 22$Å and solving Eq. (A4.1.5) by RK4 using same boundary conditions as before i.e. $\mathrm{d}z/\mathrm{d}r|_{r=0} = 0$, $z(r=0) = h_\infty$ and $\theta = 0^\circ$ we get (same data as used to plot Fig. 4.2): (a) $\theta_a = 0.0874^\circ$ for ethanol, (b) $\theta_a = 0.0897^\circ$ for water, (c) $\theta_a = 0.0894^\circ$ for ethylene glycol and (d) $\theta_a = 0.0844^\circ$ for glycerol.

CHAPTER 5

Conclusions and Future Directions

5.1 Overview

Philip and De Vries (1957) gave for the first time a flow equation based on temperature gradient. Temperature field can influence the pressure field over the whole domain. They implicitly assumed that pressure or pressure difference across meniscus (known as capillary pressure) change with temperature (temperature coefficient of P_c) is only due to surface tension change with temperature (temperature coefficient of σ). They ignored other effects implying previous results of Richards et al. (1938) and Gardner (1955) to be "uncertain". Their assumptions were justified then because of scanty experimental results. As already discussed in chapter 1, the temperature coefficient of P_c (or, $\partial P_c/\partial T|_\eta$) seems *elusive* still today (extending the comment by Grant and Bachmann, 2002). In this thesis, we have tried to answer some of the unanswered questions.

5.1.1 Plausible answers

Here we have given the plausible answers to the questions raised in Section-1.3 of Chapter-1.

Q. Can Y-L equation alone explain the existed disparity among model and experimental values? The Young-Laplace equation or in more general Laplace's theorem states:

$$P_c = \sigma \times K_m \tag{5.1}$$

We think this equation is more suitable for describing capillary pressure than usual form of Y-L equation, i.e. where K_m is replaced in Eq. (5.1) with $\frac{2\cos\theta_e}{R}$ mostly without question. In our opinion, this replacement (with an implicit spherical shape assumption) of K_m looses the meniscus information and thus affect eventually P_c and P_c-*vs.*-T relation.

Q. Is the temperature sensitivity of capillary pressure affected by the degree of saturation? Yes (see Table 4.5). Values suggest weak effect of temperature on η.

Q. Is any model consistent with the measured apparent effect of temperature on contact angles? Results of $\frac{\Delta\theta_a}{\Delta T}$ varies from one literature (King, 1981;She and Sleep, 1998; Figure 10 of Grant and Bachmann, 2002) to other (Bachmann et al., 2002; Grant, 2003). Same way result obtained from PME go with first group, whereas result from *m*PME go with the later group. These two formulations differs in terms of effect of air over meniscus. This shows that assumptions (A4/A6) of uniformity of air/air pressure in porous domain is not the case and non-uniform distribution of air may contribute to these alternating results. The effect of air or gaseous phase is an important fact to be considered as already shown by Maggi and Alonso-Marroquin (2012) in their analysis.

Q. Is the effects of temperature enough on entrapped air to influence capillary pressure? We have studied entrapped-air in terms of dead-end pores not like Peck's (1960) account of entrapped-air bubbles in the liquid. Our assumption throughout the thesis is that soil-water is homogeneous and thus free from any solutes and contaminants and as well air bubbles. Even though Grant and Bachmann (2002) mentioned the effects of entrapped air as a possible mechanism, however in their conclusions they have discarded this as contributing factor in the disparity of experimental and developed model values of temperature coefficient of P_c. Gao and Shao (2015) after modeling and experiments remarked on the entrapped air effects as a likely factor of influence. Question of influence or significance of entrapped air can be answered if one take into θ_e, R of entrapped air pore and how much of such pores are there in an averaging volume or weighting factor of such pores as mentioned in Chapter-2 (Eq. (2.29)). Value of P_c can go up to 0.579 kPa with $T = 10$ K for glass−water−air system and 1.624 kPa with $T = 10$ K for P-N-A system. Question that is the value *enough* to influence, is a contextual one and may vary one situation to another.

Now, how does the knowledge of temperature coefficient of P_c ultimately affect the unsaturated flow? We have already discussed the theory part of this question in Chapter-1 and in the following section, we discuss the same question quantitatively with state-of-the-art literatures to give some practical perspectives of the thesis topic.

5.1.2 Practical perspective

Temperature in unsaturated soil is affected by heat transfer from ground surface, specifically due to change in land cover (e.g. deforestation, snow cover, human-made surface and subsurface constructions etc.) as well as from cold or warm infiltrated rain water or seepage water from open water sources (Taylor and Stefan, 2009). This provides with the temperature gradient (∇T) in the thermal component of unsaturated soil-water flux, i.e. $-K_w \frac{\partial \psi}{\partial T}\Big|_{\eta} \nabla T$ (Philip and De Vries, 1957). In the following paragraph, we show with an example the effects of temperature on unsaturated flow.

Calculation of the thermal component of unsaturated soil-water flux (e.g. in sandy loam)

$$\psi(\eta,T) = \frac{P_c(\eta,T)}{\rho(T)\,g}. \tag{5.2}$$

$$\left.\frac{\partial\psi}{\partial T}\right|_{\eta} = \frac{1}{\rho g}\left.\frac{\partial P_c}{\partial T}\right|_{\eta} - \frac{P_c}{\rho^2 g}\frac{d\rho}{dT}. \tag{5.3}$$

As an example, we pick sandy loam (as in Gardner, 1955) from Table 4.3, 4.4 and Fig. 4.6 (a) and the values of the variables are as: $T_p = 293.15$ K, $g = 9.81$ m s^{-2}, $\phi = 0.327$, $\eta = 0.149$, $\rho(T_p = 293.15\text{ K}) = 997.84$ kg m^{-3}, $\left.{}^{\partial P_c}/_{\partial T}\right|_{\eta} = -0.8223 \times 10^3$ Pa K^{-1}, $P_c(T_p = 293.15\text{ K}) = 25 \times 10^3$ Pa, ${}^{d\rho}/_{dT} = -0.2177$ kg m^{-3} K^{-1}, $K_{\text{sat}} = 0.3192$ m day^{-1} for a sandy loam sample as calculated by Giakoumakis and Tsakiris (1999).

$$\left.\frac{\partial\psi}{\partial T}\right|_{\eta=0.149} = \frac{-0.8223\times10^3}{997.84\times9.81} - \frac{25\times10^3}{997.84^2\times9.81}\times -0.2177,$$

$$\left.\frac{\partial\psi}{\partial T}\right|_{\eta=0.149} = -0.084 + 0.00056 = -0.08344\text{ m K}^{-1}.$$

Unsaturated hydraulic conductivity can be estimated approximately as $K_w(\eta) \approx \left({}^{\eta}/_{\phi}\right) K_{\text{sat}} = 0.1454$ m day^{-1}. Assuming a linear relationship of temperature with the depth of ground in downward z-direction with ground level as reference axis as $T = T_a z + T_b$, where T_a is temperature gradient and T_b temperature at ground level. With different values of temperature gradient values $T_a = 0.1, 0.5, 1$ K m^{-1}, water pore velocities are:

$$v_z = -\frac{K_w}{\phi\eta}\left.\frac{\partial\psi}{\partial T}\right|_{\eta}\frac{dT}{dz} = -\frac{0.1454}{0.327\times0.149}\times -0.08344\times T_a = 0.249T_a;$$

$$v_z = 0.0249, 0.1245, 0.249\text{ m day}^{-1}.$$

Mean depth of unsaturated soil zone is around 5 m (Fan et al., 2013), whereas plant root depth is typically 4.6 ± 0.5 m (Canadell et al., 1996). Thus, unsaturated zone plays as a reserve of water for vegetation/plants (especially, crops). Value of the unsaturated soil-water velocity gets more with more temperature gradient, and thus this zone loses water. In more technical term, temperature can affect *water holding capacity* of the soils in term of capillary pressure. Scarcity of soil-water in unsaturated zone can impact root physiology and growth (Bao et al., 2014) and can put stress on the plants. Eventually, this may pose as a problem in agriculture without any rainfall or irrigation as Ritchie (1981) mentioned that "[T]the water problem in agriculture is related ... to the reserves of water in the soil that are available to plants".

5.2 Conclusions

We can conclude the following aspects of our study with keeping in mind of the above answers and our work in this thesis:

- Capillary pressure is a linear decreasing function of temperature regardless of the porous media or soil.
- Temperature affects the capillary pressure in dead end pores in less pronounced way than that of open end pores. As volume of entrapped air becomes less, capillary pressure becomes less sensitive with temperature and vice versa.
- Physical dimension of the pore size affects the pressure field values.
- Initial values of SCA i.e., wetting properties of the soil changes the temperature coefficient of P_c.
- Density values of air and liquid influence the sensitivity of SCA-*vs.*-T.
- Temperature is an intrinsic reason for the contact angle hysteresis.
- The assumption of spherical meniscus imposed upon Y-L equation, i.e. the usual form of Y-L equation fails to incorporate real contact angle (ACA) and fails in more general term. Inclusion of gravity effects in the formation of meniscus as PME gives the effect of ACA with temperature and liquid content (or, 1 - air content) as found in experiments (She and Sleep, 1998; Bachmann et al., 2002).
- Air phase has an impact on the relation of ACA-*vs.*-T. Presence or absence of air phase over meniscus changes the trend. Presence depicts the increasing trend and absence shows the decreasing trend of ACA (or SCA)-*vs.*-T for hydrophilic soil and for hydrophobic soil vice versa.
- The PME encompasses the whole effect of pore radius, contact angle and surface tension of liquid, whereas *m*PME lacks the information of ACA. That shows impact of both air and liquid phase over the meniscus formation. The results already confirm the effectiveness of PME over *m*PME results with respect to the experimental observations.
- Spherical shape may not be a good approximation universally, though it serves well for most cases. It is an assumption, *not* a fact.
- Emphasizing over the last point, it is very important to note that curvature is an central factor in P_c-*vs.*-T.

We recommend to use the basic relation of $P_c = \sigma \times K_m$. If one wants to use $\langle (P_c)_{\text{Y-L}} \rangle = \langle \frac{2\sigma \cos(\theta)_{\text{Y-L}}}{R} \rangle$ instead, we recommend the use of a correction factor to include the missing information of meniscus i.e. to associate the effects of air or gaseous phase following the arguments made in Section-4.4.4 as:

$$\langle (P_c)_{\text{soil}} \rangle = \mathbf{C_f} \times \langle (P_c)_{\text{Y-L}} \rangle, \tag{5.4}$$

where $\mathbf{C_f} = \langle \frac{\cos(\theta)_{\text{soil}}}{R} \rangle \langle \frac{\cos(\theta)_{\text{Y-L}}}{R} \rangle^{-1}$ = a correction factor, and by $(\theta)_{\text{Y-L}}$ and $(\theta)_{\text{soil}}$, we mean θ_e and θ_a respectively.

5.3 Future directions

Above Q&As may clarify some of the doubts. We have used many simplifications/assumptions in deriving the above equations and with every simplification/assumption comes one more limitation. Numerical solution of the above equations rather than analytical solution limits the approach and though those results give the insight into the phenomena. These limitations can be explored in future individually or as a set. We have presented the algorithm 'AoA'. This algorithm can be used for extracting values from pore space to an averaging context. As Gao and Shao (2015) pointed out about the temperature effect of soil particle on P_c, the spacing parameter d (as a function of T) can be used to include the temperature effect of soil particles. One can extend the formulation of static cases of P_c presented here to dynamic cases using DCA (Eq. (A3.1)), meniscus velocity u (see Washburn, 1921; Quéré, 1997; Maggi and Alonso-Marroquin, 2012; Das and Mitra, 2013; Delannoy et al., 2018) and dynamic CPSR as suggested in Milatz et al. (2018). More importantly, further research could and should focus on the future novel experiments and instrumentation on soil or porous media in general.

References

Abramowitz, M. and Stegun, I. A., editors (1972). *Handbook of mathematical functions with formulas, graphs, and mathematical tables*, chapter Laplace Transforms, pages 1019–1030. Dover Publications, New York. (Cited on page 59)

Adamson, A. W. (1973). Potential distortion model for contact angle and spreading. II. Temperature dependent effects. *Journal of Colloid and Interface Science*, 44(2):273–281. (Cited on pages 48 and 49)

Adomian, G. (1994). *Solving frontier problems of physics: The decomposition method*. Kluwer Academic Publishers, Boston. (Cited on page 59)

Bachmann, J., Horton, R., Grant, S. A., and van der Ploeg, R. R. (2002). Temperature dependence of water retention curves for wettable and water-repellent soils. *Soil Science Society of America Journal*, 66(1):44–52. (Cited on pages 12, 34, 71, 72, 74, 82, and 84)

Bachmann, J. and van der Ploeg, R. R. (2002). A review on recent developments in soil water retention theory: interfacial tension and temperature effects. *Journal of Plant Nutrition and Soil Science*, 165:498–478. (Cited on pages 11 and 12)

Bao, Y., Aggarwal, P., Robbins, N. E., Sturrock, C. J., Thompson, M. C., Tan, H. Q., Tham, C., Duan, L., Rodriguez, P. L., Vernoux, T., et al. (2014). Plant roots use a patterning mechanism to position lateral root branches toward available water. *Proceedings of the National Academy of Sciences*, 111(25):9319–9324. (Cited on page 83)

Batchelor, G. K. (2000). *An introduction to fluid dynamics*. Cambridge University Press, Cambridge, UK. (Cited on page 2)

Bear, J. (1972). *Dynamics of fluids in porous media*. Elsevier, Paris. (Cited on pages 7, 15, and 68)

Bear, J. and Bachmat, Y. (1990). *Introduction to modeling phenomena of transport in porous media*. Kluwer Academic Publishers, Dordrecht, The Netherlands. (Cited on pages 3 and 4)

Bear, J. and Corapcioglu, M. Y. (1981). Mathematical model for regional land subsidence due to pumping: 1. Integrated aquifer subsidence equations based on vertical displacement only. *Water Resources Research*, 17(4):937–946. (Cited on pages 3 and 4)

Bear, J., Rubinstein, B., and Fel, L. (2011). Capillary pressure curve for liquid menisci in a cubic assembly of spherical particles below irreducible saturation. *Transport in Porous Media*, 89(1):63–73. (Cited on pages 9, 55, and 70)

Bell, J. M. and Cameron, F. K. (1906). The flow of liquids through capillary spaces. *The Journal of Physical Chemistry*, 10(8):658–674. (Cited on page 55)

Beltrami, H., Ferguson, G., and Harris, R. N. (2005). Long-term tracking of climate change by underground temperatures. *Geophysical Research Letters*, 32:L19707. (Cited on page 1)

Bernoulli, D. (1738). *Hydrodynamica*. Sumptibus Johannis Reinholdi Dulseckeri, Basel. (Cited on page 2)

Biazar, J. and Shafiof, S. M. (2007). A simple algorithm for calculating adomian polynomials. *International Journal of Contemporary Mathematical Sciences*, 2(20):975–982. (Cited on page 59)

Biswas, D. and Kartha, S. A. (2017). Temperature dependence of contact angle hysteresis. In *Proc. 9th World Conf. on Experimental Heat Transfer, Fluid Mechanics, and Thermodynamics (ExHFT-9)*, page PT28 (9 Pages), Iguazu Falls, Brazil, 11-15 June, 2017. (Cited on page 13)

Biswas, D. and Kartha, S. A. (2019). Conceptual modeling of temperature effects on capillary pressure in dead-end pores. *Sādhanā*, 44(5):117. (Cited on page 13)

Blake, T. D. and Haynes, J. M. (1969). Kinetics of liquid/liquid displacement. *Journal of Colloid and Interface Science*, 30(3):421–423. (Cited on page 50)

Blundell, S. J. and Blundell, K. M. (2006). *Concepts in thermal physics*. Oxford University Press, Oxford. (Cited on page 7)

Bonn, D., Eggers, J., Indekeu, J., Meunier, J., and Rolley, E. (2009). Wetting and spreading. *Reviews of Modern Physics*, 81(2):739–805. (Cited on page 39)

Bouyoucos, G. (1915). Effect of water vapor and capillary moisture in soils. *Journal of Agricultural Research*, 5(4):141–172. (Cited on page 8)

Briggs, L. and McCall, A. (1904). An artificial root for inducing capillary movement of soil moisture. *Science*, 20(513):566–569. (Cited on page 13)

Brooks, R. H. and Corey, A. T. (1964). *Hydraulic properties of porous media, Hydrology Paper 3*. Colorado State University, Fort Collins. (Cited on page 9)

Buckingham, E. (1907). *Studies on the movement of soil moisture*. Bull. 38, USDA, Bureau of Soils, Washington D. C. (Cited on pages 3 and 6)

Butt, H.-J., Graf, K., and Kappl, M. (2003). *Physics and chemistry of interfaces*. WILEY-VCH Verlag GmbH & Co. KGaA, Weinheim. (Cited on page 7)

Canadell, J., Jackson, R., Ehleringer, J., Mooney, H., Sala, O., and Schulze, E.-D. (1996). Maximum rooting depth of vegetation types at the global scale. *Oecologia*, 108(4):583–595. (Cited on page 83)

Cass, A., Campbell, G., and Jones, T. (1984). Enhancement of thermal water vapor diffusion in soil[1]. *Soil Science Society of America Journal*, 48(1):25–32. (Cited on page 9)

Çengel, Y. A. (2003). *Heat transfer: A practical approach (2nd Edition)*. McGraw-Hill, Inc., New York. (Cited on page 7)

Çengel, Y. A. and Boles, M. A. (2015). *Thermodynamics: An engineering approach (8th Edition)*. McGraw-Hill, Inc., New York. (Cited on pages 17 and 36)

Chebbi, R. (2007). Dynamics of liquid penetration into capillary tubes. *Journal of Colloid and Interface Science*, 315(1):255–260. (Cited on page 50)

Clayton, W. S. (1999). Effects of pore scale dead-end air fingers on relative permeabilities for air sparging in soils. *Water Resources Research*, 35(10):2909–2919. (Cited on page 15)

Coats, K. and Smith, B. (1964). Dead-end pore volume and dispersion in porous media. *Society of Petroleum Engineers Journal*, 4(1):73–84. (Cited on pages 15 and 35)

Collins, R. E. (1961). *Flow of fluids through porous media*. Reinhold Pub. Corp., New York. (Cited on pages 10 and 55)

Constantz, J. (1991). Comparison of isothermal and isobaric water retention paths in nonswelling porous materials. *Water Resources Research*, 27(12):3165–3170. (Cited on page 11)

Coxeter, H. S. M. (1969). *Introduction to geometry (2nd Edition)*. Wiley, New York. (Cited on page 67)

Darcy, H. (1856). *Les Fontaines Publiques de la Ville de Dijon (In French)*. Dalmont, Paris. (Cited on page 3)

Das, S. and Mitra, S. K. (2013). Different regimes in vertical capillary filling. *Physical Review E*, 87(6):063005. (Cited on page 85)

Das, S., Mitra, S. K., and Chakraborty, S. (2012). Wenzel and Cassie-Baxter states of an electrolytic drop on charged surfaces. *Physical Review E*, 86(1):011603. (Cited on page 45)

De Gennes, P.-G., Brochard-Wyart, F., and Quéré, D. (2004). *Capillarity and wetting*

phenomena: Drops, bubbles, pearls, waves. Springer-Verlag, New York. (Cited on pages 6, 17, 18, 22, 36, 40, 41, 57, 62, and 79)

De Smedt, F. and Wierenga, P. (1979). A generalized solution for solute flow in soils with mobile and immobile water. *Water Resources Research*, 15(5):1137–1141. (Cited on page 15)

De Vries, D. A. (1987). The theory of heat and moisture transfer in porous media revisited. *International Journal of Heat and Mass Transfer*, 30(7):1343–1350. (Cited on pages 7 and 9)

De Wiest, R. J. (1966). On the storage coefficient and the equations of groundwater flow. *Journal of Geophysical Research*, 71(4):1117–1122. (Cited on page 3)

Dean, J. A. (1999). *Lange's handbook of chemistry*. McGraw-Hill, Inc., New York. (Cited on pages 22, 23, 24, 34, 44, and 70)

Delannoy, J., de Maleprade, H., Clanet, C., and Quéré, D. (2018). Capillary descent. *Soft Matter*, 14:5364–5368. (Cited on page 85)

Dullien, F. A. L., El-Sayed, M. S., and Batra, V. K. (1977). Rate of capillary rise in porous media with nonuniform pores. *Journal of Colloid and Interface Science*, 60(3):497–506. (Cited on page 55)

Dupré, A. and Dupré, P. (1869). *Théorie mécanique de la chaleur (In French)*. Gauthier-Villars, Paris. (Cited on page 7)

Durner, W. (1994). Hydraulic conductivity estimation for soils with heterogeneous pore structure. *Water Resources Research*, 30(2):211–223. (Cited on page 9)

Egloff, G. (1939). *Physical constants of Hydrocarbons Vol. I*. Reinhold Pub. Corp., New York. (Cited on page 49)

Elliott, G. E. P. and Riddiford, A. C. (1967). Dynamic contact angles: I. the effect of impressed motion. *Journal of Colloid and Interface Science*, 23(3):389–398. (Cited on pages 18 and 42)

Ellison, A. H., Klemm, R. B., Schwartz, A. M., Grubb, L. S., and Petrash, D. A. (1967). Contact angles of mercury on various surfaces and the effect of temperature. *Journal of Chemical and Engineering Data*, 12(4):607–609. (Cited on page 45)

Eppstein, D. (2001). Tangent spheres and triangle centers. *The American Mathematical Monthly*, 108(1):63–66. (Cited on page 67)

Euler, L. (1755). *Institutiones calculi differentialis*. B. G. Teubner, Leipzig. (Cited on page 2)

Extrand, C. W. and Moon, S. I. (2013). Experimental measurement of forces and energies associated with capillary rise in a vertical tube. *Journal of Colloid and Interface science*, 407:488–492. (Cited on pages 56 and 57)

Fan, Y., Li, H., and Miguez-Macho, G. (2013). Global patterns of groundwater table depth. *Science*, 339(6122):940–943. (Cited on pages 1 and 83)

Fatoorehchi, H. and Abolghasemi, H. (2016). Series solution of nonlinear differential equations by a novel extension of the laplace transform method. *International Journal of Computer Mathematics*, 93(8):1299–1319. (Cited on page 59)

Fatt, I., Maleki, M., and Upadhyay, R. N. (1966). Detection and estimation of dead-end pore volume in reservoir rock by conventional laboratory tests. *Society of Petroleum Engineers Journal*, 6(3):206–212. (Cited on page 34)

Faybishenko, B. (1983). Effect of temperature on moisture content, entropy, and water pressure in loam soils (In Russian). *Pochvevedenie*, 12:43–48. (Cited on page 16)

Fredlund, D. G. and Xing, A. (1994). Equations for the soil-water characteristic curve. *Canadian Geotechnical Journal*, 31(4):521–532. (Cited on page 9)

Gao, H. and Shao, M. (2015). Effects of temperature changes on soil hydraulic properties. *Soil and Tillage Research*, 153:145–154. (Cited on pages 12, 13, 82, and 85)

Gao, L. and McCarthy, T. J. (2006). Contact angle hysteresis explained. *Langmuir*, 22(14):6234–6237. (Cited on page 39)

Gardner, R. (1955). Relation of temperature to moisture tension of soil. *Soil Science*, 79(4):257–266. (Cited on pages 11, 72, 81, and 83)

Gardner, W. R. (1956). Calculation of capillary conductivity from pressure plate and flow data. *Soil Science Society of America, Proceedings*, 20:317–320. (Cited on page 9)

Giakoumakis, S. and Tsakiris, G. (1999). Quick estimation of hydraulic conductivity in unsaturated sandy loam soil. *Irrigation and Drainage Systems*, 13(4):349–359. (Cited on page 83)

Girifalco, L. A. and Good, R. J. (1957). A theory for the estimation of surface and interfacial energies: I. Derivation and application to interfacial tension. *The Journal of Physical Chemistry.*, 61(7):904–909. (Cited on page 23)

Glycerine Producers' Association (1963). *Physical properties of glycerine and its solutions*. Glycerine Producers' Association, New York. (Cited on page 44)

Golfman, Y. (2012). *Hybrid anisotropic materials for wind power turbine blades*. CRC Press, Florida. (Cited on pages 32 and 44)

Goodknight, R. C., Klikoff Jr, W. A., and Fatt, I. (1960). Non-steady-state fluid flow and diffusion in porous media containing dead-end pore volume. *The Journal of Physical Chemistry*, 64(9):1162–1168. (Cited on page 15)

Grant, S. A. (2003). Extension of a temperature effects model for capillary pressure saturation relations. *Water Resources Research*, 39(1):SBH–1. (Cited on pages 12, 16, 19, 25, 32, 34, 71, and 82)

Grant, S. A. and Bachmann, J. (2002). Effect of temperature on capillary pressure. In P. A. C. Raats, D. S. and Warrick, A. W., editors, *Environmental Mechanics: Water, Mass and Energy Transfer in the Biosphere: The Philip Volume*, pages 199–212. American Geophysical Union, Washington, D. C. (Cited on pages 11, 16, 25, 34, 71, 74, 81, and 82)

Grant, S. A. and Salehzadeh, A. (1996). Calculation of temperature effects on wetting coefficients of porous solids and their capillary pressure functions. *Water Resources Research*, 32(2):261–270. (Cited on pages 11 and 12)

Grifoll, J., Gasto, J. M., and Cohen, Y. (2005). Non-isothermal soil water transport and evaporation. *Advances in Water Resources*, 28(11):1254–1266. (Cited on page 9)

Gurr, C., Marshall, T., and Hutton, J. (1952). Movement of water in soil due to a temperature gradient. *Soil Science*, 74(5):335–346. (Cited on page 8)

Hager, W. H. (2012). Wilfrid Noel Bond and the Bond number. *Journal of Hydraulic Research*, 50(1):3–9. (Cited on pages 22 and 40)

Hall, W. A. (1956). An analytical derivation of the Darcy equation. *Eos, Transactions American Geophysical Union*, 37(2):185–188. (Cited on page 3)

Handy, R. L. (1973). The igloo and the natural bridge as ultimate structures. *Arctic*, 26(4):276–281. (Cited on page 40)

Hansen, R. J. and Toong, T. Y. (1971). Dynamic contact angle and its relationship to forces of hydrodynamic origin. *Journal of Colloid and Interface Science*, 37(1):196–207. (Cited on page 57)

Haridasan, M. (1970). Effect of temperature on pressure head-water content relationship and conductivity of two soils, Ph.D. dissertation, Mississippi State University, Starkville. *Diss. Abstr. 32/07b:3740*. (Cited on page 11)

Haridasan, M. and Jensen, R. (1972). Effect of temperature on pressure head-water content

relationship and conductivity of two soils[1]. *Soil Science Society of America Journal*, 36(5):703–708. (Cited on page 11)

Hassanizadeh, M. and Gray, W. G. (1979). General conservation equations for multi-phase systems: 1. Averaging procedure. *Advances in Water Resources*, 2:131–144. (Cited on page 6)

Hassanizadeh, S. M. and Gray, W. G. (1993). Thermodynamic basis of capillary pressure in porous media. *Water Resources Research*, 29(10):3389–3405. (Cited on pages 17, 19, and 42)

Hastad, J., Just, B., Lagarias, J. C., and Schnorr, C.-P. (1989). Polynomial time algorithms for finding integer relations among real numbers. *SIAM Journal on Computing*, 18(5):859–881. (Cited on page 65)

Hauksbee, F. (1710). An account of an experiment touching the ascent of water between two glass planes, in an hyperbolick figure. By Mr. Francis Hauksbee, FRS. *Philosophical Transactions*, 27(325-336):539–540. (Cited on page 50)

Hillel, D. (1980). *Fundamentals of soil physics*. Academic Press, New York. (Cited on pages 2 and 64)

Hilpert, M. (2009). Effects of dynamic contact angle on liquid infiltration into horizontal capillary tubes: (Semi)-analytical solutions. *Journal of Colloid and Interface Science*, 337:131–137. (Cited on page 50)

Hoffman, J. D. (2001). *Numerical methods for engineers and scientists (2nd Edition)*. Marcel Dekker, Inc., New York. (Cited on page 21)

Hoffman, R. L. (1975). A study of the advancing interface. I. Interface shape in liquid-gas systems. *Journal of Colloid and Interface Science*, 50(2):228–241. (Cited on page 40)

Hoffmann, M. R. (2003). *Macroscopic equations for flow in unsaturated porous media*. Ph.D. dissertation, Wageningen Universiteit, Wageningen, The Netherlands. (Cited on page 4)

Hopmans, J. and Dane, J. (1986). Temperature dependence of soil water retention curves[1]. *Soil Science Society of America Journal*, 50(3):562–567. (Cited on page 11)

Hubbert, M. K. (1940). The theory of ground-water motion. *The Journal of Geology*, 48(8, Part 1):785–944. (Cited on pages 2 and 3)

Hubbert, M. K. (1956). Darcy's law and the field equations of the flow of unsaturated fluids. *Petroleum Transactions, AIME*, 207:222–239. (Cited on page 3)

Hunt, A. (2005). Continuum percolation theory for saturation dependence of air permeability. *Vadose Zone Journal*, 4(1):134–138. (Cited on page 15)

Iden, S. C. and Durner, W. (2014). Comment on "Simple consistent models for water retention and hydraulic conductivity in the complete moisture range" by A. Peters. *Water Resources Research*, 50(9):7530–7534. (Cited on page 10)

Jaafar, R. and Likos, W. J. (2011). Estimating water retention characteristics of sands from grain size distribution using idealized packing conditions. *Geotechnical Testing Journal*, 34(5):489–502. (Cited on page 64)

Jackson, R. D. and Klute, A. (1967). Estimation of dead-end pore volume in soils from transient-and steady-state diffusion coefficients. *Soil Science Society of America Journal*, 31(1):122–123. (Cited on pages 15, 34, and 35)

Jamaloei, B. Y. and Kharrat, R. (2009). Fundamental study of pore morphology effect in low tension polymer flooding or polymer–assisted dilute surfactant flooding. *Transport in Porous Media*, 76(2):199–218. (Cited on page 15)

Jang, W. and Aral, M. M. (2009). Multiphase flow fields in in-situ air sparging and its effect on remediation. *Transport in Porous Media*, 76(1):99–119. (Cited on page 15)

Jasper, J. J. and Kring, E. V. (1955). The isobaric surface tensions and thermodynamic properties of the surfaces of a series of n-alkanes, C_5 to C_{18}, 1-alkenes, C_6 to C_{16}, and of n-decylcyclopentane, n-decylcyclohexane and n-dcylbenzene. *The Journal of Physical Chemistry*, 59(10):1019–1021. (Cited on page 49)

Johnson Jr, R. E. and Dettre, R. H. (1964). Contact angle hysteresis. III. study of an idealized heterogeneous surface. *The Journal of Physical Chemistry*, 68(7):1744–1750. (Cited on pages 19 and 39)

Jury, W. and Miller, E. (1974). Measurement of the transport coefficients for coupled flow of heat and moisture in a medium sand[1]. *Soil Science Society of America Journal*, 38(4):551–557. (Cited on page 11)

Jury, W. A. (1973). Simultaneous transport of heat and moisture through a medium sand, Ph.D. dissertation, University of Wisconsin, Madison. *Diss. Abstr. 34/08b:3585*. (Cited on page 11)

Kalman, D. (1984). The maximum and minimum of two numbers using the quadratic formula. *The College Mathematics Journal*, 15(4):329–330. (Cited on page 45)

Kar, A., Chiang, T.-Y., Ortiz Rivera, I., Sen, A., and Velegol, D. (2015). Enhanced transport into and out of dead-end pores. *ACS Nano*, 9(1):746–753. (Cited on page 15)

King, P. (1981). Comparison of methods for measuring severity of water repellence of sandy soils and assessment of some factors that affect its measurement. *Soil Research*, 19(3):275–285. (Cited on pages 71 and 82)

Knight, H. G. (1938). New size limits for silt and clay. *Soil Science Society of America Journal*, 2(C):592–592. (Cited on page 64)

Kosugi, K. (1994). Three-parameter lognormal distribution model for soil water retention. *Water Resources Research*, 30(4):891–901. (Cited on page 9)

Krischer, O. and Rohnalter, H. (1940). *Wärmeleitung und Dampfdiffusion in feuchten Gütern: mit 4 Zahlentafeln (In German)*. VDI-Verlag, Berlin. (Cited on page 8)

Kuchin, I. V. and Starov, V. M. (2016). Hysteresis of the contact angle of a meniscus inside a capillary with smooth, homogeneous solid walls. *Langmuir*, 32(21):5333–5340. (Cited on pages 19, 39, and 50)

Lamb, H. (1932). *Hydrodynamics (6th Edition)*. Cambridge University Press, Cambridge, UK. (Cited on page 5)

Laplace, P. S. (1805). *Traité de mécanique céleste, Supplément au dixiéme livre du Traité de mécanique céleste (in French)*. 4:1–79. (Cited on pages 6 and 55)

Lebeau, M. and Konrad, J.-M. (2010). A simple model for describing hydraulic conductivity in unsaturated porous media accounting for film and capillary flow. *Water Resources Research*, 46:W12554. (Cited on pages 10 and 78)

Lee, S.-L. and Lee, H.-D. (2007). Evolution of liquid meniscus shape in a capillary tube. *Journal of Fluids Engineering*, 129(8):957–965. (Cited on pages 39, 40, and 57)

Lenhard, R. J. and Parker, J. C. (1987). A model for hysteretic constitutive relations governing multiphase flow: 2. permeability-saturation relations. *Water Resources Research*, 23(12):2197–2206. (Cited on page 15)

Liechti, K. M., Schnapp, S. T., and Swadener, J. G. (1997). Contact angle and contact mechanics of a glass/epoxy interface. *International Journal of Fracture*, 86:361–374. (Cited on pages 22 and 45)

Likos, W. J. (2013). Modeling thermal conductivity dryout curves from soil-water characteristic curves. *Journal of Geotechnical and Geoenvironmental Engineering*, 140(5):04013056. (Cited on page 72)

Lipiec, J., Usowicz, B., and Ferrero, A. (2007). Impact of soil compaction and wetness

on thermal properties of sloping vineyard soil. *International Journal of Heat and Mass Transfer*, 50(19-20):3837–3847. (Cited on page 7)

Lockwood, E. H. (1961). *A book of curves*. Cambridge University Press, Cambridge, UK. (Cited on page 40)

Lu, N. and Dong, Y. (2015). Closed-form equation for thermal conductivity of unsaturated soils at room temperature. *Journal of Geotechnical and Geoenvironmental Engineering*, 141(6):04015016. (Cited on page 7)

Lu, N. and Likos, W. J. (2004). *Unsaturated soil mechanics*. John Wiley & Sons, Inc., New Jersey. (Cited on pages 17 and 42)

Lucas, R. (1918). Ueber das zeitgesetz des kapillaren aufstiegs von flüssigkeiten (in German). *Kolloid-Zeitschrift*, 23(1):15–22. (Cited on page 55)

Maggi, F. and Alonso-Marroquin, F. (2012). Multiphase capillary flows. *International Journal of Multiphase Flow*, 42:62–73. (Cited on pages 56, 57, 82, and 85)

Maggi, F. and Alonso-Marroquin, F. (2013). Temperature dependence of capillary dynamics: A multiphase and multicomponent adiabatic approach. *Physical Review E*, 88(5):053013. (Cited on pages 31, 40, 44, 51, and 70)

Makkonen, L. (2017). A thermodynamic model of contact angle hysteresis. *The Journal of Chemical Physics*, 147(6):064703. (Cited on page 19)

Marchand, A., Das, S., Snoeijer, J. H., and Andreotti, B. (2012). Contact angles on a soft solid: From Young's law to Neumann's law. *Physical Review Letters*, 109(23):236101. (Cited on page 7)

Marmur, A. (1994). Thermodynamic aspects of contact angle hysteresis. *Advances in Colloid and Interface Science*, 50:121–141. (Cited on pages 19 and 39)

Meeuwig, R. O. (1964). Effects of temperature on moisture conductivity in unsaturated soil, Ph.D. dissertation, Utah State University, Logan. *Diss. Abstr. 25/06:3180*. (Cited on page 11)

Milatz, M., Törzs, T., Nikooee, E., Hassanizadeh, S. M., and Grabe, J. (2018). Theoretical and experimental investigations on the role of transient effects in the water retention behaviour of unsaturated granular soils. *Geomechanics for Energy and the Environment*, 15:54–64. (Cited on page 85)

Miller, M. A. (1983). Laboratory evaluation of in situ steam flushing for NAPL removal from

soil, Ph.D. dissertation, Stanford University, Stanford, California. *Diss. Abstr. 44/05b:1568*. (Cited on page 11)

Milly, P. (1982). Moisture and heat transport in hysteretic, inhomogeneous porous media: A matric head-based formulation and a numerical model. *Water Resources Research*, 18(3):489–498. (Cited on page 9)

Mohr, P. J., Taylor, B. N., and Newell, D. B. (2016). Codata recommended values of the fundamental physical constants: 2014. *Reviews of Modern Physics*, 88:035009–1–035009–73. (Cited on pages 22 and 24)

Moore, R. (1941). The relation of soil temperature to soil moisture: Pressure potential, retention, and infiltration rate[1]. *Soil Science Society of America Journal*, 5(C):61–64. (Cited on pages 10 and 11)

Mosavat, N. and Torabi, F. (2016). Micro-optical analysis of carbonated water injection in irregular and heterogeneous pore geometry. *Fuel*, 175:191–201. (Cited on page 15)

Mosthaf, K., Baber, K., Flemisch, B., Helmig, R., Leijnse, A., Rybak, I., and Wohlmuth, B. (2011). A coupling concept for two-phase compositional porous-medium and single-phase compositional free flow. *Water Resources Research*, 47(10):W10522. (Cited on page 9)

Mualem, Y. (1976). A new model for predicting the hydraulic conductivity of unsaturated porous media. *Water Resources Research*, 12(3):513–522. (Cited on page 10)

Mumley, T. E., Radke, C. J., and Williams, M. C. (1986). Kinetics of liquid/liquid capillary rise: I. experimental observations. *Journal of Colloid and Interface Science*, 109(2):398–412. (Cited on page 50)

Muskat, M. and Wyckoff, R. D. (1937). *Flow of homogeneous fluids through porous media*. McGraw-Hill, Inc., New York. (Cited on page 2)

Nassar, I. and Horton, R. (1992). Simultaneous transfer of heat, water, and solute in porous media: I. Theoretical development. *Soil Science Society of America Journal*, 56(5):1350–1356. (Cited on page 9)

Nassar, I. and Horton, R. (1997). Heat, water, and solution transfer in unsaturated porous media: I. Theory development and transport coefficient evaluation. *Transport in Porous Media*, 27(1):17–38. (Cited on page 9)

Nassar, I., Horton, R., and Globus, A. (1992). Simultaneous transfer of heat, water, and solute in porous media: II. Experiment and analysis. *Soil Science Society of America Journal*, 56(5):1357–1365. (Cited on page 9)

Nassar, I., Horton, R., and Globus, A. (1997). Thermally induced water transfer in salinized, unsaturated soil. *Soil Science Society of America Journal*, 61(5):1293–1299. (Cited on page 9)

Neumann, A. W. (1974). Contact angles and their temperature dependence: Thermodynamic status, measurement, interpretation and application. *Advances in Colloid and Interface Sciences*, 4:105–191. (Cited on pages 23, 24, and 36)

Neumann, A. W., Haage, G., and Renzow, D. (1971). The temperature dependence of contact angles polytetrafluoroethylene/n-alkanes. *Journal of Colloid and Interface Science*, 35(3):379–385. (Cited on pages 25, 26, 36, 44, 45, 48, and 49)

Nimmo, J. and Miller, E. (1986). The temperature dependence of isothermal moisture vs. potential characteristics of soils[1]. *Soil Science Society of America Journal*, 50(5):1105–1113. (Cited on pages 11 and 72)

Nitao, J. J. and Bear, J. (1996). Potentials and their role in transport in porous media. *Water Resources Research*, 32(2):225–250. (Cited on page 10)

Noborio, K., McInnes, K., and Heilman, J. (1996). Two-dimensional model for water, heat, and solute transport in furrow-irrigated soil: I. theory. *Soil Science Society of America Journal*, 60(4):1001–1009. (Cited on page 7)

Nobre, R. and Thomson, N. (1993). The effects of transient temperature gradients on soil moisture dynamics. *Journal of Hydrology*, 152(1-4):57–101. (Cited on page 9)

Nordbotten, J. M., Celia, M. A., Dahle, H. K., and Hassanizadeh, S. M. (2008). On the definition of macroscale pressure for multiphase flow in porous media. *Water Resources Research*, 44(6):W06S02. (Cited on page 6)

Okandan, E. (1974). The effect of temperature and fluid composition on oil-water capillary pressure curves of limestone and sandstones and measurement of contact angle at elevated temperatures, Ph.D. dissertation, Stanford University, Stanford, California. *Diss. Abstr. 34/12b:6027*. (Cited on page 11)

Onken, U., Rarey-Nies, J., and Gmehling, J. (1989). The Dortmund Data Bank: A computerized system for retrieval, correlation, and prediction of thermodynamic properties of mixtures. *International Journal of Thermophysics*, 10(3):739–747. (Cited on pages 25 and 44)

Or, D. and Tuller, M. (1999). Liquid retention and interfacial area in variably saturated porous media: Upscaling from single-pore to sample-scale model. *Water Resources Research*, 35(12):3591–3605. (Cited on pages 10 and 55)

Parlange, M., Cahill, A., Nielsen, D., Hopmans, J., and Wendroth, O. (1998). Review of heat and water movement in field soils. *Soil and Tillage Research*, 47(1-2):5–10. (Cited on page 9)

Passioura, J. (1980). The meaning of matric potential. *Journal of Experimental Botany*, 31(4):1161–1169. (Cited on page 6)

Peck, A. (1960). Change of moisture tension with temperature and air pressure: Theoretical. *Soil Science*, 89(6):303–310. (Cited on pages 11 and 82)

Peters, A. (2013). Simple consistent models for water retention and hydraulic conductivity in the complete moisture range. *Water Resources Research*, 49(10):6765–6780. (Cited on page 10)

Peters, A. and Durner, W. (2008). A simple model for describing hydraulic conductivity in unsaturated porous media accounting for film and capillary flow. *Water Resources Research*, 44:W11417. (Cited on page 10)

Philip, J. (1968). Diffusion, dead-end pores, and linearized absorption in aggregated media. *Soil Research*, 6(1):21–30. (Cited on page 15)

Philip, J. R. and De Vries, D. A. (1957). Moisture movement in porous materials under temperature gradients. *Transactions American Geophysical Union*, 38(2):222–232. (Cited on pages 8, 34, 81, and 82)

Phirani, J., Roy, S., and Pant, H. (2018). Predicting stagnant pore volume in porous media using temporal moments of tracer breakthrough curves. *Journal of Petroleum Science and Engineering*, 165:640–646. (Cited on pages 34 and 35)

Piskunov, N. S. (1969). *Differential and integral calculus*. Mir Publisher, Moscow. (Cited on pages 41 and 62)

Pompe, T. and Herminghaus, S. (2000). Three-phase contact line energetics from nanoscale liquid surface topographies. *Physical Review Letters*, 85(9):1930–1933. (Cited on page 19)

Popiel, C. O., Wojtkowiak, J., and Biernacka, B. (2001). Measurements of temperature distribution in ground. *Experimental Thermal and Fluid Science*, 25(5):301–309. (Cited on page 24)

Poynting, J. H. and Thomson, J. J. (1902). *A textbook of physics: Properties of matter*. Griffin, London. (Cited on pages 19 and 42)

Quéré, D. (1997). Inertial capillarity. *Europhysics Letters*, 39(5):533–538. (Cited on page 85)

Quéré, D. (2008). Wetting and roughness. *Annual Review of Materials Research*, 38:71–99. (Cited on pages 19 and 39)

Rand, R. H. (1978). The dynamics of an evaporating meniscus. *Acta Mechanica*, 29:135–146. (Cited on pages 40 and 42)

Richards, L. A. (1928). The usefulness of capillary potential to soil-moisture and plant investigations. *Journal of Agricultural Research*, 37:719–742. (Cited on pages 3, 6, and 13)

Richards, L. A. (1931). Capillary conduction of liquids through porous mediums. *Journal of Applied Physics*, 1(5):318–333. (Cited on page 3)

Richards, L. A. and Neal, O. R. (1937). Some field observations with tensiometers (1). *Soil Science Society of America Journal*, 1(C):71–91. (Cited on page 10)

Richards, L. A., Russell, M. B., and Neal, O. R. (1938). Further developments on apparatus for field moisture studies[1]. *Soil Science Society of America Journal*, 2(C):55–64. (Cited on pages 10 and 81)

Richards, L. A. and Weaver, L. R. (1944). Moisture retention by some irrigated soils as related to soil moisture tension. *Journal of Agricultural Research*, 69(6):215–235. (Cited on page 10)

Ritchie, J. T. (1981). Water dynamics in the soil-plant-atmosphere system. *Plant and Soil*, 58(1):81–96. (Cited on page 83)

Rodell, M., Famiglietti, J. S., Wiese, D. N., Reager, J. T., Beaudoing, H. K., W, L. F., and Lo, M.-H. (2018). Emerging trends in global freshwater availability. *Nature*, 557:651–672. (Cited on page 1)

Rollins, R. L. (1954). Movement of soil moisture under a thermal gradient, Ph.D. dissertation, Iowa State University. *Retrospective Theses and Dissertations.*, 13247. (Cited on page 8)

Salehzadeh, A. (1990). The temperature dependence of soil moisture characteristics of agricultural soils, Ph.D. dissertation, Univ. Wisconsin, Madison. *Diss. Abstr. 51/09b:4245*. (Cited on page 11)

Santiago, C., Ghomeshi, S., Kryuchkov, S., and Kantzas, A. (2016). Pore level modeling of imbibition in heavy oil saturated media. *Journal of Petroleum Science and Engineering*, 140:108–118. (Cited on page 15)

Schutz, B. F. (1980). *Geometrical methods of mathematical physics*. Cambridge University Press, Cambridge, UK. (Cited on page 4)

Sedaghat, M. H., Hatampour, A., and Razmi, R. (2013). Investigating the role of polymer type and dead end pores' distribution on oil recovery efficiency during asp flooding. *Egyptian Journal of Petroleum*, 22(2):241–247. (Cited on page 15)

Seki, K. (2007). Swrc fit–a nonlinear fitting program with a water retention curve for soils having unimodal and bimodal pore structure. *Hydrology and Earth System Sciences Discussions*, 4(1):407–437. (Cited on page 9)

Seward III, T. P. and Vascott, T. (2005). *High temperature glass melt property database for process modeling*. The American Ceramic Society, Westerville, Ohio. (Cited on page 23)

She, H. Y. (1997). Laboratory evaluation of in-situ steam flushing for NAPL removal from soil, Ph.D. dissertation, Univ. Toronto, Toronto. *Diss. Abstr. 51/06b:2918*. (Cited on page 11)

She, H. Y. and Sleep, B. E. (1998). The effect of temperature on capillary pressure-saturation relationships for air-water and perchloroethylene-water systems. *Water Resources Research*, 34(10):2587–2597. (Cited on pages 11, 25, 72, 82, and 84)

Slattery, J. C. and Flumerfelt, R. W. (1982). Interfacial phenomena. *Handbook of Multiphase Systems*, (1):224–254. (Cited on pages 18 and 42)

Smerdon, J. E., Pollack, H. N., Cermak, V., Enz, J. W., Kresl, M., Safanda, J., and Wehmiller, J. F. (2006). Daily, seasonal, and annual relationships between air and subsurface temperatures. *Journal of Geophysical Research*, 111(D07101). (Cited on page 1)

Smith, W. (1943). Thermal transfer of moisture in soils. *Eos, Transactions American Geophysical Union*, 24(2):511–524. (Cited on page 8)

Soddy, F. (1936). The kiss precise. *Nature*, 137:1021. (Cited on page 67)

Soil Conservation Service (1975). Soil taxonomy: a basic system of soil classification for making and interpreting soil surveys. In *Agricultural Handbook no. 436*. USDA-SCS. (Cited on pages 64 and 70)

Soil Science Society of America (2008). *Glossary of soil science terms 2008*. ASA-CSSA-SSSA. (Cited on pages 2 and 33)

Sposito, G. (1986). The "physics" of soil water physics. *Water Resources Research*, 22(9):83S–88S. (Cited on page 3)

Sutula, C. L., Houtala, R., Dalla Betta, R. A., and Michel, I. A. (1967). *Abstracts*. 153rd Meeting, American Chemical Society. (Cited on page 49)

Tamura, M., Kurata, M., and Odani, H. (1955). Practical method for estimating surface tensions of solutions. *Bulletin of the Chemical Society of Japan*, 28(1):83–88. (Cited on page 51)

Taniguchi, M., Uemura, T., and Jago-on, K. (2007). Combined effects of urbanization and global warming on subsurface temperature in four asian cities. *Vadose Zone Journal*, 6(3):591–596. (Cited on page 1)

Taylor, C. A. and Stefan, H. G. (2009). Shallow groundwater temperature response to climate change and urbanization. *Journal of Hydrology*, 375(3-4):601–612. (Cited on page 82)

Taylor, S., Evans, D., and Kemper, W. (1961). Evaluating soil water. *Utah Agricultural Experiment Station Bulletin*, No 426. (Cited on page 11)

Taylor, S. A. and Cavazza, L. (1954). The movement of soil moisture in response to temperature gradients[1]. *Soil Science Society of America Journal*, 18(4):351–358. (Cited on page 8)

Tokunaga, T. K. (2009). Hydraulic properties of adsorbed water films in unsaturated porous media. *Water Resources Research*, 45(6):W06415. (Cited on page 10)

Tuller, M., Or, D., and Dudley, L. M. (1999). Adsorption and capillary condensation in porous media: Liquid retention and interfacial configurations in angular pores. *Water Resources Research*, 35(7):1949–1964. (Cited on page 10)

van Genuchten, M. T. (1978). Calculating the unsaturated hydraulic conductivity with a new closed-form analytical model, report. *Water Resources Program, Department of Civil Enginerring, Princeton University, Princeton, New Jersey*. (Cited on pages xv, 9, 10, 11, 12, and 70)

Vanderborght, J., Fetzer, T., Mosthaf, K., Smits, K. M., and Helmig, R. (2017). Heat and water transport in soils and across the soil-atmosphere interface: 1. Theory and different model concepts. *Water Resources Research*, 53(2):1057–1079. (Cited on page 9)

Vargaftik, N. B., Volkov, B. N., and Voljak, L. D. (1983). International tables of the surface tension of water. *Journal of Physical and Chemical Reference Data*, 12(3):817–820. (Cited on pages 23, 24, 44, and 70)

Visconti, G. (2001). *Fundamentals of physics and chemistry of the atmosphere*. Springer, Berlin. (Cited on page 58)

Wang, Y., Jin, M., and Deng, Z. (2018). Alternative model for predicting soil hydraulic conductivity over the complete moisture range. *Water Resources Research*, 54(9):6860–6876. (Cited on page 10)

Wang, Y., Ma, J., and Guan, H. (2016). A mathematically continuous model for describing the hydraulic properties of unsaturated porous media over the entire range of matric suctions. *Journal of Hydrology*, 541:873–888. (Cited on page 10)

Wang, Y., Ma, J., Guan, H., and Zhu, G. (2017). Determination of the saturated film conductivity to improve the emfx model in describing the soil hydraulic properties over the entire moisture range. *Journal of Hydrology*, 549:38–49. (Cited on page 10)

Washburn, E. W. (1921). The dynamics of capillary flow. *Physical Review*, 17(3):273–283. (Cited on pages 55 and 85)

Wenzel, R. N. (1936). Resistance of solid surfaces to wetting by water. *Industrial & Engineering Chemistry*, 28(8):988–994. (Cited on page 45)

Whitaker, S. (1969). Advances in theory of fluid motion in porous media. *Industrial & Engineering Chemistry*, 61(12):14–28. (Cited on page 5)

Whitaker, S. (1986). Flow in porous media I: A theoretical derivation of Darcy's law. *Transport in Porous Media*, 1(1):3–25. (Cited on pages 5 and 6)

White, F. M. (1991). *Viscous fluid flow*. McGraw-Hill, Inc., New York. (Cited on page 3)

Whyman, G., Bormashenko, E., and Stein, T. (2008). The rigorous derivation of Young, Cassie–Baxter and Wenzel equations and the analysis of the contact angle hysteresis phenomenon. *Chemical Physics Letters*, 450(4-6):355–359. (Cited on page 19)

Wilkinson, G. E. (1960). The temperature effect on the equilibrium energy status of water held by porous media, Ph.D. dissertation, University of Illinois, Urbana–Champaign. *Diss. Abstr.21/10:2916*. (Cited on page 11)

Wilkinson, G. E. and Klute, A. (1962). The temperature effect on the equilibrium energy status of water held by porous media[1]. *Soil Science Society of America Journal*, 26(4):326–329. (Cited on pages 11 and 72)

Winterkorn, H. F. (1948). Fundamental similarities between electro-osmotic and thermo-osmotic phenomena. In *Highway Research Board Proceedings*, volume 27. (Cited on page 8)

Wirner, F., Scholz, C., and Bechinger, C. (2014). Geometrical interpretation of long-time tails of first-passage time distributions in porous media with stagnant parts. *Physical Review E*, 90(1):013025. (Cited on page 35)

Young, T. (1805). III. an essay on the cohesion of fluids. *Philosophical Transactions of the Royal Society of London*, 95:65–87. (Cited on pages 6 and 7)

Yuan, Y. and Lee, T. R. (2013). Contact angle and wetting properties. In Bracco, G. and Holst, B., editors, *Surface Science Techniques*, pages 3–34. Springer, Berlin, Heidelberg. (Cited on page 39)

Zhang, L.-j. and Yue, X.-a. (2008). Displacement of polymer solution on residual oil trapped in dead ends. *Journal of Central South University of Technology*, 15(1):84–87. (Cited on page 15)